

國立交通大學

照明與能源光電博士學位學程

博士論文

有機電化學發光元件
之高能隙離子性材料及載子平衡研究



Study of High-Gap Ionic Materials and Carrier Balance in
Light-Emitting Electrochemical Cells

研究生：廖志騰

指導教授：蘇海清 助理教授

中華民國一百零一年七月

有機電化學發光元件
之高能隙離子性材料及載子平衡研究

Study of High-Gap Ionic Materials and Carrier Balance in
Light-Emitting Electrochemical Cells

研究生：廖志騰

Student : Chih-Teng Liao

指導教授：蘇海清

Advisor : Hai-Ching Su



Submitted to Graduate Program for Lighting and Energy Photonics
College of Photonics
National Chiao Tung University
in partial Fulfillment of the Requirements
for the Degree of
Doctor
In

Lighting and Energy Photonics

July 2012

Tainan, Taiwan, Republic of China

中華民國一百零一年七月

有機電化學發光元件之高能隙離子性材料及載子平衡研究

學生：廖志騰

指導教授：蘇海清

國立交通大學照明與能源光電博士學位學程

摘 要

在本論文中，我們研究有機電化學發光元件之高能隙離子性材料及載子平衡，在第一章中，我們簡介電化學發光元件原理及發展現況。接下來研究內容主要分為下列幾個部分：

一、在第二及第三章中，利用與台大化學系汪根權教授合作並由其合成之新穎三芴及二芴離子性衍生物製造出第一個深藍光及紫外光電化學發光元件，並利用載子平衡理論進行元件效率優化，有效提昇元件效能。

二、在第四章中，我們利用電化學發光元件之主客體系統進行元件效率優化工程，並使用深藍色三芴離子性衍生物為載子傳輸主體及紅色離子性銦錯合物為載子捕捉客體，此主客體系統擁有高效率能量傳輸機制，可使用極低濃度之客體搭配主體，有效調整元件載子平衡，並大幅抑制自我猝熄效應，使整體元件效能達到理想元件之特性。

三、在第五章中，我們藉由載子平衡理論基礎，利用藍色離子性銦錯合物為主要材料，並由相關文獻的回顧中，了解其元件效率並未達到理想元件之標準，且其載子傳輸特性偏向以電洞為主，因此我們利用紅外光染

料其最高佔有軌域能階之能階差，進行電洞載子捕捉，將其元件載子平衡調整至最佳狀態，使元件效率得到大幅提昇。

四、在第六章中探討載子注入效率對於元件特性之影響，我們使用兩種離子性銥錯合物為主要研究材料，分別為藍色離子性銥錯合物及橘色離子性銥錯合物，上述材料分別擁有相異之載子傳輸特性，並利用額外加入的電洞及電子注入層去研究其對元件特性的影響，研究發現，根據本體材料的載子傳輸特性，添加適當的載子注入層，可有效改善元件效率。

最後在第七章作一個總結。

關鍵字：電化學發光元件，高能隙離子性材料，載子平衡，載子注入



Study of High-Gap Ionic Materials and Carrier Balance

in Light-Emitting Electrochemical Cells

Student : Chih-Teng Liao

Advisors : Dr. Hai-Ching Su

Graduate Program for Lighting and Energy Photonics

National Chiao Tung University

ABSTRACT

In this thesis, we study the carrier balance in light-emitting electrochemical cells (LECs). First, the theory and development of LECs are discussed in chapter 1.

In chapter 2, we obtained saturated deep-blue electroluminescence (EL) from solid state LECs incorporating the ionic terfluorene derivative **1**. The peak external quantum efficiency and peak power efficiency of **1** in the presence of the ionic liquid reached 1.14% and 1.24 lm W^{-1} , respectively. These CIE coordinates are the most saturated blue emissions ever reported from LECs.

In chapter 3, UV LECs were, for the first time, achieved by the ionic 2,2'-bifluorene derivative. LEC devices incorporating bifluorene **1** exhibited UV EL emissions at 386 and 388 nm with maximum EQE and power efficiencies of

0.66 % and 0.23 lm W^{-1} . The EL emissions in the UV region are successfully achieved by LECs based on **1**, which are so far the shortest emission wavelength achieved in LECs.

In chapter 4, we report efficient host-guest solid-state LECs utilizing a cationic terfluorene derivative as the host and a red-emitting cationic transition metal complex as the guest. Experimental results confirm that in addition to reducing self-quenching of guest molecules, the strategy of utilizing a carrier transporting host doped with a proper carrier trapping guest would improve balance of carrier mobilities in the host-guest emissive layer, offering an effective approach for optimizing device efficiencies of LECs.

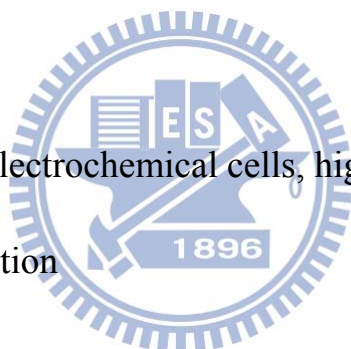
In chapter 5, we demonstrate improving balance of carrier mobilities in neat-film LECs utilizing a cationic transition metal complex (CTMC) as the emissive material and a cationic near-infrared laser dye as the carrier trapper. Experimental results confirm that balance of carrier mobilities in the CTMC neat films would be improved by doping a proper carrier trapper and such technique offers a general approach for optimizing device efficiencies of CTMC-based neat-film LECs.

In chapter 6, we study the influence of carrier injection efficiency on the performance of LECs based on a hole-preferred transporting CTMC

$[\text{Ir}(\text{dfppz})_2(\text{dtb-bpy})]^+(\text{PF}_6^-)$ (complex **1**) and an electron-preferred transporting CTMC $[\text{Ir}(\text{ppy})_2(\text{dasb})]^+(\text{PF}_6^-)$ (complex **2**). Experimental results show that even with electrochemically doped layers, ohmic contacts for carrier injection could be formed only when carrier injection barriers are relatively lower. Thus, adding carrier injection layers in LECs with relatively higher carrier injection barriers would affect carrier balance and thus would result in altered device efficiency.

Finally, the thesis is concluded in chapter 7.

Keywords: Light-emitting electrochemical cells, high-gap ionic materials, carrier balance, carrier injection



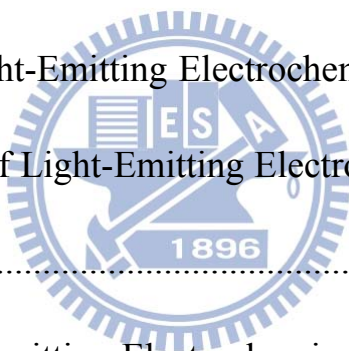
致謝

首先，由衷感謝我一輩子的恩師——蘇海清老師——給我機會加入他的研究團隊，讓我在他身旁學習他精深的知識學問、積極的實驗態度、高超的研究能力，也感謝在我修讀博士學位時，一路上支持我的人、協助我的人、鼓勵我的人、指導我的人。最後，更要感謝我的父母、岳父母、老婆無怨無悔的支持著我，讓我無後顧之憂的專注於研究之上，順利完成學業。



Contents

中文摘要.....	i
English Abstract.....	iii
致謝.....	vi
Contents.....	vii
Table Contents.....	xii
Figure Contents.....	xiii
Chapter 1 Introduction.....	1
1.1 Solid State Light-Emitting Electrochemical Cells.....	1
1.2 The Principle of Light-Emitting Electrochemical Cells.....	2
1.3 Color.....	3
1.3.1 Red Light-Emitting Electrochemical Cells.....	3
1.3.2 Yellow and Green Light-Emitting Electrochemical Cells.....	4
1.3.3 Blue Light-Emitting Electrochemical Cells.....	5
1.4 Efficiency.....	6
1.5 Stability.....	8
1.6 Turn-On Time.....	9
1.7 Summary.....	11



Chapter 2 An Ionic Terfluorene Derivative for Saturated Deep-Blue Solid State

Light-Emitting Electrochemical Cells.....	19
2.1 Introduction.....	19
2.2 Results and Discussion.....	22
2.2.1 Materials and Experimental Methods.....	22
2.2.2 Photophysical Properties.....	26
2.2.3 Atomic Force Microscopy.....	27
2.2.4 Electroluminescence.....	28
2.3 Summary.....	32

Chapter 3 UV Light-Emitting Electrochemical Cells Based on An Ionic 2,2'-

Bifluorene Derivative	42
3.1 Introduction.....	42
3.2 Results and Discussion.....	44
3.2.1 Materials and Experimental Methods.....	44
3.2.2 Photophysical Properties.....	47
3.2.3 Electroluminescence.....	49
3.3 Summary.....	54

Chapter 4 Improving the Balance of Carrier Mobilities of Host-Guest

Solid-State Light-Emitting Electrochemical Cells	63
--	----

4.1 Introduction.....	63
4.2 Materials and Experimental Methods.....	68
4.3 Results and Discussion.....	70
4.3.1 Photoluminescent Studies of the Host-Guest System.....	70
4.3.2 EL characteristics of the Host-Guest LECs.....	72
4.4 Summary.....	80
 Chapter 5 Tailoring Balance of Carrier Mobilities in Solid-State Light-Emitting Electrochemical Cells by Doping A Carrier Trapper to Enhance Device Efficiencies.....	
5.1 Introduction.....	91
5.2 Results and Discussion.....	95
5.2.1 Photoluminescent Studies.....	95
5.2.2 EL characteristics of the LEC devices.....	98
5.3 Experimental.....	107
5.3.1 Photoluminescent Characterization.....	107
5.3.2 LEC Device Fabrication and Characterization.....	107
5.4 Summary.....	109
 Chapter 6 Tailoring Carrier Injection Efficiency to Improve Carrier Balance of Solid-State Light-Emitting Electrochemical Cells.....	
	121



6.1 Introduction.....	121
6.2 Experimental.....	125
6.2.1 Materials.....	125
6.2.2 LEC Device Fabrication and Characterization.....	127
6.3 Results and Discussion.....	129
6.3.1 General LEC Device Characteristics.....	129
6.3.2 Effects of Improved Hole Injection on Device Characteristics of LECs.....	132
6.3.3 Effects of Improved Electron Injection on Device Characteristics of LECs.....	137
6.3.4 Effects of Improved Hole and Electron Injection on Device Characteristics of LECs.....	140
6.3.5 Effects of Impeded Hole, Electron and Both Hole and Electron Injection on Device Characteristics of LECs.....	144
6.4 Summary.....	148
Chapter 7 Summary.....	157
References.....	159

Table Contents

Table 2-1 Physical properties of 1	34
Table 2-2 LEC device characteristics.....	35
Table 3-1 Physical properties of 1	55
Table 3-2 LEC device characteristics.....	56
Table 4-1 Summary of the host-guest LEC device characteristics.....	82
Table 5-1 Summary of the LEC device characteristics.....	111
Table 6-1 Summary of the LEC device characteristics.....	150



Figure Contents

Figure 1-1 Schematic representations of a typical multilayer OLED and a LEC based on ionic transition metal complexes.....	12
Figure 1-2 Materials used in the first polymer-based LECs.....	13
Figure 1-3 Materials used in the first ionic transition metal complex (iTMC)-based LECs.....	14
Figure 1-4 The Principle of Light-Emitting Electrochemical Cells.....	15
Figure 1-5 Ionic iridium complexes A - H.....	16
Figure 1-6 Ionic iridium complexes I - M.....	17
Figure 1-7 The Ionic liquids of [BMIM ⁺][PF ₆ ⁻], [EMIM ⁺][PF ₆ ⁻] and [HMIM ⁺][PF ₆ ⁻].....	18
Scheme 2-1 Synthesis of 1	36
Figure 2-1 Absorption (left-hand axis) and PL (right-hand axis) spectra of 1 in acetonitrile solution (10 ⁻⁵ M) and in neat films in the presence and absence of [BMIM ⁺][PF ₆ ⁻] (10 wt%).....	37
Figure 2-2 Cyclic voltammogram of compound 1 . All potentials were recorded versus ferrocene/ferrocenium (Fc/Fc ⁺) (saturated) as a reference electrode. Inset: Differential pulse voltammetry (DPV) of the reduction region.....	38

Figure 2-3 EL spectra of device I under 3.8 V (circle) and device II under 3.4 V (square) after 0.5-hour (open symbol) and 5-hour (solid symbol) operation. PL spectra of the emissive layers are presented for comparison. Inset: CIE coordinates of the EL and PL spectra.....	39
Figure 2-4 Brightness (solid symbols) and current density (open symbols) plotted with respect to time under a constant bias voltage of (a) 3.4 – 4.2 V for device I and (b) 3.2 – 3.6 V for device II.....	40
Figure 2-5 EQE (solid symbols) and power efficiency (open symbols) plotted with respect to time under a constant bias voltage of (a) 3.4 – 4.2 V for device I and (b) 3.2 – 3.6 V for device II.....	41
Scheme 3-1 Synthesis of 1	57
Figure 3-1 Absorption (left-hand axis) and PL (right-hand axis) spectra of 1 in acetonitrile solution (10^{-5} M) and in neat film or dispersed in PMMA film (10 wt%) and the phosphorescence (Phos, right-hand axis) spectrum of 1 in EtOH solutions at 77 K.....	58
Figure 3-2 Cyclic voltammogram of compound 1 . All potentials were recorded versus Ag/AgCl (saturated) as a reference electrode.....	59
Figure 3-3 EL spectra of Device I and Device II under 4.2 V. PL spectra of the emissive layers are presented for comparison.....	60

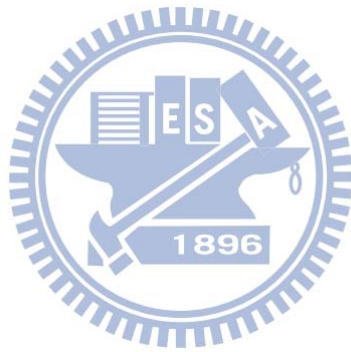
Figure 3-4	Brightness (solid symbols) and current density (open symbols) plotted with respect to time under a constant bias voltage of 4.2 and 4.6 V for (a) device I and (b) device II	61
Figure 3-5	EQE (solid symbols) and power efficiency (open symbols) plotted with respect to time under a constant bias voltage of 4.2 and 4.6 V for (a) device I and (b) device II	62
Figure 4-1	Molecular structures of the host molecule, cationic terfluorene derivative (1) and the guest molecule, $[\text{Ir}(\text{ppy})_2(\text{biq})]^+(\text{PF}_6^-)$ (2) .	83
Figure 4-2	Absorption spectrum of the neat guest films and PL spectra of the neat host and guest films. Inset: phosphorescence spectrum of the neat host films measured at 77 K.....	84
Figure 4-3	PL spectra of the host-guest films containing various guest concentrations and $[\text{BMIM}^+][\text{PF}_6^-]$ (10 wt.%). Inset: photoluminescence quantum yields vs guest concentrations of the same films.....	85
Figure 4-4	EL spectra (at 3.0 V) for the host-guest LECs with various guest concentrations and $[\text{BMIM}^+][\text{PF}_6^-]$ (10 wt.%). Inset: the energy level diagram of the host and guest molecules.....	86
Figure 4-5	(a) Brightness (solid symbols) and current density (open symbols)	

and (b) external quantum efficiency (solid symbols) and power efficiency (open symbols) as a function of time under a constant bias voltage of 3.0 – 3.4 V for Device I	87
Figure 4-6 (a) Brightness (solid symbols) and current density (open symbols) and (b) external quantum efficiency (solid symbols) and power efficiency (open symbols) as a function of time under a constant bias voltage of 2.2 – 2.3 V for Device IV	88
Figure 4-7 Peak external quantum efficiencies and peak power efficiencies (at current densities $<0.003 \text{ mA cm}^{-2}$) of the host-guest LECs as a function of the guest concentration.....	89
Figure 4-8 Schematic diagrams of the position of exciton recombination zone for (a) host-only device, (b) Device I and (c) Device III . Electrochemically doped regions near electrodes are omitted for clarity.....	90
Figure 5-1 Molecular structures of the CTMC $[\text{Ir}(\text{dfppz})_2(\text{dtb-bpy})]^+(\text{PF}_6^-)$ and the carrier trapper DOTCI.....	112
Figure 5-2 PL spectrum of the $[\text{Ir}(\text{dfppz})_2(\text{dtb-bpy})]^+(\text{PF}_6^-)$ neat film and absorption/PL spectra of DOTCI in ethanol solution (10^{-5} M)	113

Figure 5-3 PL spectra of the $[\text{Ir}(\text{dfppz})_2(\text{dtb-bpy})]^+(\text{PF}_6^-)$ films containing various concentrations of DOTCI and $[\text{BMIM}^+][\text{PF}_6^-]$ (20 wt.%)	114
Figure 5-4 EL spectra for the LECs based on $[\text{Ir}(\text{dfppz})_2(\text{dtb-bpy})]^+(\text{PF}_6^-)$ containing various concentrations of DOTCI and $[\text{BMIM}^+][\text{PF}_6^-]$ (20 wt.%) at 3.3 V.....	115
Figure 5-5 Maximum current density vs voltage characteristics for the LECs based on $[\text{Ir}(\text{dfppz})_2(\text{dtb-bpy})]^+(\text{PF}_6^-)$ containing various concentrations of DOTCI and $[\text{BMIM}^+][\text{PF}_6^-]$ (20 wt.%). Inset: the energy level diagram of $[\text{Ir}(\text{dfppz})_2(\text{dtb-bpy})]^+(\text{PF}_6^-)$ and DOTCI molecules.....	116
Figure 5-6 (a) Brightness (solid symbols) and current density (open symbols) and (b) external quantum efficiency (solid symbols) and power efficiency (open symbols) as a function of time under a constant bias voltage of 3.3 – 3.7 V for Device II	117
Figure 5-7 Peak external quantum efficiencies and peak power efficiencies (at current densities $<0.1 \text{ mA cm}^{-2}$) of the LECs as a function of the DOTCI concentration.....	118
Figure 5-8 Schematic diagrams of the position of exciton recombination zone	

for (a) Device I , (b) Device II and (c) Device III . Electrochemically doped regions near electrodes are omitted for clarity.....	119
Figure 5-9 (a) Turn-on time and (b) lifetime as a function of bias voltage for the LECs based on $[\text{Ir}(\text{dfppz})_2(\text{dtb-bpy})]^+(\text{PF}_6^-)$ containing various concentrations of DOTCI and $[\text{BMIM}^+][\text{PF}_6^-]$ (20 wt.%)	120
Figure 6-1 Molecular structures of $[\text{Ir}(\text{dfppz})_2(\text{dtb-bpy})]^+(\text{PF}_6^-)$ (1) and $[\text{Ir}(\text{ppy})_2(\text{dasb})]^+(\text{PF}_6^-)$ (2)	151
Figure 6-2 Device configurations, energy level alignments and schematic diagrams of the position of carrier recombination zone for the LECs under study. Electrochemically doped regions near electrodes are omitted for clarity.....	152
Figure 6-3 EL spectra of Device 1-S, 1-H, 1-E and 1-HE at 3.5 V and Device 2-S, 2-H, 2-E, 2-HE, 2-IH, 2-IE, 2-IHE at 2.4 V.....	153
Figure 6-4 (a) Current density, (b) brightness and (c) external quantum efficiency as a function of time for Device 1-S, 1-H, 1-E and 1-HE at 3.5 V.....	154
Figure 6-5 (a) Current density, (b) brightness and (c) external quantum efficiency as a function of time for Device 2-S, 2-H, 2-E and 2-HE at 2.4 V.....	155

Figure 6-6 (a) Current density, (b) brightness and (c) external quantum efficiency as a function of time for **Device 2-S, 2-IH, 2-IE** and **2-IHE** at 2.4 V.....156



Chapter 1 Introduction

1.1 Solid State Light-Emitting Electrochemical Cells

Solid State light-emitting electrochemical cells (LECs) possess several advantages over conventional organic light-emitting diodes (OLEDs). OLEDs typically require sophisticated multilayer structures and low-work-function cathodes to achieve high efficiencies and low operating voltages, while LECs generally require only a single emissive layer, which can be easily processed from solutions, and can conveniently use air-stable electrodes, as show in Figure 1-1. The mobile ions in emissive layers enable LECs to use air-stable metals (such as Au, Ag or Al) as cathodes and the device can be operated under low driving voltages. With these advantages (single-layer, solution-process, air-stable cathodes, low driving voltages, etc.), LECs will be promising candidates for future solid-state lighting application.[1-8]

The LECs have two main material systems: polymers or small molecules. A polymer blend sandwiched between two electrodes comprised the first solid-state LEC device. (Figure 1-2) [1] The polymer blend was composed of an emissive conjugated polymer, a lithium salt (lithium trifluoromethane sulfonate), and an ion-conducting polymer (poly(ethylene oxide); PEO). The salt provided

mobile ions, and the ion-conducting polymer prevented the blend film from phase separation, the induction of which could result from polarity discrepancies between the conjugated polymer and the lithium salt. More recently, cationic transition-metal complexes (CTMCs) have also been used in LECs (Figure 1-3), and show several advantages over conventional polymer LECs.[5, 9-20] In such devices, no ion-conducting material is needed because the metal complexes are intrinsically ionic. In general, they show good thermal stabilities and charge-transport properties. Furthermore, high electroluminescence (EL) efficiencies can be expected because of the phosphorescent nature of the metal complexes. The first solid-state LEC based on transition-metal complexes, in which a ruthenium polypyridyl complex was utilized as the emissive material, was reported in 1996.[9] Since then, many efforts have been made to improve the performance characteristics of such LECs.

1.2 The Principle of Light-Emitting Electrochemical Cells

The emissive layer of LECs contains mobile ions, which can drift toward electrodes under an applied bias. The spatially separated ions induce doping (oxidation and reduction) of the emissive materials near the electrodes, i.e., *p*-type doping near the anode and *n*-type doping near the cathode. (Figure 1-4)

[1] The doped regions induce ohmic contacts with the electrodes, and

consequently facilitate the injection of both holes and electrons that recombine at the junction between *p*-type and *n*-type regions. As a result, a single-layered LEC device can be operated at very low voltages (close to E_g/e , where E_g is the energy gap of the emissive material and e is the elementary charge, 1.602×10^{-19} C) with balanced carrier injection, giving high power efficiencies. Furthermore, air-stable metals (e.g., Al, Au and Ag) can be used because carrier injection in LECs is relatively insensitive to the work functions of the electrodes.

1.3 Color

1.3.1 Red Light-Emitting Electrochemical Cells

To achieve efficient white emission LECs for future lighting application, the red-emitting iridium complexes should be developed. To obtain the red emission color, their energy gap should be narrowed by this two strategies: increasing the conjugation length of ligands or attaching electron-withdrawing groups onto the ancillary ligands.[21-27] Tamayo *et al.*[22] reported the most efficient red-emitting LEC based on complex A (Figure 1-5). They increased the conjugation length of bpy-type ancillary ligands. Operated at 3 V, the device brightness at the peak external quantum efficiency (EQE) (7.4%) was 7500 cd m^{-2} . The CIE coordinates of (0.67, 0.32) and a peak power efficiency of 10 lm W^{-1} . Meanwhile, Su *et al.*[23] developed a red emitting ($\lambda_{max} = 656$ nm)

complex B (Figure 1-5) and used it to fabricate efficient white LECs.

The deep-red-emitting LECs were reported by Chen *et al.*[28] They synthesized a red-emitting complex C (Figure 1-5) by adding an electron-withdrawing diphenylamino group to the ancillary ligand. The LEC based on complex C showed a peak current efficiency of 0.013 cd A^{-1} .

1.3.2 Yellow and Orange Light-Emitting Electrochemical Cells

LECs based on the yellow-emitting (560 nm) iridium complex $[\text{Ir}(\text{ppy})_2(\text{dtb-bpy})]\text{PF}_6$ (ppy: phenylpyridine; dtb-bpy: 4,4'-ditertbutyl-2,2'-bipyridine) were reported in 2004, exhibiting efficiencies of 5% and 10 lm W^{-1} . [29-30] Replacement of the ppy ligands by F-mpy ligands (F-mpy: 2-(4'-fluorophenyl)-5-methylpyridine) resulted in green emission (531 nm) and an EL efficiency of 1.8 %. [30-31] On the other hand, the use of $\text{dF}(\text{CF}_3)\text{ppy}$ ligands ($\text{dF}(\text{CF}_3)\text{ppy}$: 2-(2,4-difluorophenyl)-5-trifluoromethylpyridine) increased the energy gap of the iridium complexes and shifted the EL emission to blue-green (500 nm, with an EQE of 0.75 %). [32] In 2009, Costa *et al.* reported the orange-emitting LECs (570-590 nm) based on iridium complex $[\text{Ir}(\text{ppy})_2(\text{bpy})]\text{PF}_6$ and $[\text{Ir}(\text{ppy})_2(\text{phen})]\text{PF}_6$ (bpy: 2,2'-bipyridine, phen: 1,10-phenanthroline). The device efficiency was optimized through adjustment of doping concentration of

ionic liquid in the active layers. It showed a peak EQE of 5.6% and a peak power efficiency of 16.3 lm W^{-1} . [33] Moreover, to enhance the efficiency of orange LECs, Su *et al.* synthesized iridium complex ($[\text{Ir}(\text{ppy})_2\text{SB}]\text{PF}_6$) (SB is 4,5-diaza-9,9'-spirobifluorene, and ppy is 2-phenylpyridine). with a bulky ancillary ligand. The complex can be used to make highly efficient single-layered, solid-state orange LECs, with EL efficiencies (7.1 %, 22.6 lm W^{-1}) among the highest reported. [34]

1.3.3 Blue Light-Emitting Electrochemical Cells

In recent years, to toward lighting applications in future, blue emission with good color purity and high device efficiency was certainly needed. [4] There were two major methods that could be used to make blue-emitting LECs. First, the functional ligands, such as electron-withdrawing substitutes ($-\text{F}$, or $-\text{CF}_3$), could be attached onto the cyclometalating ligands to stabilize the highest occupied molecular orbitals (HOMOs). The other was to replace electron-donating substitutes ($-\text{N}(\text{CH}_3)_2$) onto the ancillary ligands to destabilize the lowest unoccupied molecular orbitals (LUMOs). [4,31-32,35] The energy gaps of iridium complexes could be enlarged by these methods and thus lead to the emissive wavelength shift toward blue emission region. Therefore several new types of cyclometalating and ancillary ligands have been

developed.[16,29-30,36-37]

The blue-emitting iridium complex with the fastest response was reported by Myldak *et al.* in 2010.[36] These complexes based on a series of 1,2,3-triazole ancillary ligands. The photoluminescence (PL) emission in solution showed a blue peak wavelength (ca. 452 nm) and peak brightness ranging from 14 to 45 cd m⁻². Furthermore, LECs based on them exhibited blue-green emission with a peak wavelength (ca. 488 nm) and shoulder wavelength (ca. 460 nm). On the other hand, He *et al.* proposed to insert electron-donating atoms (N) into the ancillary ligands of the complexes.[17] The strategy would be increased the electron density on the ancillary ligands significantly, thus resulted in enhancing the LUMO levels of the complexes. The LEC based on [Ir(ppy)₂(pzpy)]PF₆ [pzpy is 2-(1-phenyl-1H-pyrazol-3-yl)pyridine, and ppy is 2-phenylpyridine] showed blue emission with CIE coordinates of (0.20, 0.28). Form ever reported, this is among the bluest LEC.

1.4 Efficiency

In general, LECs are composed of neat films of emissive materials, which very often suffer self-quenching induced by interactions between closely packed molecules. Many efforts have been made to enhance device efficiencies of LECs

based on CTMCs by reducing self-quenching of the emissive materials. Modifying the molecular structures, such as adding bulky substituents on ligands [14,38-39] or utilizing bulky auxiliary ligands[40] have been shown to suppress interchromophore interaction to some degree, improving device efficiencies of LECs.

He *et al.* attached a bulky side group, 4-tritylphenyl to the imidazole-type ancillary ligand, the blue-green-emitting complex D (Figure 1-5) with the sterically bulky ancillary ligand was developed.[41-43] In neat film, the self-quenching effect was significantly suppressed by enhanced steric hindrance. Under 3.2 V, the efficient blue-green LEC based on complex D shown a peak wavelength at 474 and 494 nm (CIE = 0.22, 0.41) and a peak power efficiency of 18.0 lm W⁻¹.

On the other hand, a new strategy was demonstrated by Chen *et al.*[44] They incorporated electron-withdrawing groups in the alkyl chain to enhance device performance. They employed riazole-pyridine as the ancillary ligands and developed sky-blue and blue-green-emitting complexes E–H (Figure 1-5). Their ancillary ligands employed riazole-pyridine and developed sky-blue and blue-green-emitting complexes E–H. The efficiencies of devices based on complexes G and H which included cyanogen groups in the side alkyl chains of

the ancillary ligand were significantly enhanced by 10 times and 4 times. The author explained that the device efficiencies were improved by the interaction between cyanogens group and electrodes and reduced electrical impedance.

1.5 Stability

Recently, the stability of LECs is the major challenge for future practical applications. The water-assisted ligand-exchange reactions occur during the operation of LECs based on ionic ruthenium complexes, which degrades the emitting complexes and the stability of LECs.[45-47] On the other hand, the degradation mechanisms of LECs based on ionic iridium complexes have not been reported so far. But the similar water-assisted ligand-exchange reactions is a critical factor in the degradation of LECs.[48-51]

From ever reported, addition of the hydrophobic groups on the periphery of ligands and intramolecular π - π stacking interactions can suppress the water-assisted degradation in LECs. The stability of LECs based on ionic iridium complexes were significantly improved by this two strategies.[41,48-55]

Recently, a series of ionic iridium complexes with hydrophobic methyl or phenyl groups attached to bpy ancillary ligands. (complexes I, J and K, Figure 1-6) were reported by Costa *et al.*[49] Complex K has the highest luminescent efficiencies in films and the highest stability in LECs among these three

complexes. Because it added both methyl and phenyl groups upon its bpy ancillary ligands.

In 2008, the long-lived LECs based on Ir- ionic transition metal complexes (iTMCs) was reported by Bolink *et al.* up to date.[50] Complex L (Figure 1-6) attached a pendant phenyl ring at the 6 position of the bpy ancillary ligand. The pendant phenyl ring stacked to the phenyl group of the ppy ligand, forming a strong intramolecular π - π stacking interaction which could make the complex more robust and reduce the degradation reactions. It also exerted a cage effect that restricted the opening of the structure of complex L in the excited 3MC (metal-centered) states. Under a high voltage pulse, the LEC based on complex L shown a peak brightness of 290 cd m^{-2} , a $t_{1/2}$ (lifetime, which is defined as the time for the brightness to decay from the maximum to half of the maximum) value of more than 3000 h.

1.6 Turn-On Time

The turn-on time of LECs is defined as the time to reach maximum brightness under constant biases. Under constant biases, the current density and brightness of LECs increase depend with time because the motion and redistribution of ions in LECs.[1,56] However, since the ionic conductivity in the LECs is low, it needs more time to become operative, generally ranges from

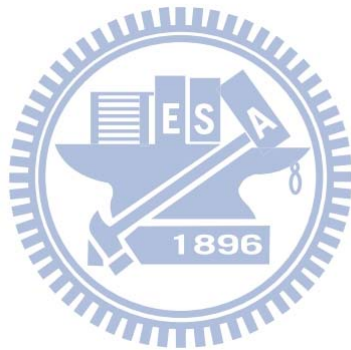
a few minutes to hundreds of hours. For future practical applications, the turn-on time should be shortened. In the last few years, several approaches in reducing turn-on time have been reported.

Kwon *et al.*[57] developed complex M (Figure 1-6), which attached sodium sulfonate to the ligand of a neutral ionic iridium complexes and with an Na^+ counter cation. The cation Na^+ has a better mobility than bulky PF_6^- or BF_4^- , therefore compare with the LECs based on an ionic iridium complexes with a PF_6^- counter anion, the turn-on time of LECs based on complex M exhibited a several times shorter.

Recently, Costa *et al.* studied the effect of some different ionic liquids. They used different ionic conductivities with similar chemical structures on the same LECs.[58] They tested 1-ethyl-3-methylimidazolium hexafluorophosphate $[\text{EMIM}^+][\text{PF}_6^-]$ and 1-hexyl-3-methylimidazolium hexafluorophosphate $[\text{HMIM}^+][\text{PF}_6^-]$, which ionic conductivities increased from $[\text{EMIM}^+][\text{PF}_6^-]$ to $[\text{HMIM}^+][\text{PF}_6^-]$ as the alkyl chain length decreased. (Figure 1-7). Therefore, the author found that by adding a proper amount of ionic liquids with high conductivity (molar ratio Ir-CTMC: $[\text{EMIM}^+][\text{PF}_6^-]$ 4:1), it was possible to improve the turn-on time without sacrificing the stability of the device.

1.7 Summary

In this introduction, we have provided an overview on the state-of-the art of the characteristic of LECs, which have achieved remarkable performance cover all the visible spectral region, from blue to red. However, for future application in solid-state lighting or display technique, the performance of LECs should be further improved. Thus, in this thesis, we would develop the novel high-gap materials to be used for LECs and study the effect of carrier balance in LECs.



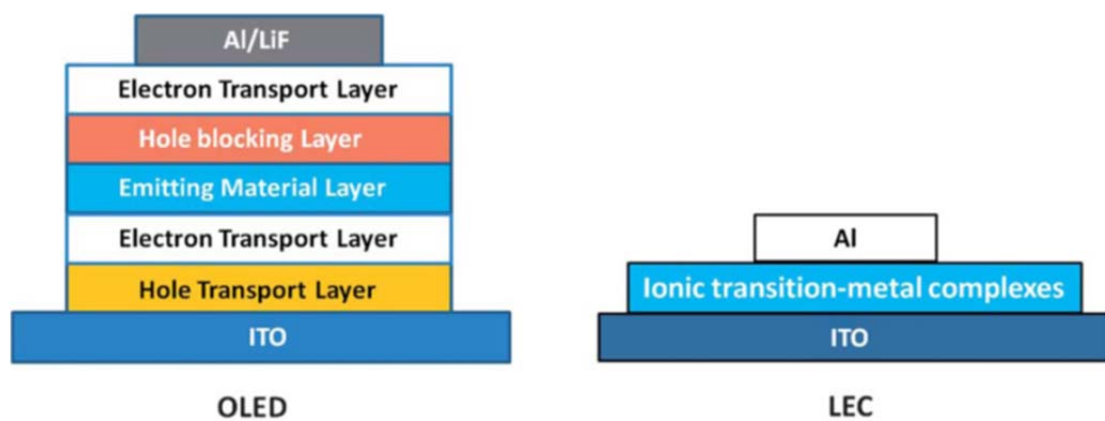


Figure 1-1 Schematic representations of a typical multilayer OLED and a LEC based on ionic transition metal complexes.

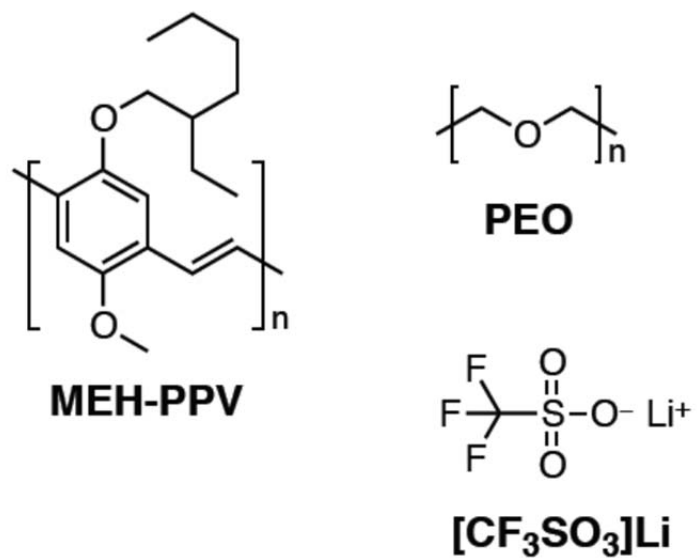


Figure 1-2 Materials used in the first polymer-based LECs.

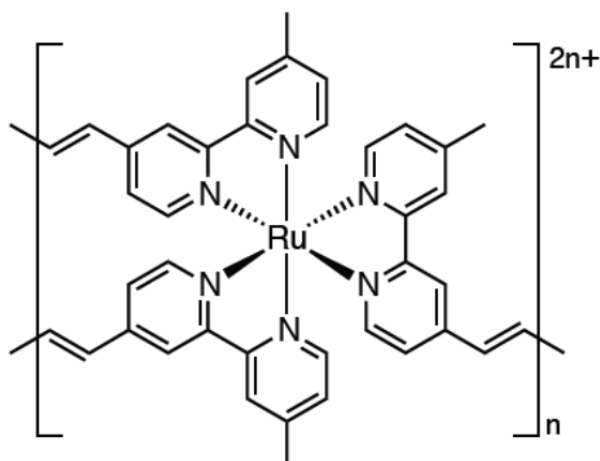


Figure 1-3 Materials used in the first ionic transition metal complex (iTMC)

-based LECs.



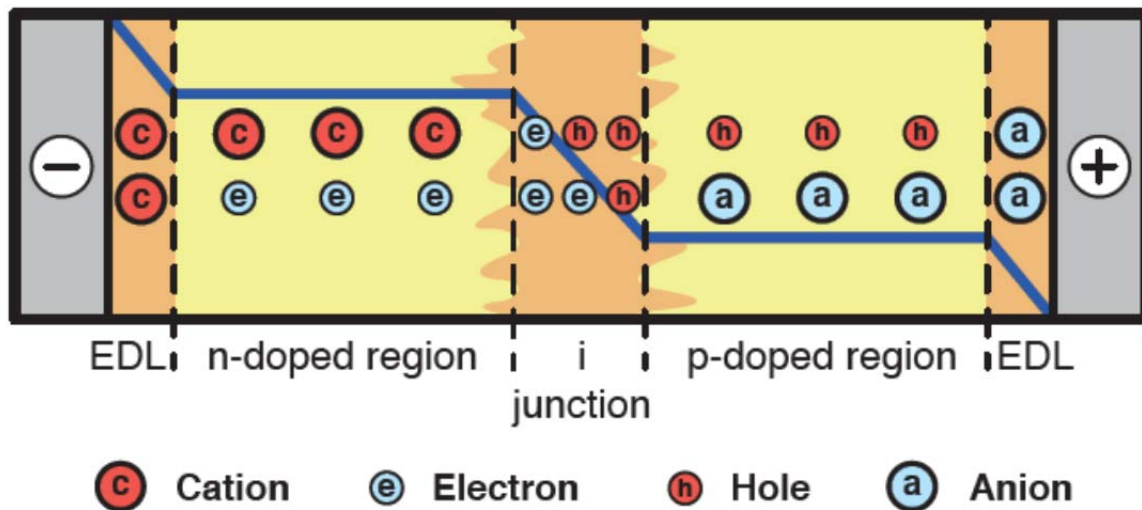


Figure 1-4 The Principle of Light-Emitting Electrochemical Cells

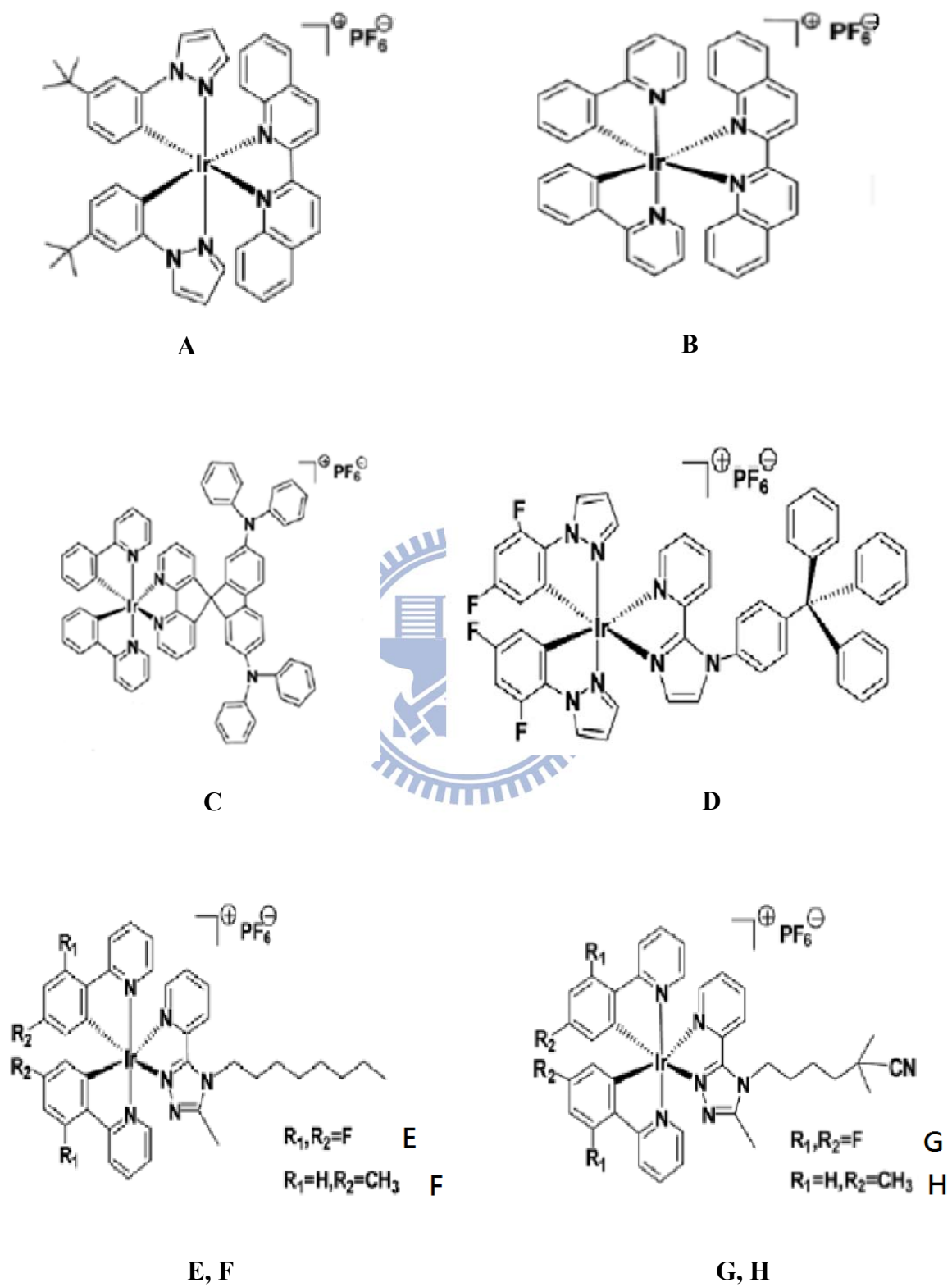


Figure 1-5 Ionic iridium complexes **A - H**.

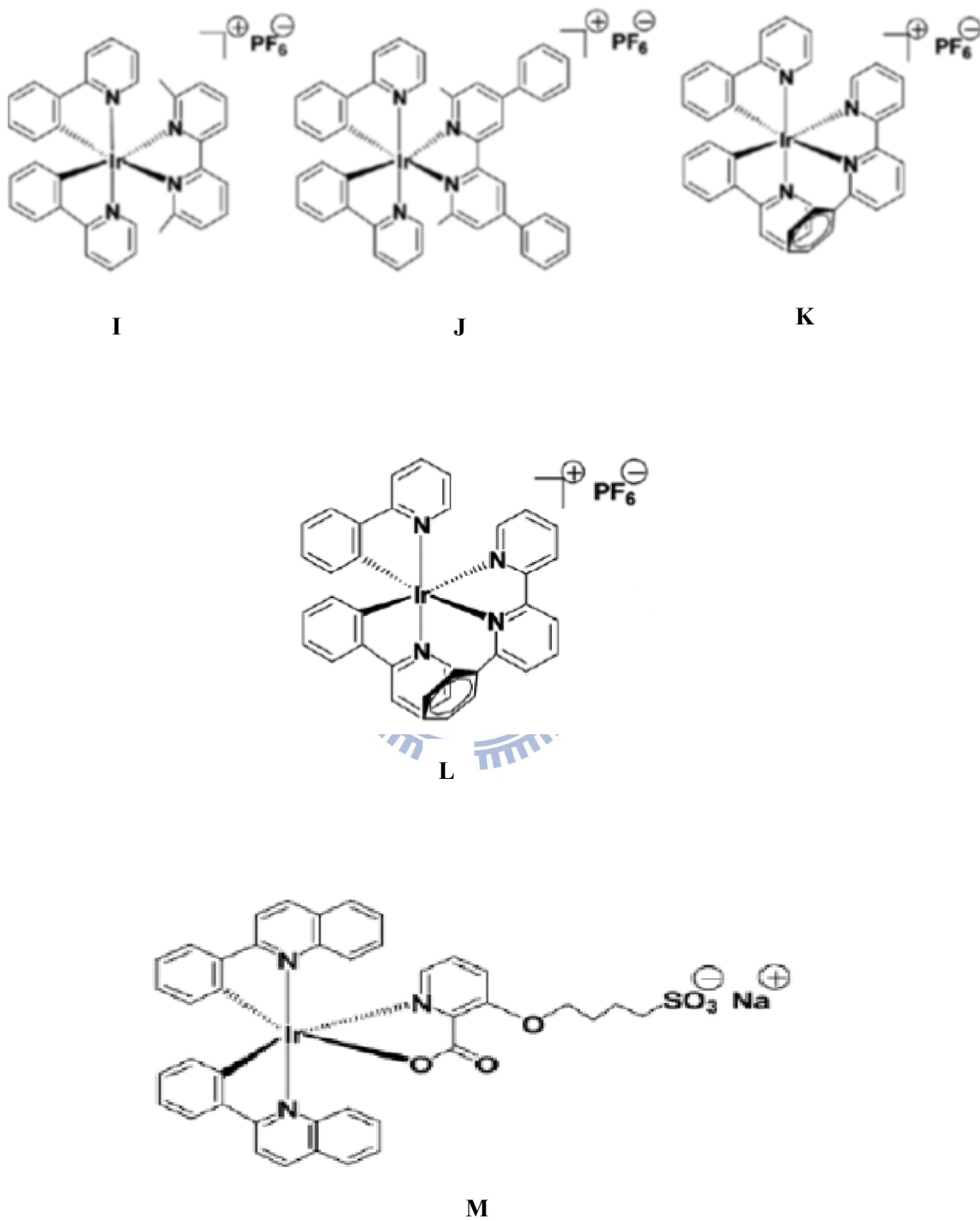


Figure 1-6 Ionic iridium complexes I - M.

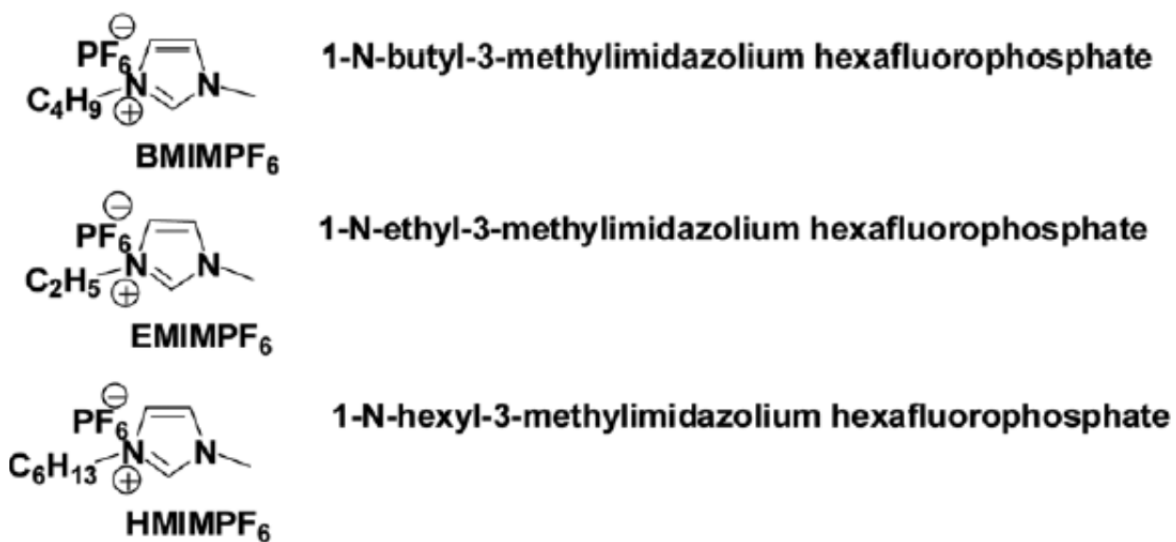


Figure 1-7 The Ionic liquids of [BMIM⁺][PF₆⁻], [EMIM⁺][PF₆⁻] and [HMIM⁺][PF₆⁻].

Chapter 2 An Ionic Terfluorene Derivative for Saturated Deep-Blue Solid State Light-Emitting Electrochemical Cells

2.1 Introduction

LECs possess several advantages over conventional OLEDs. In LECs, electrochemically doped regions induced by spatially separated ions under a bias form ohmic contacts with electrodes, resulting in balanced carrier injection and low operating voltages and, consequently, high power efficiencies.[1,59] As such, LECs generally require only a single emissive layer, which can be processed readily from solution, and, conveniently, they can feature air-stable electrodes, whereas OLEDs typically require more sophisticated multilayer structures and low-work-function cathodes.[60-61]

Recently, cationic Ir complexes have been explored widely for their use in LECs because of their high luminescence efficiencies, tunable light emission colors, and high compatibility with ionic electrolytes. By tailoring the structures of their chelating ligands, emissions from cationic Ir complexes can cover such a large color range to achieve full-color displays and white light emission.[8,22,30] To date, however, the development of efficient saturated blue-emitting ionic Ir complexes has lagged behind those of other colors. The complexes that have been prepared with large optical band gaps have mainly exhibited emissions in

the bluish-green region. Recently, He *et al.* reported a blue-emitting cationic Ir complex exhibiting EL centered at 460 nm.[17] Bolink *et al.* found that the origin of the large spectral shift in the EL, ranging from 476 to 560 nm, of the blue-emitting cationic Ir complex $[\text{Ir}(\text{ppy-F}_2)_2\text{Me}_4\text{phen}]\text{PF}_6$ was related to the concentration of the ionic transition metal complex in the thin film.[63] The difficulty in effecting color-shifting toward the deep-blue region with Ir-based cationic complexes is mainly due to the intrinsically narrow energy gaps in such cationic complexes relative to those of neutral ones [e.g., $\text{Ir}(\text{dfppy})_2(\text{pic})$, where dfppy is 2-(2,4-difluorophenyl)pyridine and pic is picolinic acid], thereby limiting the possibility of spectral tuning through molecular design.[64-65] Moreover, thermal population to accessible ligand field states (a possible nonradiative decay pathway) leads to low emission efficiencies, which further restricts the development of blue-emitting cationic Ir complexes.[66] Therefore, alternative approaches for the development of saturated blue-emitting materials for the use in LECs remain in high demand to complete the emitting color gap of cationic Ir complexes.

Polyfluorenes (PFs) are used widely as efficient blue emitters in polymer light-emitting diodes (PLEDs) because they generally possess high PL quantum efficiencies and high thermal stabilities.[67-69] The rigidity of the

coplanar fluorene structure in the conjugated backbone and the flexibility of functionalization on the C9 position have crucial effects on the characteristics and processability of the resulting polymers, as well as modulating their intermolecular interactions when in the form of thin films. LECs based on PF/PEO mixtures were reported by Yang *et al.* as early as 1997. Blue-green LECs incorporating an emissive layer blend comprising a PF featuring polyether-type side groups and lithium triflate has achieved an EQE of 4%.^[70] In this case, however, the emission resulted mainly from aggregation of PF, shifting the emission wavelength to the green region.^[71] Although much effort has been exerted to improve the compatibility of the polymer and the ionic electrolytes [e.g., introducing oligo(ethylene glycol) units at the C9 positions of the PF or directly end-capping C9-substituted alkyl chains with ionic species],^[75] no LECs based on PFs have yet avoided the phenomena of green emissions generated from either aggregation or keto defects.^[69]

In this study, to avoid the intrinsic tendency of aggregation that is widely observed for PF derivatives, we selected members of the terfluorene family—low-molecular-weight analogues of PFs—to realize saturated blue-emitting LECs. Terfluorene derivatives possess emission wavelengths in the deep-blue region with ultra-high luminance quantum yields (close to

unity).[76-77] They also exhibit bipolar carrier transport capability ($\mu_{\text{h}}, \mu_{\text{e}} > 10^{-4}$ $\text{cm}^2 \text{V}^{-1} \text{s}^{-1}$), which is beneficial to device performance.[78-79] Herein, we report the use of a terfluorene-based ionic compound (**1**) to achieve saturated deep-blue EL from two LEC devices: **device I** and **device II** provided Commission Internationale de l'Eclairage (CIE)[80] coordinates (x, y) of (0.151, 0.122) and (0.159, 0.115), respectively, extremely close to the blue coordinates (0.14, 0.08) in the NTSC color gamut. We prepared the ionic terfluorene derivative **1** through simple attachment of 1-methylimidazolium moieties to the terminal positions of the alkyl substituents of the central fluorene moiety, rendering a hydrophobic terfluorene core bearing movable anions, enabling the formation of homogeneous films through spin-coating and, consequently, efficient blue-emitting LECs.

2.2 Results and Discussion

2.2.1 Materials and Experimental Methods

Materials

Scheme 2-1 outlines the synthesis of the ionic compound **1**. This ionic compound **1** is synthesized and provided by Prof. Wong's group of chemistry department in National Taiwan University. They obtained the key bromo-substituted intermediate **1-Br** in 68% yield after performing a modified

one-pot Suzuki coupling[18] of 2-bromo-9,9-dihexylfluorene (**2**)[82] with 2,7-dibromo-9,9-bis(6-bromohexyl)fluorene (**3**).[83] They isolated compound **1** in 81% yield after treating **1-Br** with an excess of 1-methylimidazole, followed by ion exchange with potassium hexafluorophosphate.

Figure 2-1 displays the electrochemical characteristics of **1**, as probed using cyclic voltammetry (CV). This figure measures and provides by Prof. Wong's Group of chemistry department in National Taiwan University. They observed two discrete reversible oxidation potentials [at 0.87 and 1.02 V (vs. Fc/Fc⁺)] for **1** in acetonitrile (0.1 M *n*-Bu₄NPF₆ as supporting electrolyte) and two reversible reduction potentials [at -2.69 and -2.89 V (vs. Fc/Fc⁺)] for **1** in THF (0.1 M *n*-Bu₄NClO₄ as supporting electrolyte). They assign both the oxidation and reduction peaks to electron transfer processes that occurred on the terfluorene backbone, verifying the prominent bipolar carrier transport observed in terfluorene derivatives. The reductions were relatively poorly resolved, with a lower peak current during the positive sweep relative to that of the oxidations, presumably because the pendent imidazolium units could interact with the reduced species and, consequently, retard the diffusion toward the electrode.[86] The pronounced potential differences in the oxidation (150 mV) and reduction (200 mV) regions indicate efficient resonance delocalizations of the radical

cation and the radical anion over the entire terfluorene backbone.

Experimental Methods

^1H and ^{13}C NMR spectra of compounds were recorded at room temperature using a 400 MHz spectrometer. Photophysical characteristics of complexes in solutions were recorded at room temperature using 10^{-5} M acetonitrile solutions of all compounds, which were carefully purged with N_2 prior to measurements. The neat and 1-butyl-3-methylimidazolium hexafluorophosphate [BMIM^+][PF_6^-] blended films for PL studies were spin-coated onto quartz substrates from acetonitrile solutions. The thickness of each spin-coated film was ca. 200 nm, as measured using profilometry. UV-Vis absorption spectra were recorded using a Hitachi U2800A spectrophotometer. PL spectra were recorded using a Hitachi F9500 fluorescence spectrophotometer. PL quantum yields (PLQYs) for solution and thin-film samples were determined using a calibrated integrating sphere system (Hamamatsu C9920). Oxidation and reduction potentials of **1** were determined using CV; a CH Instruments model 619B electrochemical analyzer was operated at a scan rate of 100 mV s^{-1} using either an acetonitrile or THF solution (1.0 mM). A glassy carbon electrode and a Pt wire were used as the working and counter electrodes, respectively. All potentials were recorded versus the Ag/AgCl (saturated) reference electrode and calibrated with the

ferrocene/ferrocenium redox couple (reversible oxidation potential at 0.44 V in ACN and 0.56 V in THF). Oxidation CV was performed using 0.1 M tetra-n-butylammonium hexafluorophosphate (TBAPF₆) in acetonitrile as the supporting electrolyte; for reduction CV, 0.1 M tetra-n-butylammonium perchlorate (TBAP) in THF was used as the supporting electrolyte. AFM images of films of **1** spin-coated onto PEDOT:PSS/ITO glass in the presence and absence of [BMIM⁺][PF₆⁻] were obtained using a scanning probe microscope (Nano Navi L-trace II) operated in tapping mode.

ITO-coated glass substrates were cleaned and treated with UV/ozone prior to use. A PEDOT:PSS layer was spin-coated onto the ITO substrate in air and then the structure was baked at 150 °C for 30 min. The emissive layer (ca. 200 nm) was spin-coated from an acetonitrile solution of **1**. To reduce the turn-on time of the LEC device, the [BMIM⁺][PF₆⁻] was added to enhance the ionic conductivity of the thin film of **1**. [84] After spin-coating the emissive layer, the samples were baked at 70 °C for 10 h and subjected to thermal evaporation of an 100-nm-thick Al top contact in a vacuum chamber (ca. 10⁻⁶ torr). The electrical and emission characteristics of the LEC devices were measured using a source-measurement unit and a Si photodiode calibrated with a Photo Research PR-650 spectroradiometer. The accuracy of optoelectronic measurement system

closed to 10^{-12} A, therefore our measurement results have ultra-high accuracy.

All device measurements were performed under a constant bias voltage. EL spectra of LEC devices were recorded using a calibrated CCD spectrograph.

2.2.2 Photophysical Properties

Figure 2-2 depicts the UV–Vis absorption and PL spectra of **1** in solution (acetonitrile, 10^{-5} M) and in the form of neat films. Table 2-1 summarizes the photophysical data. To speed up the device response, the ionic liquid [BMIM⁺][PF₆⁻] is commonly used as an additive providing additional mobile anions.[84] Therefore, we also examined the emission properties of thin films of **1** in the presence of [BMIM⁺][PF₆⁻] (10 wt %). In solution, **1** exhibits an absorption signal centered at 352 nm, which we assign to the lowest π – π^* transition of the terfluorene backbone. In its PL spectrum, **1** reveals intense fluorescence with an emission maximum centered at 393 nm along with vibronic features at *ca.* 413 and 441 nm and an excellent quantum yield of 100%. These PL features are characteristic of terfluorene derivatives.[76-77] The absorption spectra of neat films of **1** exhibited spectral broadening, possibly due to its wide conformational distribution and a certain degree of intermolecular interactions in the solid state. Nevertheless, no significant emission peaks appeared in the green region in the solid state PL spectra of **1**. Instead, we observed only slightly

red-shifted emission signals, centered at 417 and 418 nm, which we attribute to an enhanced molecular polarization effect.[85] The emission quantum yields of **1** in the form of neat films remained high (up to 0.76) despite the presence of intermolecular interactions. More importantly, the addition of the ionic liquid in the neat film did not affect the emission properties of **1**. The highly retained PL properties and the high emission quantum yield of **1** in neat film, compared with those of PF derivatives, suggested that **1** would be suitable for use as a deep-blue emitter in LECs.

2.2.3 Atomic Force Microscopy

The addition of polar salts into conjugated polymer films can result in the formation of aggregates or phase separation as a result of discrepancies in polarity.[87-89] To study the effect of [BMIM⁺][PF₆⁻] on the morphology of the neat film of **1**, Prof. Wong's group used atomic force microscopy (AFM) to probe the surface. AFM images of films of **1** on ITO glass substrates, in the presence and absence of [BMIM⁺][PF₆⁻], exhibited no significant differences, with root-mean-square (RMS) roughnesses of 6.44 and 7.79 nm, respectively. At a doping concentration of [BMIM⁺][PF₆⁻] in **1** of 1:1.77 (molar ratio), we observed no particular aggregation features or phase separation, giving uniform spin-coated thin films. The comparable roughnesses of the two samples indicate

the high compatibility between **1** and the added salt, presumably imparted by the ionic nature of **1**. Remarkably, the composite thin film of **1** in the presence of [BMIM⁺][PF₆⁻] did not exhibit particular emission quenching: the emission quantum yield was comparable with that of the thin film of **1** formed in the absence of [BMIM⁺][PF₆⁻] (Table 2-1).

2.2.4 Electroluminescence

The promising physical properties of the ionic terfluorene **1** rendered it suitable for LEC applications. Table 2-2 summarizes the device characteristics of structures having the configuration glass substrate/ITO/(PEDOT:PSS, 30 nm)/emissive layer (ca. 200 nm)/Al (100 nm), where the emissive layer was a film of compound **1** for device **I** and a film of compound **1** containing 10 wt% [BMIM⁺][PF₆⁻] for device **II**. In device **II**, we added [BMIM⁺][PF₆⁻] to enhance the ionic conductivity.[84] Measurements of both device properties were performed under constant bias voltages.

Figure 2-3 compares the EL spectra of the LEC devices with the PL spectra of their emissive layers. The similarity of the EL spectra of both devices indicates that the addition of [BMIM⁺][PF₆⁻] did not alter the EL of **1**. Notably, the signals in the EL spectra are broadened relative to those in the PL spectra. The longer emission wavelengths (450–500 nm) were significantly enhanced

under electrical driving; presumably, this spectral change is primarily related to thermal rearrangement of the molecules and, consequently, the enhanced formation of intermolecular excimer species.[90] Possibly because of its shorter conjugation length, the excimer EL emission band of the ionic terfluorene **1** was, however, predominantly centered in the sky-blue region (Figure 2-3), whereas LECs based on PF derivatives[70, 72-75] or copolymers containing crown ether spacers[91] exhibit significant green or yellow interchain excimer emissions. Therefore, the LEC devices based on **1** retained their deep-blue EL emissions, with CIE coordinates for the EL signals of devices **I** and **II** of (0.151, 0.122) and (0.159, 0.115), respectively. The inset to Figure 2-3 reveals that the CIE coordinates of the EL signals for both LEC devices approached the blue apex of the National Television System Committee (NTSC) color gamut—indeed, they are the bluest EL emissions ever to have been reported for blue LECs.[17,36,63] Thus, the ionic terfluorene **1** is a promising candidate for use as a deep-blue emitting material in LECs.

Figure 2-4 presents the time-dependent brightness and current densities of devices **I** and **II** when operated under various bias voltages. These LEC devices exhibited similar electrical characteristics. The brightness and device current first increased with time after the bias was applied, reaching maximum values

before undergoing gradual decreases over time. The time required for the brightness to reach its maximum value decreased as the bias voltage increased (Table 2-2), presumably because a higher accumulation rate of mobile ions facilitated the formation of doped regions under a higher electric field. Under the same bias voltage, device **II** required a significantly shorter time for its brightness to reach the maximum value relative to that of device **I** (e.g., 30 and 161 min, respectively, at 3.4 V). This result indicates that the additional mobile ions provided by the electrolyte $[\text{BMIM}^+][\text{PF}_6^-]$ increased the rate of accumulation of ions near the electrodes, leading to accelerated formation of doped regions. The decreases in brightness and current densities over time after reaching the maximum values are associated with degradation of the emissive material during LEC operation. The maximum brightness and current density obtained in the first measurement were not fully recoverable in subsequent measurements, even under the same driving conditions. Under a constant bias, the lifetime of each device, defined as the time required for the brightness of the device to decay from the maximum value to half of the maximum value, decreased upon increasing the bias voltage. For instance (Table 2-2), the lifetime of device **I** (device **II**) decreased from 462 to 78 min (427 to 49 min) upon increasing the bias voltage from 3.4 to 4.2 V (from 3.2 to 3.6 V). We suspect that

the higher current density induced by a higher bias voltage led to a higher rate of irreversible multiple oxidation and subsequent decomposition of the emissive material,[84,93] thereby accelerating the degradation of the LEC devices. Similarly, device **II**, which exhibited higher current densities induced by more mobile ions, had shorter lifetimes than device **I** under the same bias voltage (Table 2-2).

Figure 2-5 presents the time-dependent EQEs and corresponding power efficiencies of devices **I** and **II** operated under various bias voltages. Both devices exhibited similar time evolutions of their EQEs. Immediately after a forward bias was applied, the EQE was rather low because of unbalanced carrier injection. During the formation of the doped regions near the electrodes, the balance of the carrier injection was improved and, accordingly, the EQE of the device increased rapidly. The peak EQE and peak power efficiency were 1.04% and 0.63 lm W^{-1} , respectively, for device **I** under 3.4 V and 1.14% and 1.24 lm W^{-1} , respectively, for device **II** under 3.2 V. Addition of $[\text{BMIM}^+][\text{PF}_6^-]$ (device **II**) decreased the operating voltage and, therefore, increased the power efficiency relative to that of the parent neat-film device (device **I**). Thus, LEC devices based on **1** can exhibit deep-blue EL emissions and good device efficiencies, making them potential candidates for use in full-color

power-effective displays.

2.3 Summary

Prof. Wong's group has synthesized an efficient deep-blue-emitting terfluorene derivative, **1**, that allows the realization of saturated deep-blue-emitting LECs. They achieved the essential ionic character required for LECs by chemically tethering methylimidazolium moieties as pendent groups to the terfluorene. Furthermore, we successfully demonstrate deep-blue LECs utilizing a terfluorene derivative **1** as the emissive material. The introduction of these methylimidazolium moieties not only allowed uniformly spin-coated thin films to be formed (without particular aggregation features or phase separation) in either the absence or presence of the ionic liquid [BMIM⁺][PF₆⁻] but also retained the attractive characteristics (deep-blue emission, extremely high quantum yield, reversible redox behavior) of terfluorene derivatives. An LEC device incorporating a neat film of **1** achieved a deep-blue EL emission centered at 424 nm with CIE coordinates of (0.151, 0.122), an EQE of 1.04%, and a peak power efficiency of 0.63 lm W⁻¹ under 3.4 V. Incorporating the ionic liquid [BMIM⁺][PF₆⁻] in the emitting layer of device **II** increased the accumulation rate of mobile ions near the electrodes, leading to accelerated formation of doped regions. The highest peak EQE and power efficiency of device **II** were

1.14% and 1.24 lm W^{-1} , respectively, at 3.2 V. The CIE coordinates of the EL signals from these two devices approached the blue apex of the NTSC color gamut—notably, these values represent the bluest EL emissions ever obtained from LECs.



Table 2-1 Physical properties of **1**

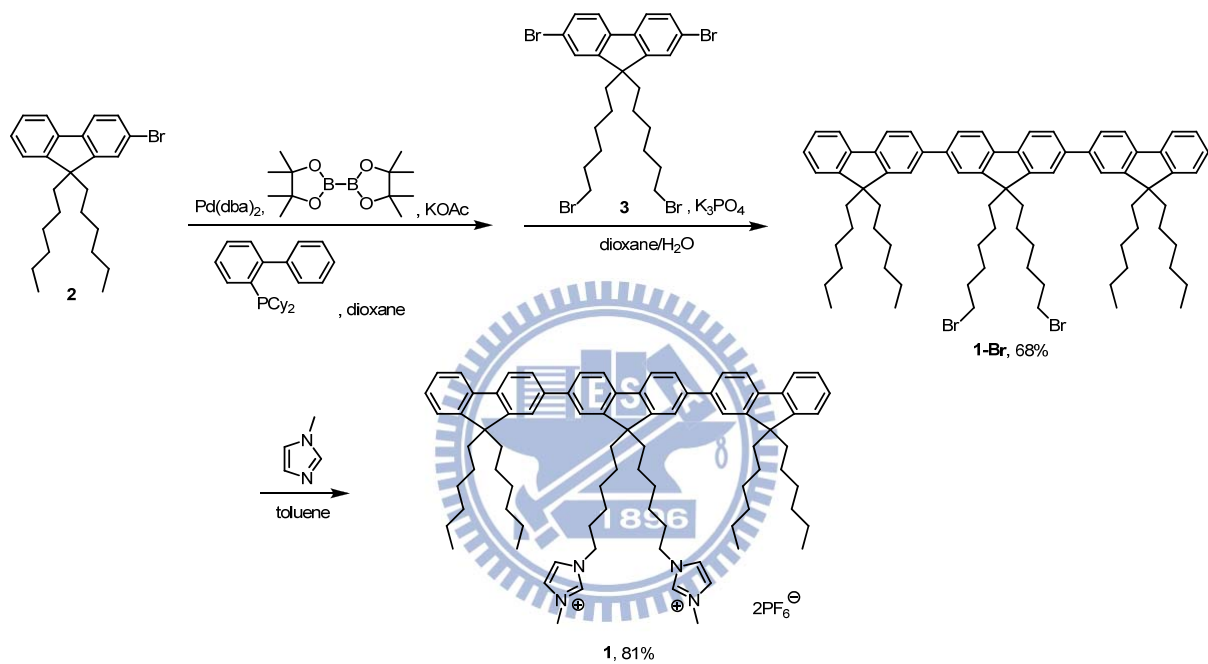
	$\lambda_{\text{max, PL}}$ (nm) ^b		PLQY ^c		$E_{1/2}^{\text{ox}}$ (V) ^d	$E_{1/2}^{\text{red}}$ (V) ^e	$\Delta E_{1/2}$ (V) ^f
	Solution ^a	Film	Solution ^a	Film			
1	393	418	1.00	0.76	+0.87, +1.02 ^g	-2.69, -2.89 ^h	3.56
1 with 10 wt% BMIM·PF ₆	—	417	—	0.75	—	—	—

[a] Measured in CH₂Cl₂ (10⁻⁵ M) at room temperature. [b] PL peak wavelength. [c] Photoluminescence quantum yields. [d] Oxidation potential vs ferrocene/ferrocenium redox couple. [e] Reduction potential vs. ferrocene/ferrocenium redox couple. [f] The electrochemical gap $E_{1/2}$ is the difference between $E_{1/2}^{\text{ox}}$ and $E_{1/2}^{\text{red}}$. [g] 0.1 M TBAPF₆ in acetonitrile. [h] 0.1 M TBAP in THF.

Table 2-2 LEC device characteristics

Device	Bias Voltage (V)	$\lambda_{\max, \text{EL}}$ (nm) ^a	CIE (x, y) ^b	t_{\max} (min) ^c	L_{\max} (cd m ⁻²) ^d	$\eta_{\text{ext, max}}$ (%) ^e	$\eta_{\text{p, max}}$ (lm W ⁻¹) ^f	Lifetime (min) ^g
I	3.4			161	0.31	1.04	0.63	462
	3.8	424	(0.151, 0.122)	62	1.48	0.99	0.52	156
	4.2			35	2.43	0.69	0.31	78
II	3.2			51	0.34	1.14	1.24	427
	3.4	423	(0.159, 0.115)	30	0.52	1.03	0.72	211
	3.6			11	1.69	0.77	0.47	49

[a] EL peak wavelength. [b] CIE coordinates of EL spectra. [c] Time required to reach the maximal brightness. [d] Maximal brightness achieved at a constant bias voltage. [e] Maximal external quantum efficiency achieved at a constant bias voltage. [f] Maximal power efficiency achieved at a constant bias voltage. [g] The time for the brightness of the device to decay from the maximum to half of the maximum under a constant bias voltage.



Scheme 2-1 Synthesis of **1**.

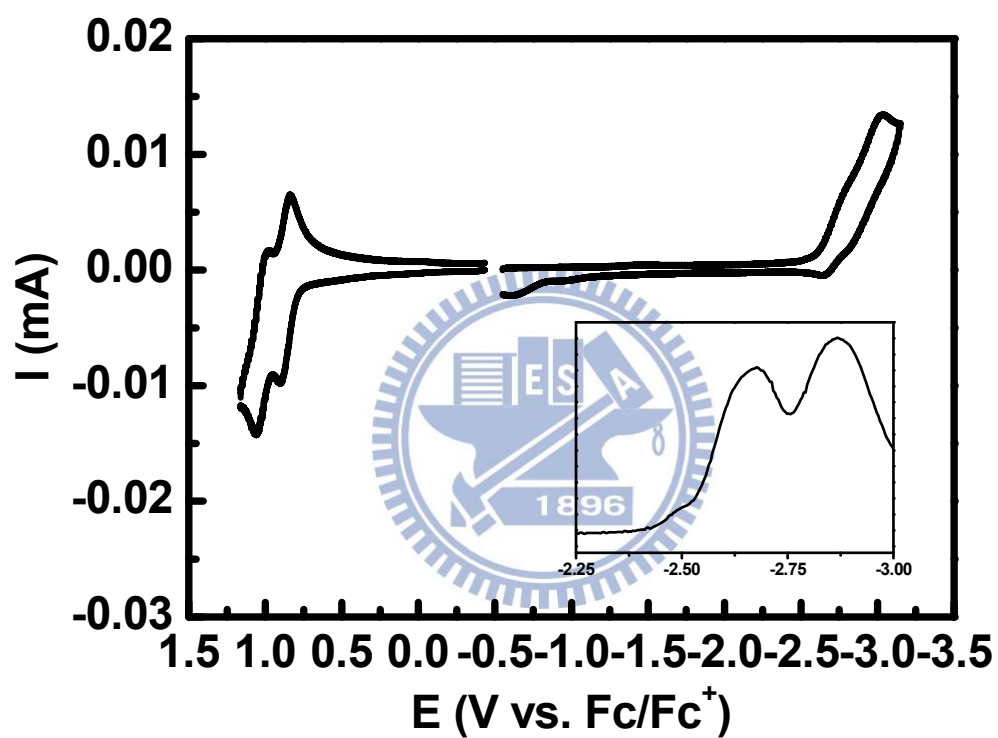


Figure 2-1 Cyclic voltammogram of compound **1**. All potentials were recorded versus ferrocene/ferrocenium (Fc/Fc^+) (saturated) as a reference electrode. Inset: Differential pulse voltammetry (DPV) of the reduction region.

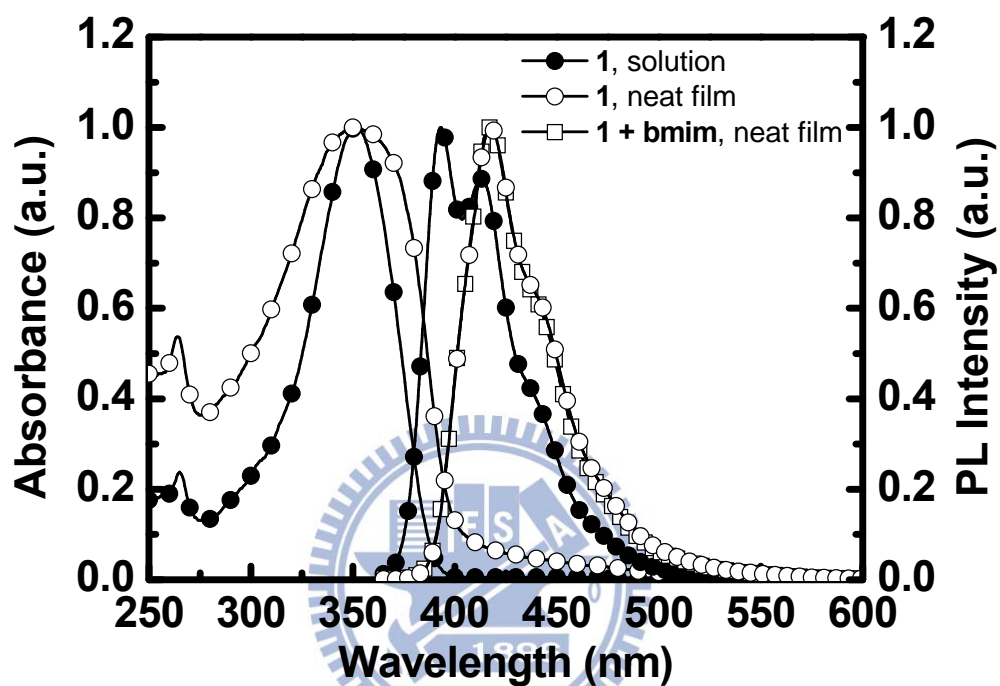


Figure 2-2 Absorption (left-hand axis) and PL (right-hand axis) spectra of **1** in acetonitrile solution (10^{-5} M) and in neat films in the presence and absence of $[\text{BMIM}^+][\text{PF}_6^-]$ (10 wt%).

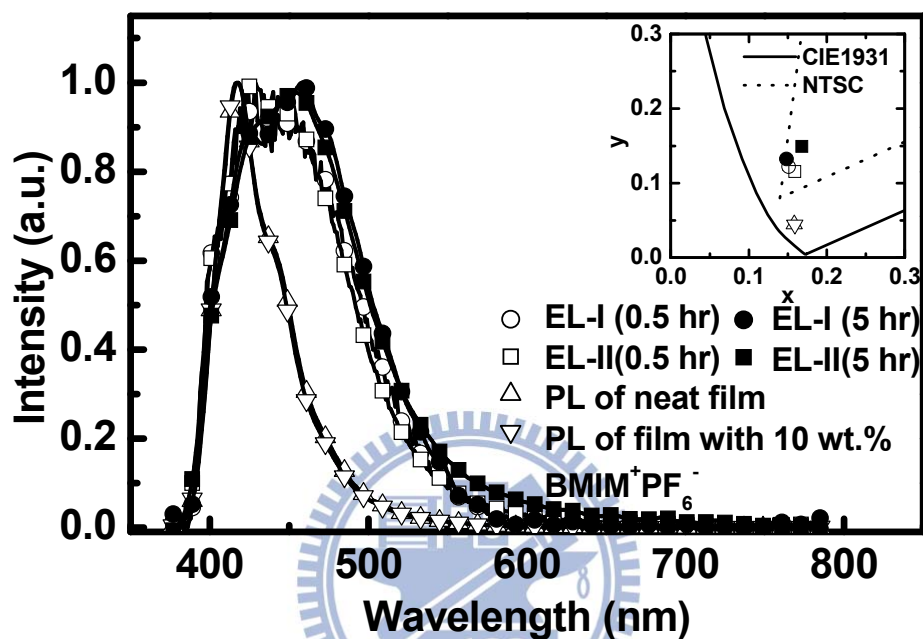


Figure 2-3 EL spectra of device I under 3.8 V (circle) and device II under 3.4 V (square) after 0.5-hour (open symbol) and 5-hour (solid symbol) operation. PL spectra of the emissive layers are presented for comparison. Inset: CIE coordinates of the EL and PL spectra.

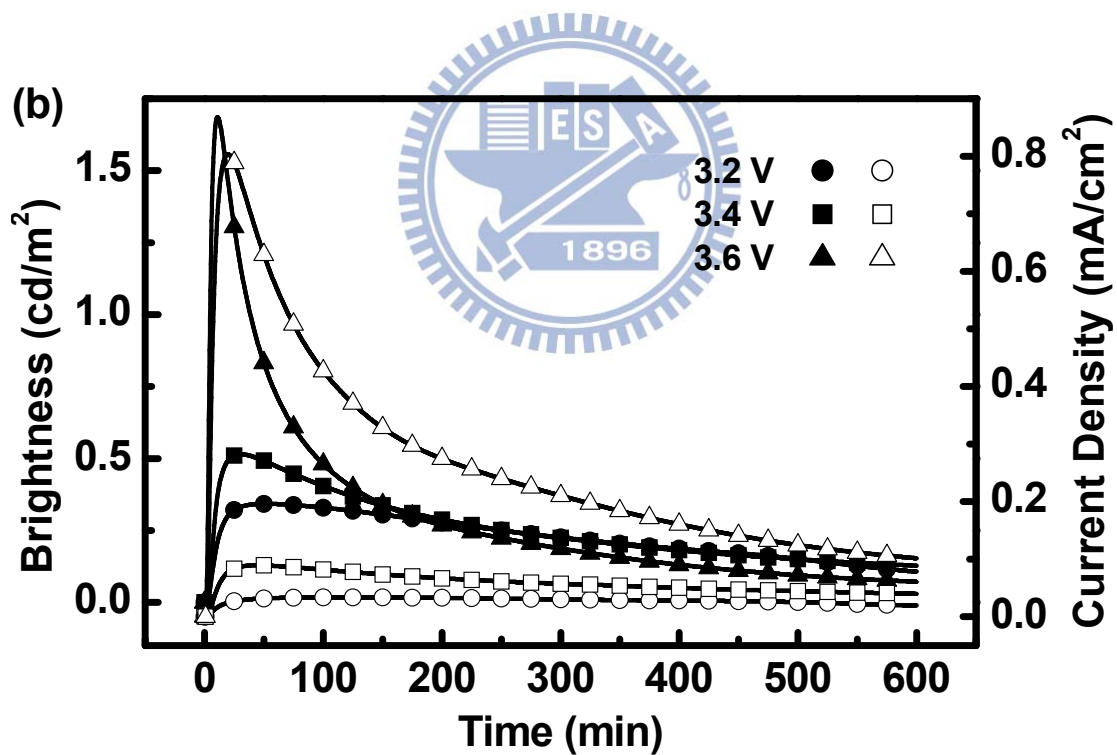
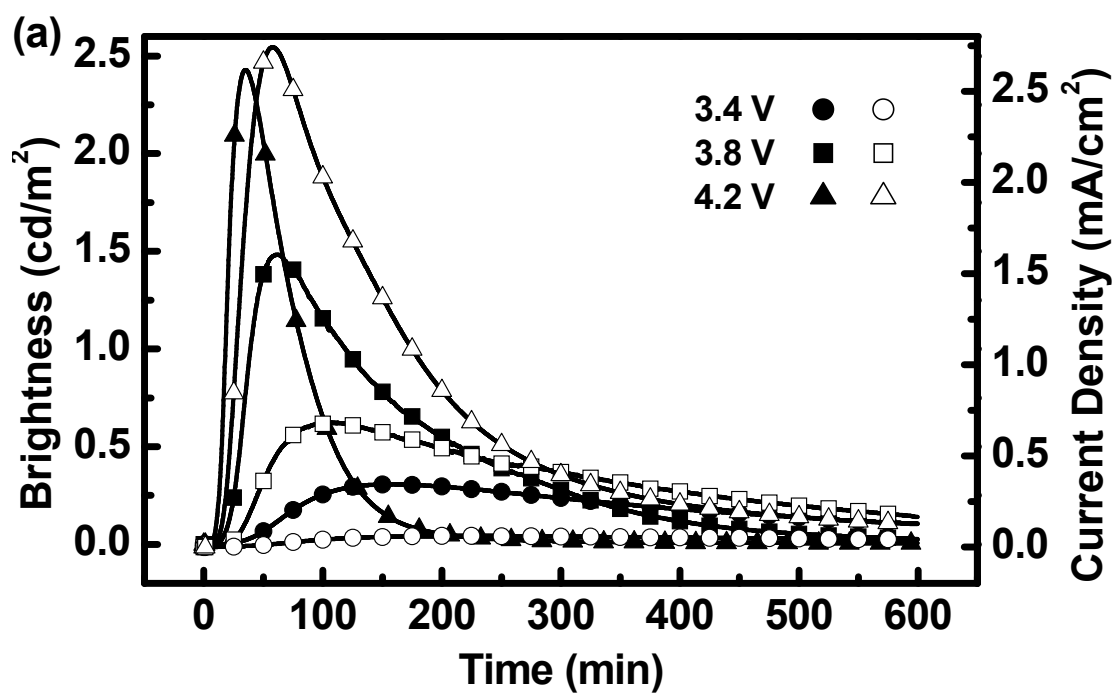


Figure 2-4 Brightness (solid symbols) and current density (open symbols) plotted with respect to time under a constant bias voltage of (a) 3.4–4.2 V for device I and (b) 3.2–3.6 V for device II.

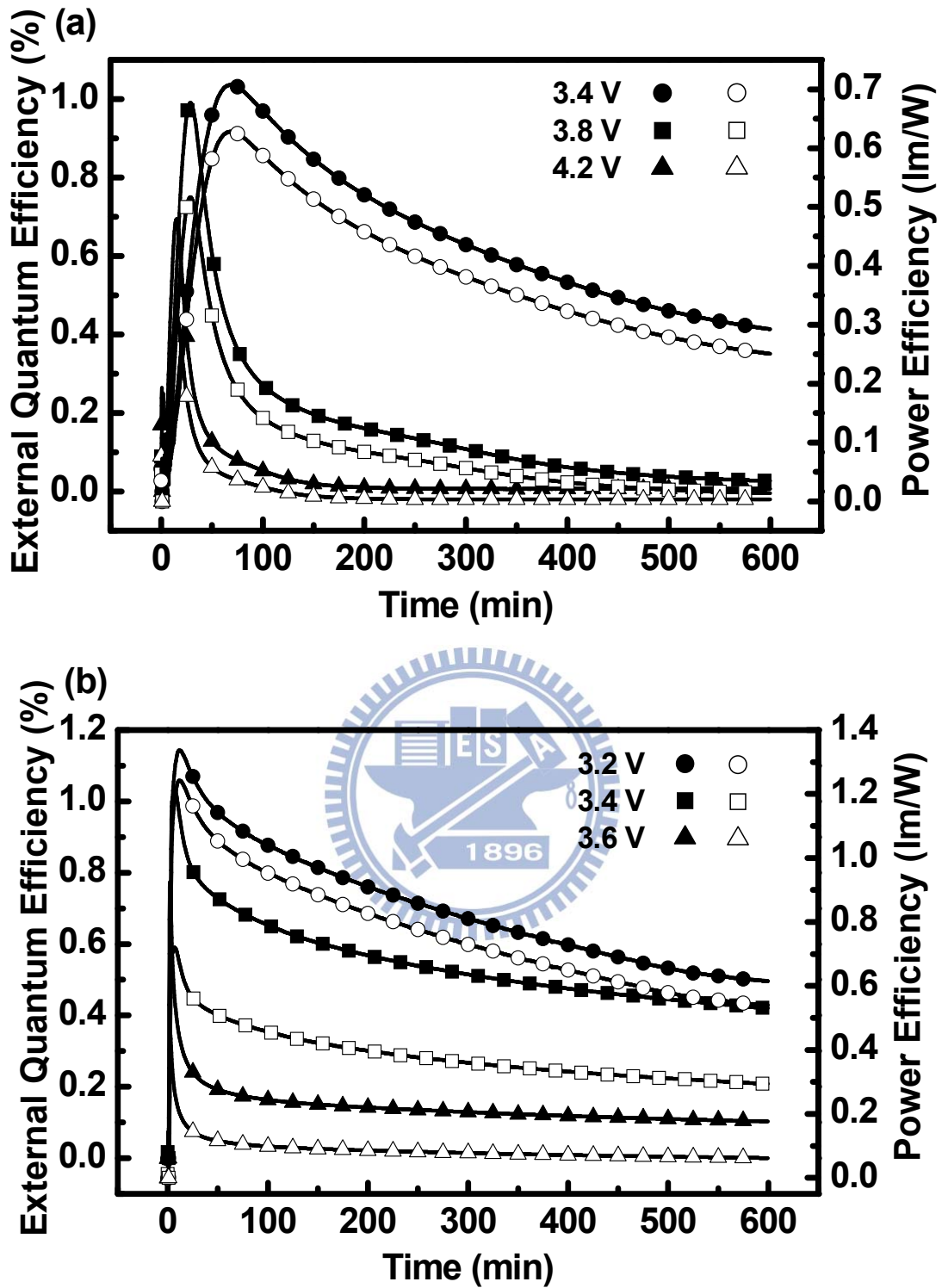


Figure 2-5 EQE (solid symbols) and power efficiency (open symbols) plotted with respect to time under a constant bias voltage of (a) 3.4–4.2 V for device I and (b) 3.2–3.6 V for device II.

Chapter 3 UV Light-Emitting Electrochemical Cells Based on An Ionic 2, 2'- Bifluorene Derivative

3.1 Introduction

Solid state LECs possess solution-processable simple device architecture and high compatibility with air-stable electrodes such as gold, silver, and aluminum.[1] In LEC devices, electrochemically doped regions induced by spatially separated ions under an applied voltage generate ohmic contacts with electrodes, resulting in balanced carrier injection and low operating voltages and, consequently, high power efficiencies. These promising advantages render this type of electroluminescent device competitive with conventional OLEDs as a cost-effective alternative for display and lighting.[94-97]

LECs based on CTMCs have shown several advantages including (i) high compatibility with ionic electrolytes imparted by intrinsic ionicity of CTMCs; (ii) high EL efficiencies due to phosphorescent nature, and (iii) tunable emission colors. Particularly, the most widely used CTMCs for single-component LEC devices are based on cationic iridium(III) complexes owing to their facile synthetic pathways and a full coverage of emission wavelength in the visible region by tailoring the structures of their chelating ligands.[8,22,23,26,30,34,62,86,99,100-103] However, intrinsic narrow energy

gaps and accessible non-radiative ligand field states of cationic iridium complexes substantially restrict their practical use for achieving blue-emitting LEC devices.[64-66] To achieve saturated blue-emitting LEC devices, we have successfully demonstrated so far the bluest electroluminescence from the LEC based on ionic terfluorene derivative.[104] The ionic fluorescent emitter was achieved by covalent tethering of 1-methylimidazolium moieties as pendant groups, rendering a hydrophobic terfluorene core bearing movable anions to form homogeneous films through spin-coating. The efficient and successful strategy for accomplishing blue-emitting LEC propelled us to further explore the molecules with larger energy gaps, which is highly desired for host materials or excitation light source for light-emitting devices.

The development of wide-gap materials is rather limited to a few functionalized structural features such as materials containing carbazoles[105] and silane[8] moieties in order to obtain a confined conjugation length. The emissions of these wide-gap materials are generally above 400 nm, *i.e.*, violet-blue emission. However, limited π -conjugation considerably complicates the molecular design since it also constraints the molecular size and coplanarity which are related to the molecular morphological stability and luminescent properties. It is rather difficult to construct a molecule which meets most general

requirements for optoelectronic materials such as high thermal stability, good carrier mobility, and ionic (for LEC application) in a limited conjugation and dimension. As a result, with meticulous selection on the wide-gap chromophores, we have demonstrated several UV OLEDs based on 2,2'-bifluorene derivatives with remarkable short emission wavelength centered at 370 nm and external quantum efficiency up to 3.6%.^[111-112] Distinguish and efficient UV emission below 400 nm is rarely reported for organic materials and has never been done for LEC application. Herein, we present the first UV LEC achieved by 2,2'-bifluorene derivative with ionic pendant 1-methylimidazolium moieties, achieving the EL as short as 386 nm. The successful demonstration of UV LEC once again proved that our judicious molecular design strategy for ionic emitters is much suitable for LEC application.

3.2 Results and Discussion

3.2.1 Materials and Experimental Methods

Materials

Scheme 3-1 outlines the synthetic route of the ionic bifluorene (**1**). This ionic bifluorene (**1**) was synthesized and provided by Prof. Wong's group of chemistry department in National Taiwan University. They obtained the bromo-substituted 2,2'-bifluorene **1-Br** after homo-coupling *via* modified

one-pot Suzuki coupling[81] of 2-bromo-9,9-bis(6-bromohexyl)fluorene (**2**) in 46% yield. After treating **1-Br** with excess amount of 1-methylimidazole followed by ion-exchange with potassium hexafluorophosphate, they isolated compound **1** in 81% yield.

Figure 3-1 displays the electrochemical characteristics of **1**, as probed by C. A quasi-reversible oxidation potential [at +1.04 V (vs. Fc/Fc⁺)] in acetonitrile (0.1 M *n*-Bu₄NPF₆ as supporting electrolyte) and a quasi-reversible reduction potential [at -2.66 V (vs. Fc/ Fc⁺)] in acetonitrile (0.1 M *n*-Bu₄NClO₄ as supporting electrolyte) were distinctly observed for **1**. This figure was measured and provided by Prof. Wong's group of chemistry department in National Taiwan University. They unambiguously assign both the oxidation and reduction peaks to electron transfer processes that occurred on the bifluorene backbone, consistent with the published bifluorene derivatives.[111-112] The reduction peak is less reversible in terms of a lower peak current in the reverse scan as compared with that of oxidation. It is presumably due to the pendent imidazolium units interacting with the reduced species and, consequently, retarding the diffusion toward the electrode.[86] **1** possesses a more positive oxidation and a less negative reduction than those of neutral bifluorene derivatives (where the oxidation and reduction potentials are in a range of +0.89

to +0.99 V and -2.74 to -2.94 V, respectively, vs. Fc/ Fc⁺)[111], suggesting a substantial inductive effect given by methylimidazolium units.

Experimental Methods

¹H and ¹³C NMR spectra of compounds were collected on a 400 MHz spectrometer at room temperature. Photophysical characteristics of complexes in solutions were collected at room temperature by using 10⁻⁵ M acetonitrile solutions of all compounds, which were carefully purged with nitrogen prior to measurements. The thickness of spin-coated films was ~200 nm, as measured by profilometry. UV-visible absorption spectra were recorded on a spectrophotometer (HITACHI U2800A). PL spectra were measured with a fluorescence spectrophotometer (HITACHI F9500). PLQYs for solution and thin-film samples were determined with a calibrated integrating sphere system (HAMAMATSU C9920). Oxidation and reduction potentials of all complexes were determined by CV at a scan rate of 100 mV/s in acetonitrile solutions (1.0 mM). A glassy carbon electrode and a platinum wire were used as the working electrode and the counter electrode, respectively. All potentials were recorded versus the Ag/AgCl (sat'd) reference electrode. Oxidation CV was performed using 0.1 M TBAPF₆ in acetonitrile. For reduction CV, 0.1 M TBAP in acetonitrile was used as the supporting electrolyte.

ITO-coated glass substrates were cleaned and treated with UV/ozone prior to use. A PEDOT:PSS layer was spin-coated onto the ITO substrate in air and then the structure was baked at 150 °C for 30 min. For device **I**, the emissive layer (ca. 400 nm) was spin-coated from an acetonitrile solution of **1**. For device **II**, the emissive layer was spin-coated from a mixed acetonitrile solution containing a mass ratio of 1/ poly(methyl methacrylate) (PMMA) = 0.9:0.1. All solution preparing and spin-coating processes were carried out under ambient conditions. After spin-coating the emissive layer, the samples were baked at 70 °C for 10 h in a nitrogen glove box (oxygen and moisture levels below 1 ppm) and the subjected to thermal evaporation of a 100-nm-thick Ag top contact in a vacuum chamber (ca. 10^{-6} torr). The electrical and emission characteristics of the LEC devices were measured using a source-measurement unit and a Si photodiode calibrated with a Photo Research PR-650 spectroradiometer. All device measurements were performed under a constant bias voltage in a nitrogen glove box. EL spectra of LEC devices were recorded using a calibrated CCD spectrograph.

3.2.2 Photophysical Properties

Figure 3-2 depicts the UV–Vis absorption and PL spectra of **1** in solution (acetonitrile, 10^{-5} M) and in the form of neat films. Table 1 summarizes the

photophysical data. To increase the film quality, we also dispersed compound **1** into inert PMMA which can efficiently fill out the defect sites of the film to diminish the current leakage of the device.[14] Thus, the emission properties of compound **1** dispersed in PMMA (10 wt%) is also examined. In solution, **1** exhibits an absorption signal centered at 328 nm, which we assign to the lowest $\pi-\pi^*$ transition of the bifluorene backbone. In its PL spectrum, **1** reveals intense fluorescence with an emission maximum centered at 373 nm and an excellent quantum yield of 100%. These values correspond with the published results of bifluorene derivatives.[111-112] Both absorption and PL spectra of **1** in neat films are red-shifted by *ca.* 10 nm as compared with those in solutions, possibly due to a certain degree of intermolecular interactions ($\pi-\pi$ stacking) in the solid state. Interestingly, by adding 10 wt% PMMA in the films of **1**, no significant change is observed for the absorption and PL spectra as compared to that without PMMA, indicating that **1** is still in the form of small aggregates instead of completely dispersion in PMMA. The amphiphilic property of **1**, imparted by solvophilic imidazolium and solvophobic bifluorene backbone, renders a substantial hydrophobic effect to potentially organize nano-scale architectures by non-covalent interactions.[114-115] The addition of PMMA is speculated to give certain extent of separation to these small aggregates, evidenced by the

identical absorption and PL spectra for **1** with and without the presence of PMMA, respectively. The triplet energy of **1** (2.33 eV) was determined from the highest energy vibronic sub-band of the phosphorescence spectra recorded in ethanol (EtOH) at 77 K. The low E_T value indicates a significant exchange stabilization energy of the bifluorene chromophore.

3.2.3 Electroluminescence

To examine the electroluminescence properties of **1**, LEC devices based on **1** were fabricated and the device characteristics are summarized in Table 3-2. The device structures are glass/ITO (120 nm)/PEDOT:PSS (30 nm)/emissive layer (400 nm)/Ag (100 nm) (where the emissive layer was a thin film of **1** for Device **I** and a thin film of **1** containing 10 wt% PMMA for Device **II**). In device **II**, PMMA was added to improve film quality and thus to decrease the leakage current during device operation, enhancing device efficiency.[12] Measurements of both device properties were performed under constant bias voltages. Figure 3-3 compares the EL spectra of the LEC devices under 4.2 V and the PL spectra of their emissive layers. The similarity of the EL spectra of both devices indicates that the addition of PMMA did not significantly alter the EL of **1**. Slight discrepancies in intensities of EL vibronic peaks between the two devices may be attributed to altered molecular potential energy surfaces of **1** in

media with different polarities[116] under applied electric fields. Notably, the signals in the EL spectra are slightly broadened at 420-500 nm relative to those in the PL spectra. It is primarily related to thermal rearrangement of the molecules and, consequently, the enhanced formation of intermolecular excimer species.[90] Since such effect is not significant in LEC devices based on **1**, both devices exhibited EL emissions centered at UV region ($\lambda_{\text{max}} = 386$ and 388 nm for device **I** and device **II**, respectively), which are bluest EL emissions ever to have been reported for LECs. Therefore, **1** is a promising candidate for use as a UV emitting or a high-gap host material in LECs.

Figure 3-4(a) and 3-4(b) presents the time-dependent brightness and current densities when operated under 4.2 and 4.6 V for devices **I** and **II**, respectively. The driving voltages are chosen to be close to the energy gap of **1** (3.7 eV in solutions, Table 3-1) to improve the device stability.[34] Furthermore, the UV EL emissions of both devices exhibited poor overlap with the luminosity function[117] and thus lead to relatively lower brightness (Table 3-2). Both LEC devices exhibited similar electrical characteristics. The brightness and device current first increased with time after the bias was applied, reaching maximum values before undergoing gradual decreases over time. The time required for the brightness to reach its maximum value decreased as the bias voltage increased

(Table 3-2), presumably because a higher accumulation rate of mobile ions facilitated the formation of doped regions under a higher electric field. Both devices showed similar time required to reach maximum brightness under the same bias voltage (e.g., 5.0 and 4.8 min for device **I** and **II**, respectively, at 4.2 V). This result indicates that addition of inert PMMA could not significantly alter the ionic mobility of the emissive layer possibly due to a high density of mobile ions in the films of **1** (4 PF₆⁻ anions per molecule). However, device **II** exhibited a lower maximum device current density under the same bias voltage as compared to device **I** (e.g., 2.27 and 1.51 mA cm⁻² for device **I** and **II**, respectively, at 4.2 V). Since the emissive layers of both devices have similar thicknesses, lowered device current density of device **II** may be attributed to impeded charge hopping between dispersed **1** in PMMA matrix. Furthermore, improved film quality by adding PMMA may also reduce the leakage current of the emissive layer, rendering a lower device current. The decreases in brightness and current densities over time after reaching the maximum values are associated with degradation of the emissive material during LEC operation. The maximum brightness and current density obtained in the first measurement were not fully recoverable in subsequent measurements, even under the same driving conditions. Under a constant bias, the lifetime of each device, defined as the

time required for the brightness of the device to decay from the maximum value to half of the maximum value, decreased upon increasing the bias voltage. For instance (Table 3-2), the lifetime of device **I** (device **II**) decreased from 5.8 to 3.3 min (4.9 to 3.0 min) upon increasing the bias voltage from 4.2 to 4.6 V. It results from that higher current density induced by a higher bias voltage led to a higher rate of irreversible multiple oxidation and subsequent decomposition of the emissive material, thereby accelerating the degradation of the LEC devices.[84,93]

Figure 3-5(a) and 3-5(b) presents the time-dependent EQEs and corresponding power efficiencies operated under 4.2 and 4.6 V for devices **I** and **II**, respectively. Both devices exhibited similar time evolutions of their EQEs. Immediately after a forward bias was applied, the EQE was rather low because of unbalanced carrier injection. During the formation of the doped regions near the electrodes, the balance of the carrier injection was improved and, accordingly, the EQE of the device increased rapidly. The peak EQE and peak power efficiency were 0.15% and 0.06 lm W^{-1} , respectively, for device **I** under 4.2 V and 0.66% and 0.23 lm W^{-1} , respectively, for device **II** under 4.2 V. The device efficiency of device **II** is much higher than that of device **I** under the same bias voltage. Since the PLQYs of **1** in the films with and without PMMA

are similar (0.41 and 0.45, respectively, Table 1), enhanced device efficiency of LECs based on **1** containing 10 wt% PMMA cannot be attributed to reduced self-quenching of **1** dispersed in PMMA matrix. Possible reason for this phenomenon would come from reduced device current due to impeded charge hopping between dispersed molecules in PMMA matrix. Lower current density suppresses collision-induced exciton dissociation and consequently reduces efficiency roll-off. Thus, a higher device efficiency would be obtained at a lower device current density. In addition, reduced leakage current of the emissive layer due to improved film quality by adding PMMA may also enhance device efficiency. However, the maximum EQEs (0.66%) of LEC devices based on **1** are lower than the upper limit (~2 %) that one would expect from the PLQYs in the films of **1** containing 10 wt% PMMA (0.41, Table 3-1), when considering fluorescent spin statistics (ca. 25%) and an optical out-coupling efficiency of ca. 20% from a typical layered light-emitting device structure. It may mainly result from imperfect carrier balance of **1** in the films containing 10 wt% PMMA. These results shown above reveal that LEC devices based on **1** can exhibit UV EL emissions and moderate device efficiencies, making them potential candidates of UV emitting materials or high-gap host materials for use in LECs.

3.3 Summary

Prof Wong's group has synthesized a UV-emitting ionic bifluorene derivative, **1**, that realized the unprecedented UV-emitting LECs. They achieved the essential ionic character required for LECs by chemically tethering methylimidazolium moieties as pendent groups to the bifluorene. Incorporating the inert PMMA in the emitting layer of device **II** impeded charge hopping between dispersed molecules as well as improved the film quality, leading to a reduced current density and current leakage. The highest peak EQE was over four times larger in the device with PMMA (device **II**) than that without PMMA (device **I**). The EQE and power efficiency of device **II** were 0.66% and 0.23 lm W⁻¹, respectively, at 4.2 V. Both devices **I** and **II** exhibited UV EL emissions at 386 and 388 nm, respectively, which are the first example of UV LEC ever reported.

Table 3-1 Physical properties of **1**

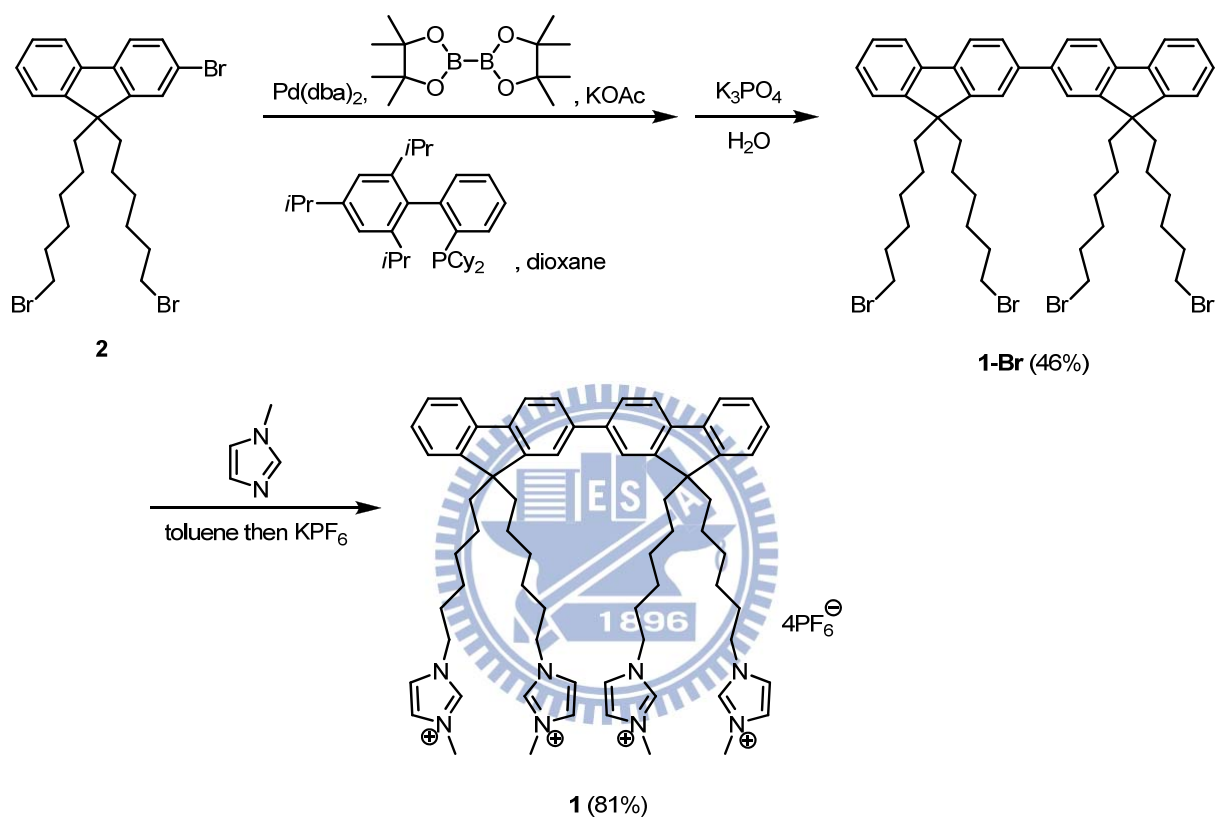
	$\lambda_{\text{max, PL}}$ (nm) ^b		PLQY ^c		$E_{1/2}^{\text{ox}}$ (V) ^d	$E_{1/2}^{\text{red}}$ (V) ^e	$E_{1/2}$ (V) ^f	E_{T} (eV)
	Solution ^a	Film	Solution ^a	Film				
1	373	385	1.00	0.45	+1.04 ^g	-2.66 ^h	3.70	2.33
1 with 10 wt% PMMA	—	385	—	0.41	—	—	—	—

[a] Measured in acetonitrile (10^{-5} M) at room temperature. [b] PL peak wavelength. [c] Photoluminescence quantum yields. [d] Oxidation potential vs ferrocene/ferrocenium redox couple. [e] Reduction potential vs. ferrocene/ferrocenium redox couple. [f] The electrochemical gap $E_{1/2}$ is the difference between $E_{1/2}^{\text{ox}}$ and $E_{1/2}^{\text{red}}$ [g] 0.1 M TBAPF₆ in acetonitrile. [h] 0.1 M TBAP in acetonitrile.

Table 3-2 LEC device characteristics

Device ^a	Bias Voltage (V)	$\lambda_{\max, \text{EL}}$ (nm) ^b	t_{\max} (min) ^c	J_{\max} (mA cm ⁻²) ^d	L_{\max} (cd m ⁻²) ^e	$\eta_{\text{ext, max}}$ (%) ^f	$\eta_{\text{p, max}}$ (lm W ⁻¹) ^g	Lifetime (min) ^h
I	4.2	386	5.0	2.27	0.34	0.15	0.06	5.8
	4.6		4.0	4.30	0.54	0.14	0.05	3.3
II	4.2	388	4.8	1.51	0.66	0.66	0.23	4.9
	4.6		3.2	3.78	1.08	0.64	0.20	3.0

[a] Device structures: Glass/ITO (120 nm)/PEDOT:PSS (30 nm)/emissive layer (Device **I**: 100 wt% **C6**, Device **II**: 90 wt.% **C6** + 10 wt.% PMMA) (400 nm)/Ag (100 nm). [b] EL peak wavelength. [c] Time required to reach the maximal brightness. [d] Maximal device current density achieved at a constant bias voltage. [e] Maximal brightness achieved at a constant bias voltage. [f] Maximal external quantum efficiency achieved at a constant bias voltage. [g] Maximal power efficiency achieved at a constant bias voltage. [h] The time for the brightness of the device to decay from the maximum to half of the maximum under a constant bias voltage.



Scheme 3-1 Synthesis of **1**.

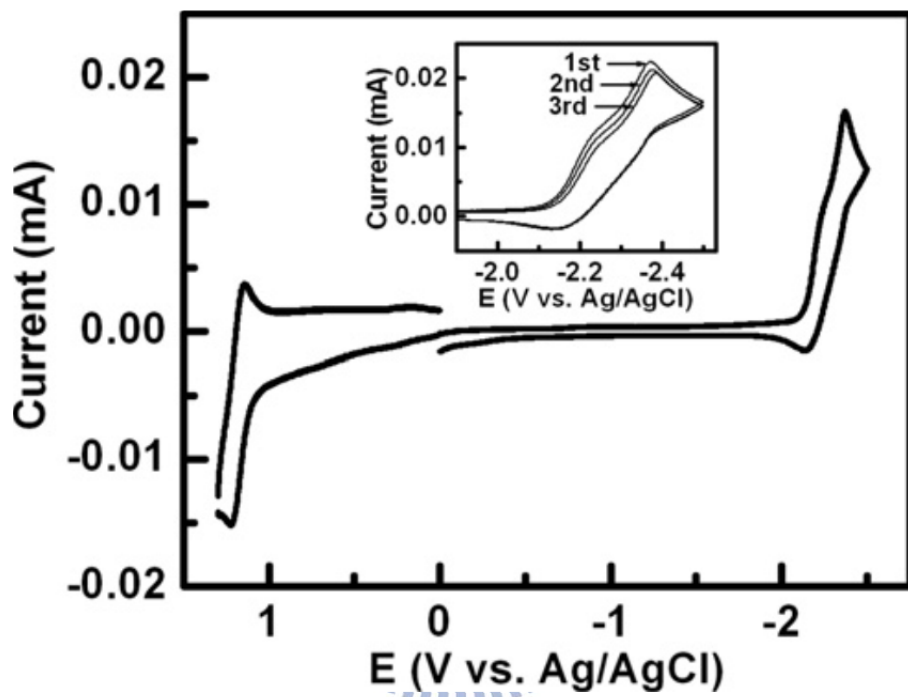


Figure 3-1 Cyclic voltammogram of compound **1**. All potentials were recorded versus Ag/AgCl (saturated) as a reference electrode.

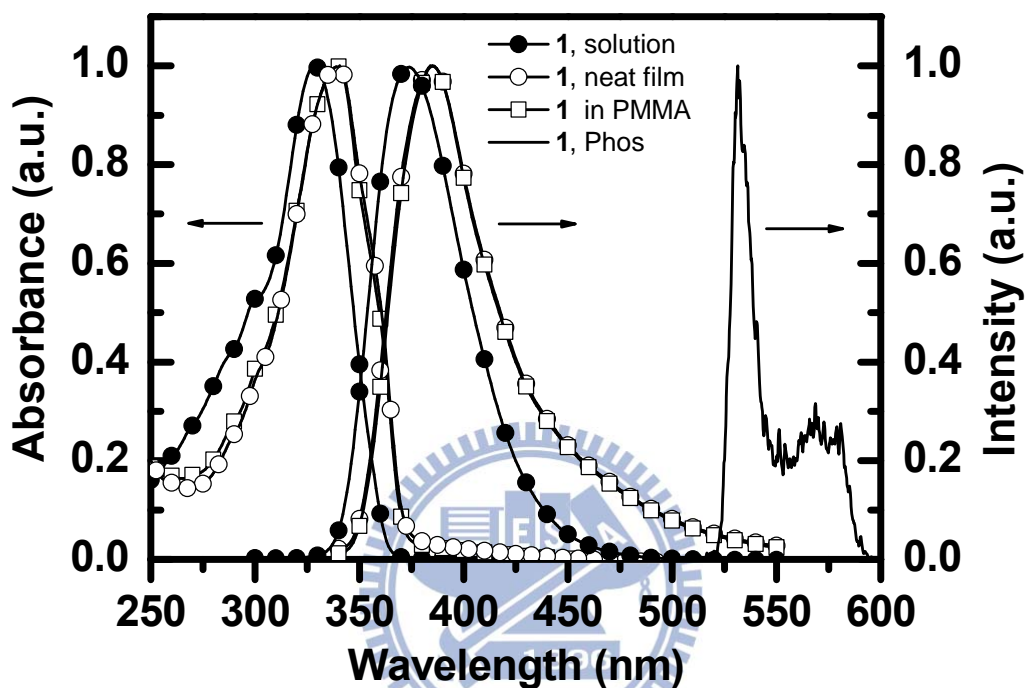


Figure 3-2 Absorption (left-hand axis) and PL (right-hand axis) spectra of 1 in acetonitrile solution (10^{-5} M) and in neat film or dispersed in PMMA film (10 wt%) and the phosphorescence (Phos, right-hand axis) spectrum of 1 in EtOH solutions at 77 K.

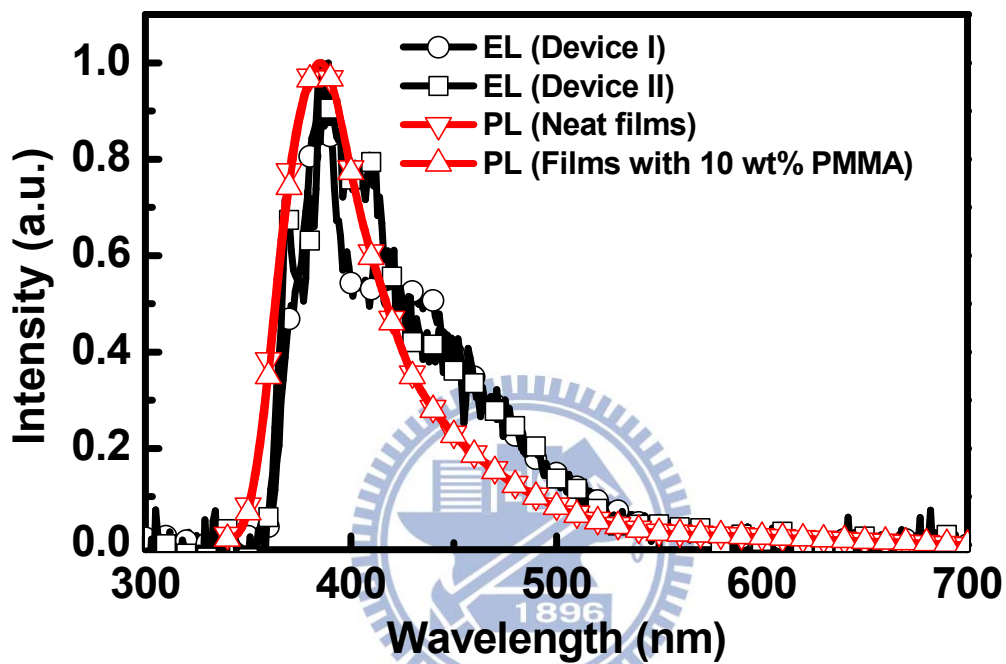


Figure 3-3 EL spectra of Device I and Device II under 4.2 V. PL spectra of the emissive layers are presented for comparison.

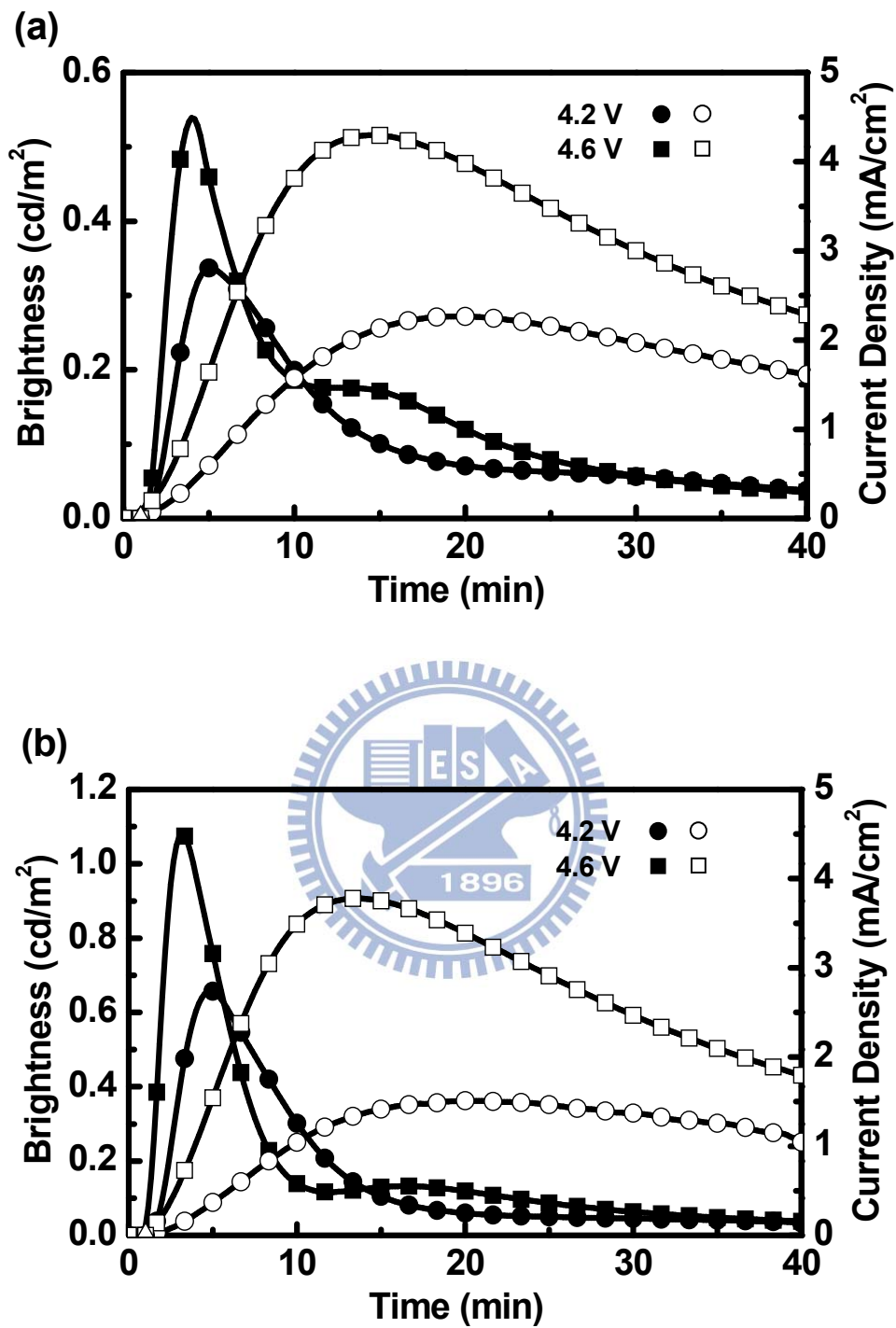


Figure 3-4 Brightness (solid symbols) and current density (open symbols) plotted with respect to time under a constant bias voltage of 4.2 and 4.6 V for (a) device I and (b) device II.

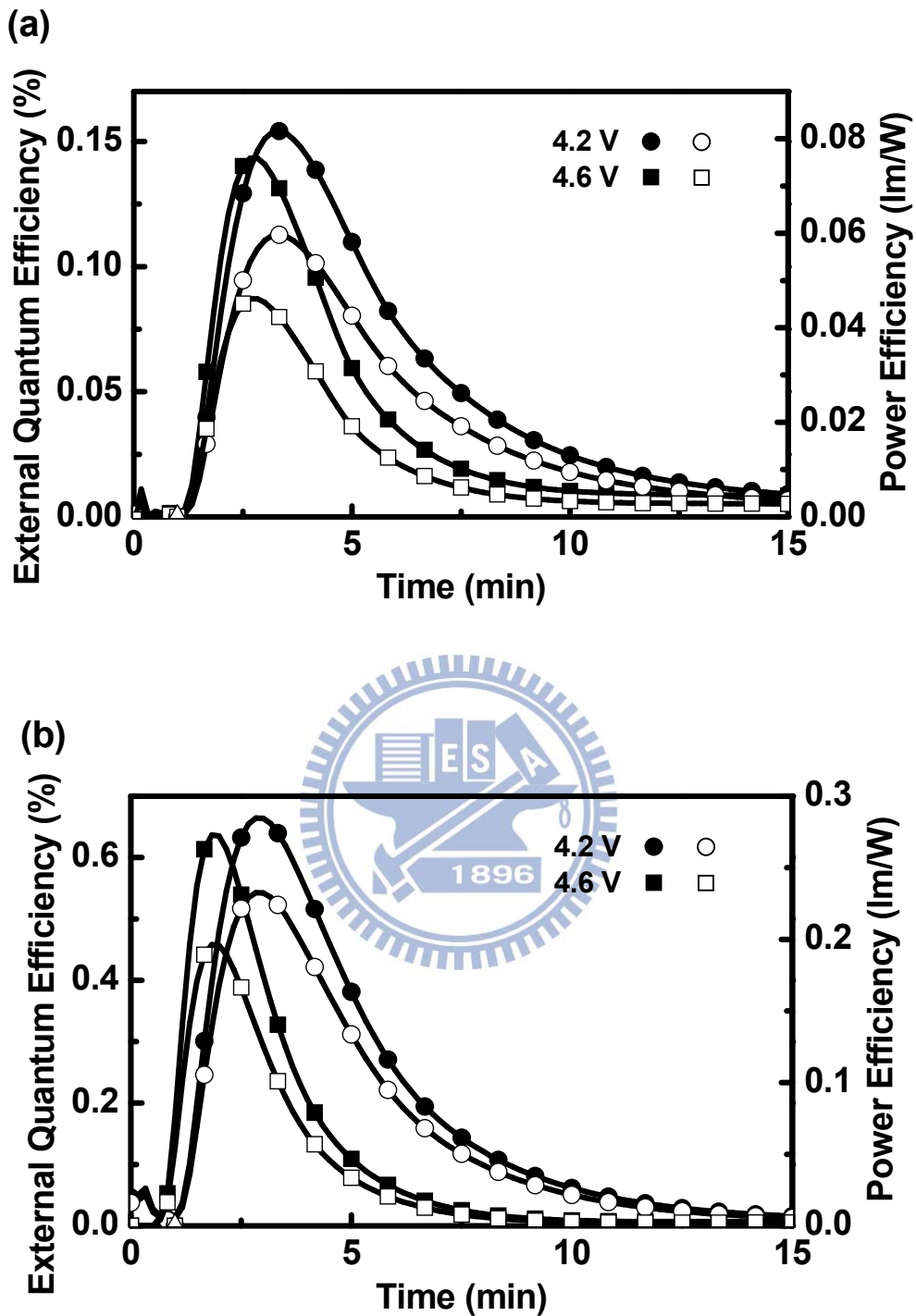


Figure 3-5 EQE (solid symbols) and power efficiency (open symbols) plotted with respect to time under a constant bias voltage of 4.2 and 4.6 V for (a) device I and (b) device II.

Chapter 4 Improving the Balance of Carrier Mobilities of Host-Guest Solid-State Light-Emitting Electrochemical Cells

4.1 Introduction

Solid-state LECs possess several advantages over conventional OLEDs. In LECs, electrochemically doped regions induced by spatially separated ions under a bias form Ohmic contacts with electrodes, giving balanced carrier injection, low operating voltages, and consequently high power efficiencies.[1,59] As such, LECs generally require only a single emissive layer, which can be easily processed from solutions and can conveniently use air-stable electrodes, while OLEDs typically require more sophisticated multilayer structures and low-work-function cathodes.[60-61] Compared with conventional polymer LECs that are usually composed of an emissive conjugated polymer, a salt and an ion-conducting polymer,[1,59] LECs based on CTMCs show several further advantages and have attracted much attention in recent years.[4-5,9-12] In such devices, no ion-conducting material is needed since these CTMCs are intrinsically ionic. Furthermore, higher EL efficiencies are expected due to the phosphorescent nature of CTMCs.

In general, LECs are composed of neat films of emissive materials, which very often suffer self-quenching induced by interactions between closely packed

molecules. Many efforts have been made to enhance device efficiencies of LECs based on CTMCs by reducing self-quenching of the emissive materials. Modifying the molecular structures, such as adding bulky substituents on ligands[14,38-39] or utilizing bulky auxiliary ligands[34] have been shown to suppress interchromophore interaction to some degree, improving device efficiencies of LECs. However, self-quenching is still significant in neat films even composed of materials with bulky molecular structures and thus limits device efficiencies. To further reduce self-quenching and increase EL efficiency, one feasible approach is to spatially disperse an emitting guest into a transporting host matrix, as previously reported for conventional OLEDs[61] and solid-state LECs.[18,23,39,62,99,119,126] Among the reported host-guest LECs, CTMCs were the most commonly used host materials and high EQE up to 10.4% photon/electron has been demonstrated in host-guest LECs based on CTMCs.[62] To optimize device efficiencies, sophisticated molecular design for CTMC-based host materials with balanced carrier mobilities is generally required to ensure the carrier recombination zone to situate at the center of the emissive layer and consequently to avoid exciton quenching near electrodes[127] in single-layered LEC devices. Nevertheless, adjusting carrier transporting characteristics of CTMCs by modifying their ligands would simultaneously alter

their energy gaps, influencing the effectiveness of energetic confinement for guest excitons when CTMCs are utilized as hosts. For instance, the neat-film PL maximum of the model compound $[\text{Ir}(\text{ppy})_2(\text{dtb-bpy})]^+(\text{PF}_6^-)$ (where ppy is 2-phenylpyridine and dtb-bpy is 4,4'-di-tert-butyl-2,2'-dipyridyl) centers at 558 nm[29] while the functionalized bipolar compound with dtb-bpy replaced by 4,5-diaza-2',7'-bis(diphenylamino)-9,9'-spirobifluorene, in which the 4,5-diazafluorene and diphenylamino substituents act as electron and hole transporting moieties, respectively, exhibits significant bathochromic shift in neat-film PL (maximum at 638 nm).[26] Such reduced energy gap would impede functionalized bipolar CTMCs to be used as host materials for guest materials emitting in the visible region. Furthermore, utilizing expensive phosphorescent CTMCs containing rare metals as host materials, which require a vast amount of material usage to form the emissive layer, increases the fabrication costs of LECs.

Compared with CTMC-based hosts, relatively inexpensive fluorescent polymers[70] and small-molecule materials[104] are feasible for independent tailoring of carrier transporting properties and energy gaps and thus would be more suitable for use as host materials in LECs. Host-guest phosphorescent LECs based on poly[9,9-bis(3,6-dioxaheptyl)-fluorene-2,7-diyl] (BDOH-PF)[54]

as the host and a red-emitting iridium complex bis[2-(2'-benzothienyl)-pyridinato-N,C^{3'}]iridium(acetylacetonate) [Btp₂Ir(acac)] as the guest has been reported.[126] The host-only (BDOH-PF) LEC devices showed a high EQE up to 4%, which approaches the upper limit that one would expect from the PLQY of the neat host films (0.73) when considering spin statistics ~25% for singlet excitons and an optical out-coupling efficiency of ~20% from a typical layered light-emitting device structure, suggesting balanced carrier mobilities in BDOH-PF neat films.[70] However, the maximum power efficiency (1 lm/W) of the host-guest LECs based on BDOH-PF doped with [Btp₂Ir(acac)][126] was much lower than that obtained in [Btp₂Ir(acac)] doped OLEDs (4.6 lm/W),[128] in which multilayered structures were utilized to confine excitons in the emissive layer sandwiched between electron and hole transporting layers and thus to prevent exciton quenching near electrodes. These results reveal that when doped with guest, balance of carrier mobilities of host films would deteriorate due to carrier trapping induced by the offset in energy levels between the host and the guest and the carrier recombination zone would consequently move to the proximity of electrodes, leading to exciton quenching and thus reduced device efficiencies. Hence, to optimize the device efficiencies of the host-guest LECs, balancing carrier mobilities of the emissive layer to

keep the carrier recombination zone away from electrodes would be a critical issue. In this work, we demonstrate improving balance of carrier mobilities in host-guest LECs utilizing a cationic terfluorene derivative as the host and a red-emitting CTMC as the guest. Carrier trapping induced by the energy offset in the LUMO levels between the host and the guest impedes electron transport in the host-guest films and thus improves balance of carrier mobilities of the host films intrinsically exhibiting electron preferred transporting characteristics. PL measurements show efficient energy transfer in this host-guest system and thus ensure predominant guest emission at low guest concentrations, rendering significantly reduced self-quenching of guest molecules. EL measurements show that the peak EQE (power efficiency) of the host-guest LECs reaches 3.62% (7.36 lm/W), which approaches the upper limit that one would expect from the PLQY of the emissive layer (~ 0.2) and an optical out-coupling efficiency of $\sim 20\%$ and consequently indicates superior balance of carrier mobilities in such host-guest emissive layer. These results are among the highest reported for red-emitting LECs[18,22,24,38,57,119,121] and thus confirm that in addition to reducing self-quenching of guest molecules, the strategy of utilizing a carrier transporting host doped with a proper carrier trapping guest would improve balance of carrier mobilities in the host-guest emissive layer, offering an

effective approach for optimizing device efficiencies of LECs.

4.2 Materials and Experimental Methods

Materials

Molecular structures of the host and guest materials used in this study are shown in Fig. 4-1. All compounds were synthesized according to the procedures reported in the literatures.[23,104] The cationic terfluorene derivative (**1**) reported recently by Chen *et al.* to be used in saturated deep-blue-emitting LECs was used as the host.[104] Compound **1** in dilute solutions possesses PL emission wavelengths in the deep-blue region with a high PLQY close to unity.[104] The PLQY of **1** in the form of neat films remained high (up to 0.76) despite the presence of intermolecular interactions.[104] More importantly, the addition of the ionic liquid [BMIM⁺][PF₆⁻], which provides additional mobile ions in the emissive layer to fasten the device response, in the neat film did not affect the emission properties of **1**. [104] Thus, it would be suitable for use as the host material in host-guest LECs. [Ir(ppy)₂(biq)]⁺(PF₆⁻) (**2**) (where biq is 2,2'-biquinoline), which was used as the red-emitting complex in white LECs reported by Su *et al.*,[30] was utilized as the red-emitting guest. Complex **2** exhibits saturated red PL emission in both solutions and neat films and thus suitable for use as the red-emitting guest in host-guest LECs.

Experimental Methods

Thin films for PL studies were spin-coated at 3000 rpm onto quartz substrates using mixed solutions (in acetonitrile) of various ratios. Since in LECs, an ionic liquid [BMIM⁺][PF₆⁻] of 10 wt.% was added to provide additional mobile ions and to shorten the device response time,^[16] photophysical properties of the [BMIM⁺][PF₆⁻] blended host-guest films were characterized. The mass ratio of solute component [1:2: [BMIM⁺][PF₆⁻]] in acetonitrile solutions for spin coating of the host-guest films containing x wt.% guest is (90-x):x:10. The thickness of each spin-coated film was ca. 200 nm, as measured using profilometry. The concentrations of all solutions for spin coating are 80 mg/mL. UV-Vis absorption spectra were recorded using a Hitachi U2800A spectrophotometer. PL spectra were recorded using a Hitachi F9500 fluorescence spectrophotometer. PLQYs for thin-film samples were determined using a calibrated integrating sphere system (Hamamatsu C9920).

ITO-coated glass substrates were cleaned and treated with UV/ozone prior to use. A PEDOT:PSS layer was spin-coated at 4000 rpm onto the ITO substrate in air and baked at 150 °C for 30 min. The emissive layer (~200 nm, as measured by profilometry) was then spin-coated at 3000 rpm from the acetonitrile solutions under ambient conditions. To reduce the turn-on time of the LEC

device, the ionic liquid [BMIM⁺(PF₆)⁻] (10 wt.% for the host-guest devices and 20 wt.% for the guest-only devices) was added to enhance the ionic conductivity of thin films.[84] The mass ratio of solute component and the concentrations of solutions for spin coating of the emissive layers were the same as that used for spin coating of the host-guest films for PL studies described above. After spin coating, the thin films were then baked at 70 °C for 10 hours in a nitrogen glove box (oxygen and moisture levels below 1 ppm), followed by thermal evaporation of a 100-nm Al top contact in a vacuum chamber (~10⁻⁶ torr). The electrical and emission characteristics of LEC devices were measured using a source-measurement unit and a Si photodiode calibrated with the Photo Research PR-650 spectroradiometer. All device measurements were performed under a constant bias voltage (3.0, 3.2 and 3.4 V) in a nitrogen glove box. The EL spectra were taken with a calibrated CCD spectrograph.

4.3 Results and Discussion

4.3.1 Photoluminescent Studies of the Host-Guest System

PL spectra of the neat host and guest films are shown in Fig. 4-2. Neat films of the high-gap host (1) exhibit deep-blue fluorescent PL centered at 418 nm and yellow phosphorescent PL centered at 562 nm (the inset of Fig. 4-2, measured at 77 K), corresponding to a triplet energy of 2.21 eV. Neat films of

the guest (**2**) show saturated red phosphorescent PL emission centered at 662 nm, which is equal to a triplet energy of 1.87 eV. Therefore, the triplet level of the host is higher than that of the guest and thus triplet-triplet back energy transfer from guest to host can be prevented, eliminating a potential path way of energy loss in a host-guest system.[129] The absorption spectrum of the guest neat films is also shown in Fig. 4-2. Since the absorption spectrum of the guest and the PL spectrum of the host exhibit considerable spectral overlap, efficient host-guest energy transfer is expected (calculated Förster radius ca. 3 nm for this host-guest system) and thus the guest emission could dominate PL at low guest concentrations, resulting in significantly reduced self-quenching of guest molecules.

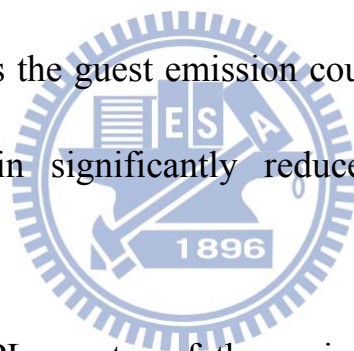


Fig. 4-3 depicts the PL spectra of the emissive layers of the host-guest LECs, i.e. the host-guest films containing various guest concentrations and [BMIM⁺][PF₆⁻] (10 wt.%). The ionic liquid [BMIM⁺][PF₆⁻] was added to provide additional mobile ions and to shorten the device response time.[84] Addition of [BMIM⁺][PF₆⁻] (10 wt.%) has been reported not to affect the PL emission properties of the neat host films.[104] With the increase of the guest concentration, the relative intensity of the guest emission with respect to the residual host emission is larger due to a higher host-guest energy transfer rate at

a higher guest concentration. It is noted that the PL emissions of the guest at low concentrations (0.5~2.0 wt.%, Fig. 4-3) center at ca. 610 nm and exhibit significant blue shift ca. 50 nm as compared to those of the neat guest films (Fig. 4-2), indicating reduced intermolecular interactions of dispersed guest molecules in a host matrix. PLQYs of the host-guest films containing various guest concentrations and [BMIM⁺][PF₆⁻] (10 wt.%) are shown in the inset of Fig. 4-3. PLQYs of the host-guest films decrease as the guest concentration increases from 0 to 2 wt.% since the guest emission, which exhibits a lower PLQY than the host emission, dominates PL emission at relatively higher guest concentrations. At the guest concentration of 2 wt.%, most PL emission (ca. 90%) of the host-guest films comes from the guest and the PLQY of the host-guest films is 0.2, which is comparable with that of the guest in dilute (10⁻⁵ M) dichloromethane solutions.[23] Thus, the PLQY of the guest molecules dispersed at low concentrations in the host films would be estimated to be ~0.2. Such PLQY is much higher as compared with that of the neat guest films (0.09)[23] and thus confirms significantly reduced self-quenching of guest molecules dispersed in the host matrix.

4.3.2 EL characteristics of the Host-Guest LECs

To clarify the EL properties of the host-guest system, EL characteristics of

host-guest LECs containing various guest concentrations were measured and are summarized in Table 4-1. The host-guest LECs have the structure of ITO/PEDOT:PSS (30 nm)/emissive layer (200 nm)/Al (100 nm), where the emissive layer contains [host (89.5 wt.%), guest (0.5 wt.%) and [BMIM⁺][PF₆⁻] (10 wt.%) for **Device I**, [host (89.0 wt.%), guest (1.0 wt.%) and [BMIM⁺][PF₆⁻] (10 wt.%) for **Device II**, [host (88.0 wt.%), guest (2.0 wt.%) and [BMIM⁺][PF₆⁻] (10 wt.%) for **Device III** and [host (0.0 wt.%), guest (80.0 wt.%) and [BMIM⁺][PF₆⁻] (20 wt.%) for **Device IV**. The ionic liquid [BMIM⁺][PF₆⁻] was added to provide additional mobile ions and to shorten the device response time.[84] The EL spectra of the host-guest LECs with various guest concentrations under 3 V are shown in Fig. 4-4. The host-guest LECs with guest concentrations of 0.5~2.0 wt.% exhibited similar saturated red EL spectra with a Commission Internationale de l'Eclairage (CIE)[80] coordinate of (0.62, 0.37). The EL spectra resemble the guest emission in the PL spectra of the corresponding host-guest emissive layers (Fig. 4-3), indicating similar emission mechanisms. However, the residual host emissions appeared in the PL spectra of the host-guest films are absent in the EL spectra of the host-guest LECs. These results could be understood by energy level alignments of the host and guest molecules (estimated by cyclic voltammetry)[23,104] depicted in the inset of

Fig. 4-4. For host-guest LECs, electrochemically doped regions of the emissive layer result in ohmic contact with metal electrodes and consequently facilitate carrier injection onto both the host and the guest. Hence, both exciton formation on the host followed by host-guest energy transfer and direct exciton formation on the guest induced by charge trapping contribute to the guest emission. At lower biases, such energy level alignments favor electron injection and trapping on the smaller-gap guest, resulting in direct carrier recombination/exciton formation on the guest (rather than host-guest energy transfer). Thus, compared with the PL spectra (Fig. 4-3), the EL spectra (Fig. 4-4) are independent on the guest concentration and exhibit predominant guest emission even at a low guest concentration of 0.5 wt.%.

The host-guest LECs with various guest concentrations exhibited similar time-dependent EL characteristics under constant-bias operation. Fig. 4-5(a) shows the time-dependent brightness and current density under constant biases of 3.0~3.4 V for **Device I**. After the bias was applied, the current first increased and then stayed rather constant. On the other hand, the brightness first increased with the current and reached the maxima of 0.13, 0.57 and 2.77 cd/m² under biases of 3.0, 3.2 and 3.4 V, respectively. The brightness then dropped with time with a rate depending on the bias voltage (or current). Corresponding

time-dependent EQEs and power efficiencies of the same device are shown in Fig. 4-5(b). When a forward bias was just applied, the EQE was rather low due to poor carrier injection. During the formation of the p- and n-type regions near electrodes, the capability of carrier injection was improved and the EQE thus rose rapidly. The peak EQE (peak power efficiency) at 3.0, 3.2 and 3.4 V are 3.62% (7.36 lm/W), 2.99% (3.33 lm/W) and 2.13% (2.81 lm/W), respectively. The drop of efficiency and brightness after reaching the peak value, as commonly seen in solid-state LECs, may be associated with a few factors. Before the device current reaches a steady value, the carrier recombination zone may keep moving closer to one electrode due to discrepancy in electron and hole mobilities, which would induce exciton quenching. Further, the decrease in brightness and efficiency under a constant bias may be rationally attributed to the degradation of the emissive material during the LEC operation.[45]

For comparison, time-dependent brightness/current density and EQE/power efficiency of the guest-only LECs (**Device IV**) are shown in Fig. 4-6(a) and Fig. 4-6(b), respectively. The guest-only (Fig. 4-6(a)) and the host-guest LECs (Fig. 4-5(a)) exhibited similar characteristics in time-dependent brightness and current density. However, much larger current densities were measured in the guest-only devices even at significantly lower biases due to the lower electrochemical band

gap of the guest complex **2**. The peak EQE (peak power efficiency) of the guest-only devices at 2.3 V is 0.38% (0.44 lm/W), which is much lower than that of the host-guest LECs (Table 4-1). Further reducing the bias voltage (2.2 V) leads to an even lower EQE (0.04%). As revealed in previous studies,[118] as bias voltage decreases, the width of the intrinsic layer between the p- and n-type doped layers extends due to shrinking of the doped layers, resulting in reduced electric field in the recombination zone. Thus, reduced device efficiency under a lower bias may be attributed to deteriorated balance of carrier mobilities caused by field-dependent electron and hole mobilities.

Peak EQEs and peak power efficiencies (at current densities <0.003 mA/cm²) of the host-guest LECs with various guest concentrations are shown in Fig. 4-7. All LEC devices contain 10 wt.% [BMIM⁺][PF₆⁻] in the emissive layer. The peak device efficiency first increases then decreases as the guest concentration increases from 0 to 90 wt.%. The fluorescent host-only [mass ratio of host:guest: [BMIM⁺][PF₆⁻] = 90:0:10] devices show an EQE ~1%, which is much lower than that one would expect (3.8%) from the PLQY of the neat host films (0.76)[104] when considering spin statistics ~25% for singlet excitons and an optical out-coupling efficiency of ~20% from a layered structure. Since the electrochemically doped regions near electrodes of LECs ensure balanced

carrier injection,[59] such lowered device efficiency would be attributed to imperfect balance of carrier mobilities in the host films. As the carrier injection at both electrodes are becoming balanced, the carrier recombination zone may consequently locate near one of the electrodes due to discrepancy in electron and hole mobilities of the emissive layer. The recombination zone in the vicinity of an electrode may cause exciton quenching such that the EQE of the device would decrease. Terfluorene derivatives with alkyl substitutions on the tetrahedral C9 carbon have been reported to exhibit higher electron mobilities than hole mobilities.[130] Furthermore, imidazole moieties, which are tethered at the ends of the alkyl chains on **1**, have been used in electron transporting materials for OLEDs.[131] Therefore, electron preferred transporting characteristics of **1** would rationally be responsible for lowered device efficiencies of the host-only devices. The schematic diagram of the position of exciton recombination zone for the host-only device is shown in Fig. 4-8(a). Since electron mobility is higher than hole mobility in the host, the exciton recombination zone would locate near the anode and thus exciton quenching occurs, deteriorating device efficiency. However, with a guest concentration of 0.5 wt.%, the peak EQE (peak power efficiency) of the host-guest LECs reach 3.62% (7.36 lm/W), which is among the highest reported for red-emitting LECs.[18,22,24,38,57,119,121] It

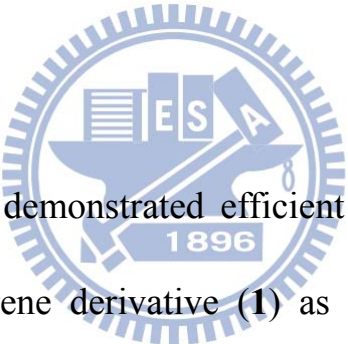
is noted that such an EQE approximately approaches the upper limit (~4%) that one would expect from the PLQY of the guest dispersed at low concentrations in host films (~0.2), when considering spin statistics ~100% (both singlet and triplet excitons can be harvested for a CTMC) and an optical outcoupling efficiency of ~20% from a typical layered light-emitting device structure. This result implies superior balance of carrier mobilities of the host-guest films with a guest concentration of 0.5 wt.%. As shown in the inset of Fig. 4-4, balance of carrier mobilities would be significantly altered in the host-guest films due to the large energy offset (1.32 eV) in the LUMO levels between the host and the guest molecules. Electron trapping induced by the host-guest energy offset in the LUMO levels would reduce the electron mobility while the hole mobility would remain relatively unchanged due to similar energies in the HOMO levels of the host and the guest molecules. Since the host intrinsically possesses electron preferred transporting characteristics, balance of carrier mobilities would be improved in the host-guest devices doped with an electron-trapping guest at a proper concentration. As shown in Fig. 4-8(b), the exciton recombination zone of the host-guest LECs with a guest concentration of 0.5 wt.% would be pushed toward the center of the emissive layer due to reduced electron mobility. Thus, exciton quenching would be effectively eliminated, leading to high device

efficiency. However, over-doping of the electron-trapping guest would further impede electron transporting and consequently would result in higher hole mobility than electron mobility, deteriorating balance of carrier mobilities of the host-guest films as well. Thus, with a guest concentration higher than 0.5 wt.%, the device efficiency of the host-guest devices decreases as the guest concentration further increases (Fig. 4-7). As shown in Fig. 4-8(c), the exciton recombination zone of the host-guest LECs with a guest concentration of 2.0 wt.% would be pushed to the proximity of cathode due to reduced electron mobility. Exciton quenching occurs again and the device efficiency is consequently low.

On the other hand, the guest-only [mass ratio of host:guest: [BMIM⁺][PF₆⁻] = 0:80:20] LECs under a low bias voltage of 2.3 V exhibit a low EQE of 0.38%, which is approximately an order of magnitude lower than that achieved in the host-guest LECs doped with 0.5 wt.% guest. However, the estimated upper limit of EQE of the guest-only LECs from the PLQY of the neat guest films (0.09)[23] when considering an optical out-coupling efficiency ~20% should reach ca. 1.8%. Thus, the low EQE obtained in the guest-only devices may be attributed to poor balance of carrier mobilities of the neat guest films. Except for a few reported LECs based on materials with balanced carrier mobilities,[34,70,125]

in which only PLQY of the emissive layer and optical outcoupling efficiency of layered device structure limits the device efficiency, balance of carrier mobilities in single-layered LECs is a common bottleneck in optimizing device efficiencies. The research results of this work confirm that in addition to reducing self-quenching of guest molecules as revealed in previous reports,[62,119,126] the strategy of utilizing a carrier transporting host doped with a proper carrier trapping guest would also improve balance of carrier mobilities of the emissive layer and thus would be effective in optimizing device efficiencies of LECs.

4.4 Summary



In summary, we have demonstrated efficient host-guest solid-state LECs utilizing a cationic terfluorene derivative (**1**) as the host and a red-emitting CTMC $[\text{Ir}(\text{ppy})_2(\text{biq})]^+(\text{PF}_6^-)$ as the guest (**2**). Carrier trapping induced by the offset in the LUMO levels between the host and the guest impedes electron transport in the host-guest films and thus improves balance of carrier mobilities of the host films intrinsically exhibiting electron preferred transporting characteristics. PL measurements show efficient host-guest energy transfer in this host-guest system and thus ensure predominant guest emission at low guest concentrations, rendering significantly reduced self-quenching of guest molecules. EL measurements show that the peak EQE (power efficiency) of the

host-guest LECs reaches 3.62% (7.36 lm/W), which approaches the upper limit that one would expect from the PLQY of the emissive layer (~ 0.2) and an optical out-coupling efficiency of $\sim 20\%$ and consequently indicates superior balance of carrier mobilities in such host-guest emissive layer. These results are among the highest reported for red-emitting LECs and thus confirm that in addition to reducing self-quenching of guest molecules, the strategy of utilizing a carrier transporting host doped with a proper carrier trapping guest would improve balance of carrier mobilities in the host-guest emissive layer, offering an effective approach for optimizing device efficiencies of LECs.



Table 4-1 Summary of the host-guest LEC device characteristics.

Device (guest concentration)	Bias (V)	t_{\max} (min) ^a	L_{\max} (cd m^{-2}) ^b	$\eta_{\text{ext, max}}$ (%) ^c	$\eta_{\text{p, max}}$ (lm W^{-1}) ^d	Lifetime (min) ^e
I (0.5 wt.%)	3.0 V	97	0.13	3.62	7.36	527 ^f
	3.2 V	33	0.57	2.99	3.33	248
	3.4 V	11	2.77	2.13	2.81	46
II (1.0 wt.%)	3.0 V	132	0.04	2.37	3.25	539 ^f
	3.2 V	78	0.59	1.74	2.15	245
	3.4 V	13	4.70	1.37	1.73	37
III (2.0 wt.%)	3.0 V	131	0.02	1.01	1.18	617 ^f
	3.2 V	114	0.38	0.98	1.14	399
	3.4 V	40	3.05	0.70	0.77	102
IV (80.0 wt.%) ^g	2.2 V	600	1.09	0.04	0.05	— ^h
	2.3 V	349	13.6	0.38	0.44	1221 ^f

[a] Time required to reach the maximal brightness. [b] Maximal brightness achieved at a constant bias voltage. [c] Maximal external quantum efficiency achieved at a constant bias voltage. [d] Maximal power efficiency achieved at a constant bias voltage. [e] The time for the brightness of the device to decay from the maximum to half of the maximum under a constant bias voltage. [f] Extrapolated. [g] Guest-only device [mass ratio of host:guest:BMIM⁺(PF₆⁻) = 0:80:20]. [h] Extrapolation can not be performed since brightness have not yet decreased after 10-hr continuous operation.

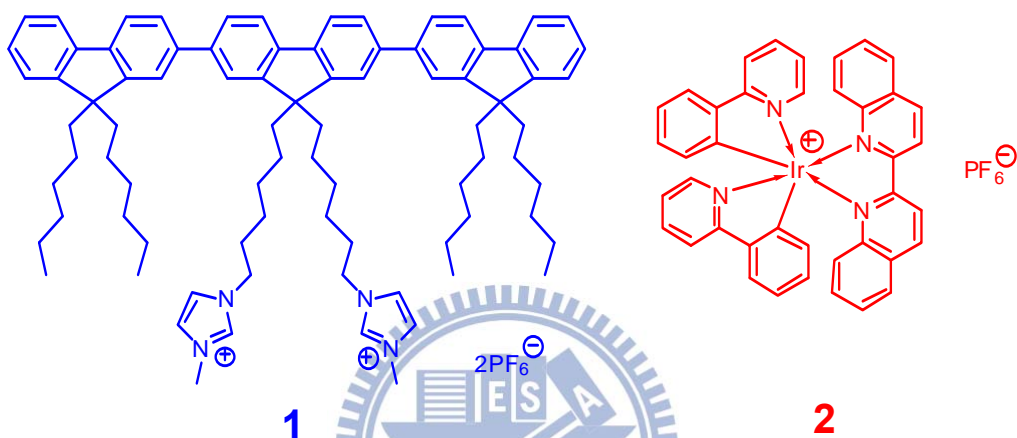


Figure 4-1 Molecular structures of the host molecule, cationic terfluorene derivative (**1**) and the guest molecule, $[\text{Ir}(\text{ppy})_2(\text{biq})]^+(\text{PF}_6^-)$ (**2**).

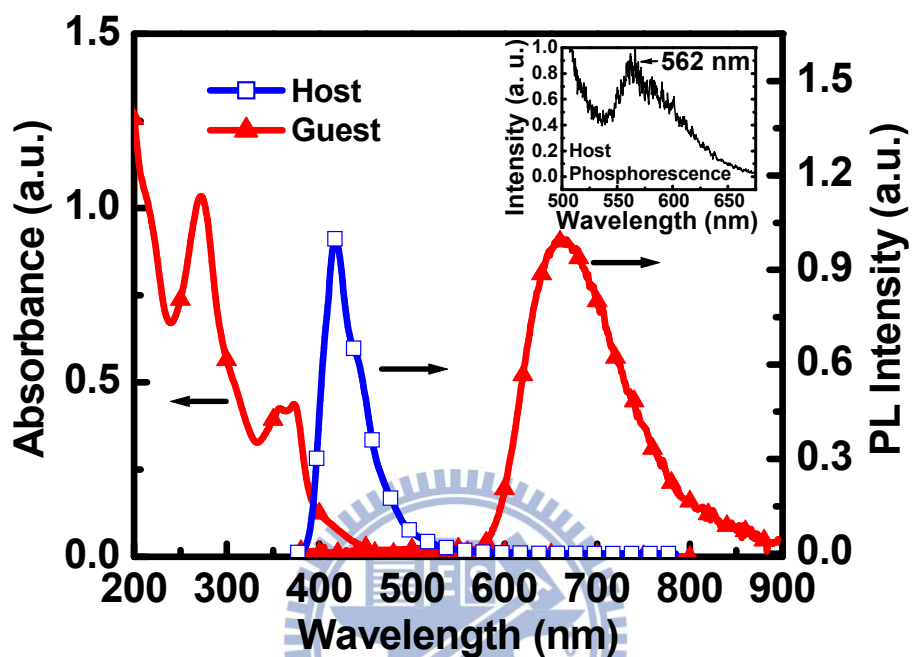


Figure 4-2 Absorption spectrum of the neat guest films and PL spectra of the neat host and guest films. Inset: phosphorescence spectrum of the neat host films measured at 77 K.

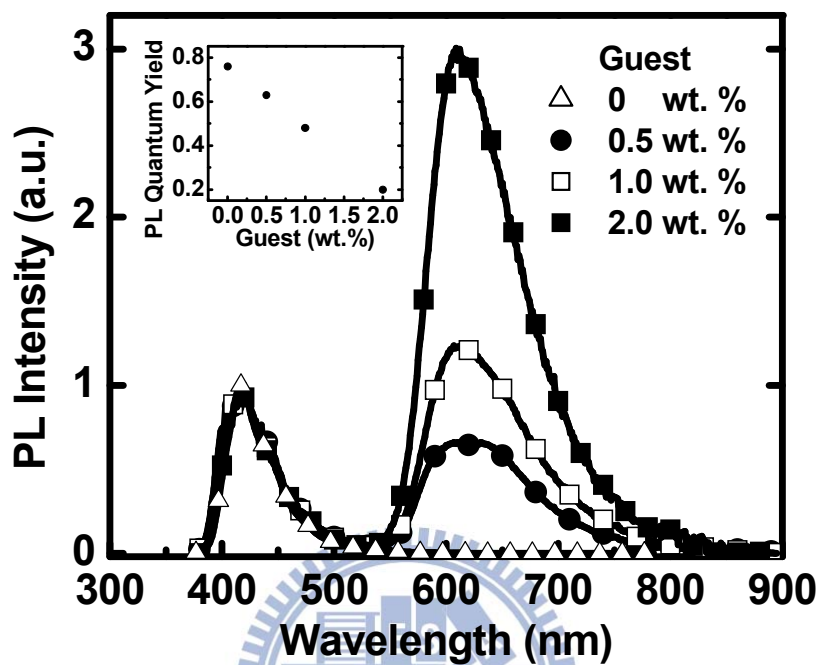


Figure 4-3 PL spectra of the host-guest films containing various guest concentrations and [BMIM⁺][PF₆⁻] (10 wt.%). Inset: photoluminescence quantum yields vs guest concentrations of the same films.

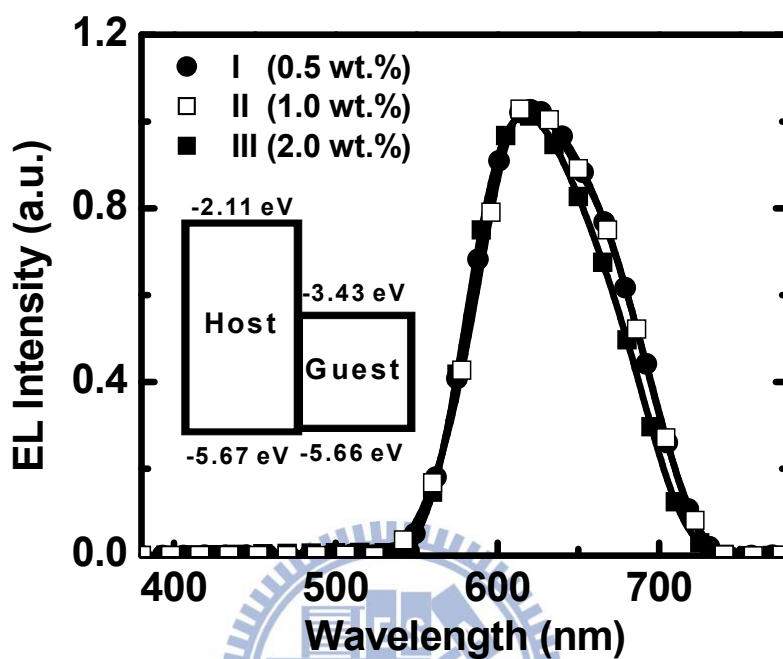


Figure 4-4 EL spectra (at 3.0 V) for the host-guest LECs with various guest concentrations and [BMIM⁺][PF₆⁻] (10 wt.%). Inset: the energy level diagram of the host and guest molecules.

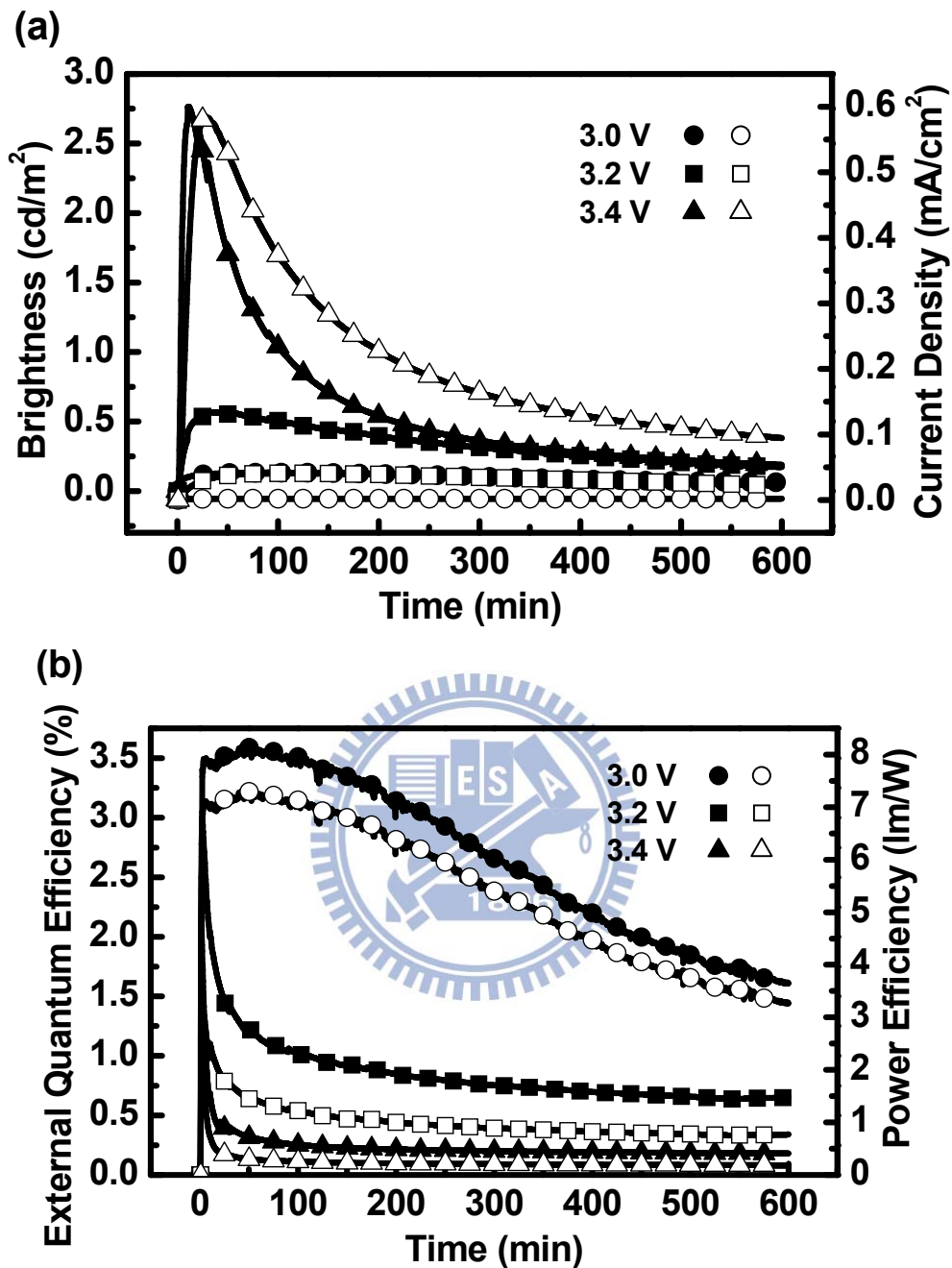


Figure 4-5 (a) Brightness (solid symbols) and current density (open symbols) and (b) external quantum efficiency (solid symbols) and power efficiency (open symbols) as a function of time under a constant bias voltage of 3.0–3.4 V for Device I.

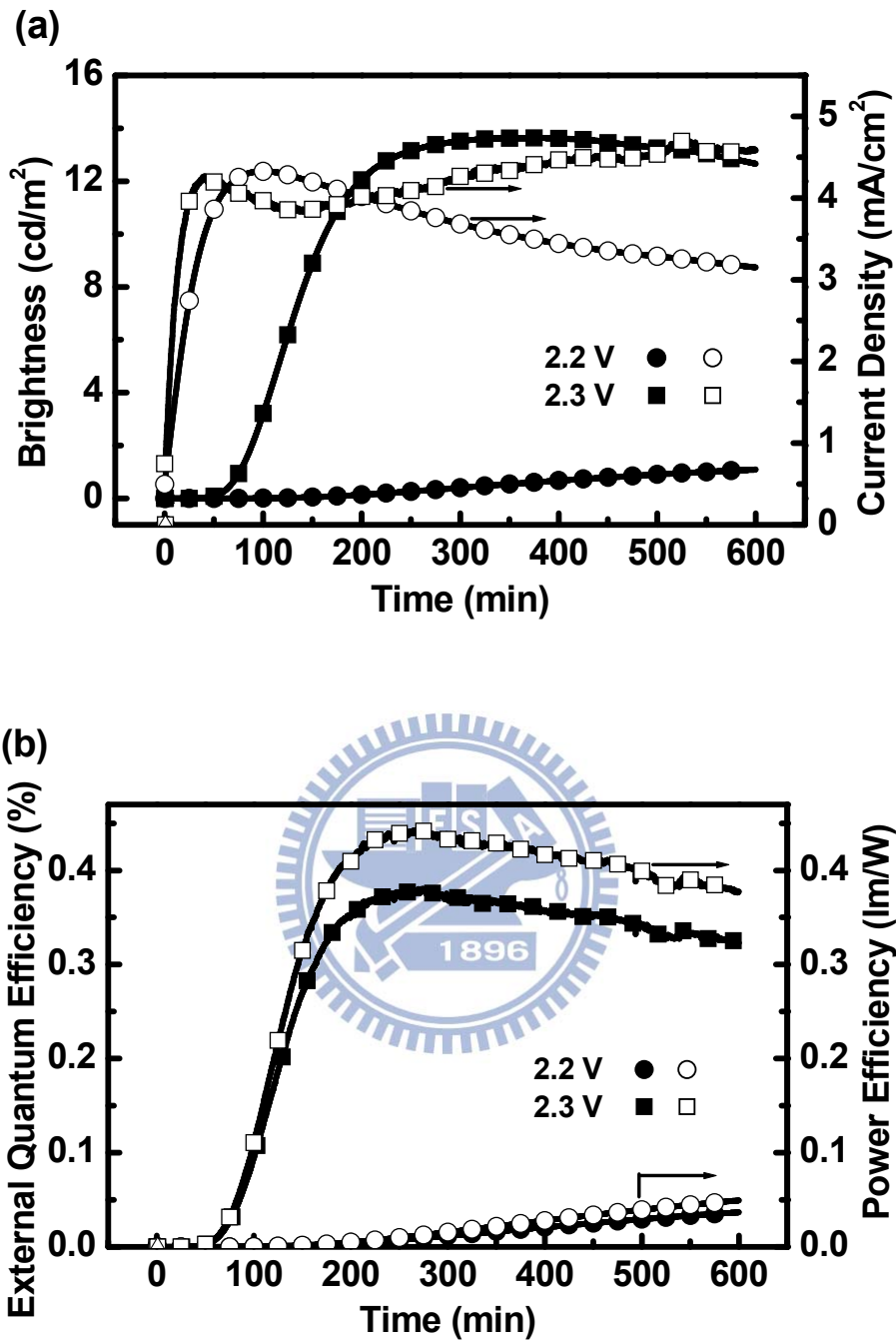


Figure 4-6 (a) Brightness (solid symbols) and current density (open symbols) and (b) external quantum efficiency (solid symbols) and power efficiency (open symbols) as a function of time under a constant bias voltage of 2.2–2.3 V for Device IV.

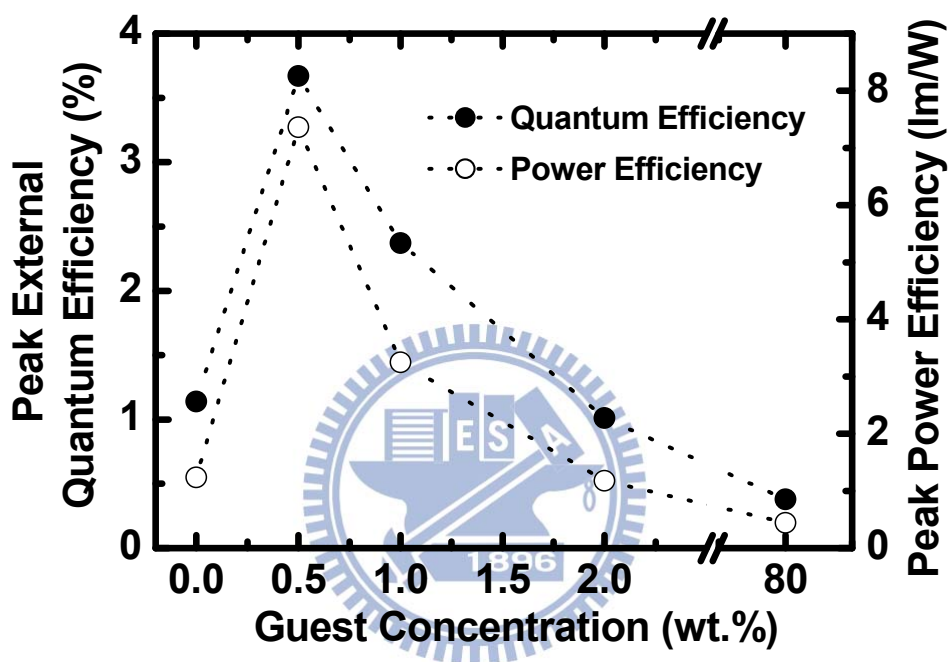


Figure 4-7 Peak external quantum efficiencies and peak power efficiencies (at current densities $<0.003 \text{ mA cm}^{-2}$) of the host-guest LECs as a function of the guest concentration.

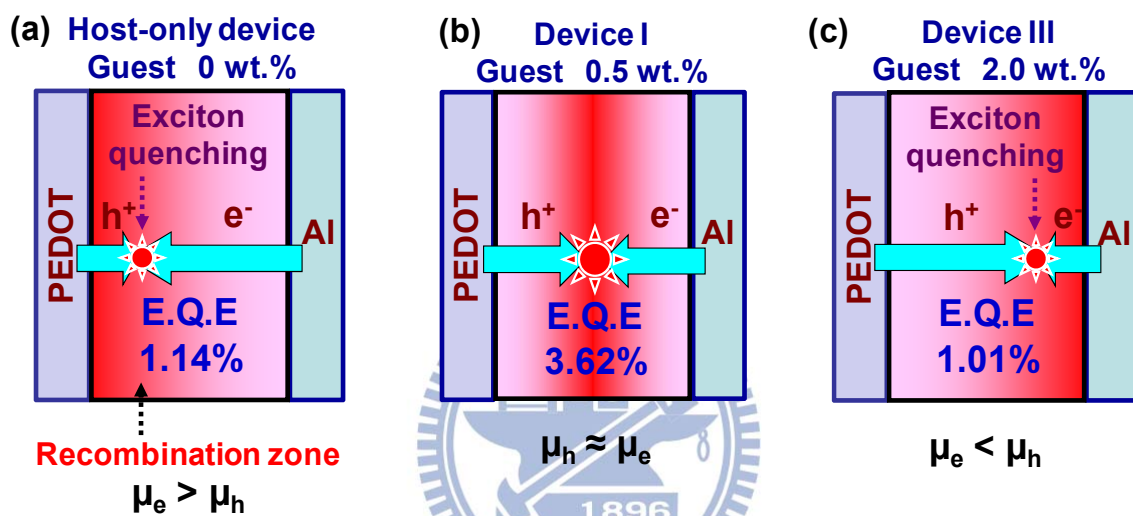


Figure 4-8 Schematic diagrams of the position of exciton recombination zone for (a) host-only device, (b) **Device I** and (c) **Device III**. Electrochemically doped regions near electrodes are omitted for clarity.

Chapter 5 Tailoring Balance of Carrier Mobilities in Solid-State Light-Emitting Electrochemical Cells by Doping A Carrier Trapper to Enhance Device Efficiencies

5.1 Introduction

Solid-state LECs possess several advantages over conventional OLEDs. In LECs, electrochemically doped regions induced by spatially separated ions under a bias form ohmic contacts with electrodes, giving balanced carrier injection, low operating voltages, and consequently high power efficiencies.[1,59]

As such, LECs generally require only a single emissive layer, which can be easily processed from solutions,[132-134] and can conveniently use air-stable electrodes, while OLEDs typically require more sophisticated multilayer structures and low-work-function cathodes.[60-61,135-137] Compared with conventional polymer LECs that are usually composed of an emissive conjugated polymer, a salt and an ion-conducting polymer,[1,59] LECs based on CTMCs show several further advantages and have attracted much attention in recent years.[11-14,138-142] In such devices, no ion-conducting material is needed since these CTMCs are intrinsically ionic. Furthermore, higher EL efficiencies are expected due to the phosphorescent nature of CTMCs.

In general, CTMC-based LECs are composed of neat films of emissive materials.[11-14,138-142] Since the electrochemically doped regions form ohmic contacts with electrodes, the carrier injection at both electrodes is balanced and the carrier recombination zone may consequently locate near one of the electrodes due to a discrepancy in electron and hole mobilities of the emissive layer. The recombination zone in the vicinity of an electrode may cause exciton quenching such that the device efficiency would decrease.[127] Balanced electron and hole mobilities would be beneficial in keeping the recombination zone near the center of the emissive layer and thus would prevent exciton quenching. However, only a few reports successfully demonstrated perfect EQEs of CTMC-based LECs reaching the upper limits estimated from the PLQYs of the emissive layers and an optical out-coupling efficiency of ~20% from a typical layered lightemitting device structure.[34,122,125] Most reported LECs commonly suffered deteriorated device efficiencies due to the intrinsically imperfect balance of carrier mobilities in the neat-film emissive layers. Hence, to generally optimize the device efficiencies of neat-film LECs based on CTMCs, tailoring the balance of carrier mobilities in the emissive layer to keep the carrier recombination zone away from electrodes would be a critical issue.

Sophisticated design of carrier transporting substituents on CTMCs or introducing proper carrier trappers into the neat-film CTMC emissive layers would be two possible ways to alter carrier mobilities and thus to improve the balance of carrier mobilities. The former method could be implemented by modifying ligands of efficient CTMCs with substituents containing electron and hole transporting moieties.[58] However, adjusting carrier transporting characteristics of CTMCs by modifying their ligands would simultaneously alter their energy gaps and PLQYs, influencing the EL spectra and device efficiencies of LECs.[26] It could not be a general technique for applying to all reported efficient CTMCs. On the other hand, introducing carrier trappers into neat-film CTMC emissive layers could impede carrier transport due to the energy offset in the HOMO levels or in the LUMO levels between the CTMCs and the carrier trappers. Different amounts of energy offset in the HOMO levels and in the LUMO levels between the CTMCs and the carrier trappers lead to different degrees of impeding in hole and electron transport, respectively. Therefore, the balance of carrier mobilities in CTMC-based neat-film LECs could be generally optimized by introducing carrier trappers possessing proper HOMO and LUMO levels into the emissive layers.

In this work, we demonstrate improvements in the balance of carrier

mobilities in neat-film LECs utilizing a cyan-emitting phosphorescent CTMC as the emissive material and a cationic fluorescent near-infrared (NIR) laser dye as the carrier trapper. This low-gap carrier trapper is chosen such that a significant energy offset in the HOMO levels between the CTMC and the carrier trapper impedes hole transport in the emissive layers while similar LUMO levels of these two materials result in relatively unaffected electron transport. Therefore, the balance of carrier mobilities of the neutral light-emitting layer between the p- and n-type electrochemically doped layers in CTMC neat films, which would intrinsically exhibit characteristics of preferred transport of holes, would be improved by doping such a carrier trapper. PL measurements reveal inefficient energy transfer between the CTMC and the carrier trapper due to poor spectral overlap between the CTMC emission and the carrier-trapper absorption, ensuring unapparent carrier-trapper emission and thus reducing color shift in the CTMC emission at low doping concentrations of the carrier trapper. However, even at low doping concentrations, carrier trapping would still be effective due to the large energy offset in the HOMO levels between the CTMC and the carrier trapper. EL measurements show that the peak EQE (power efficiency) of the neat-film LECs doped with the carrier trapper reaches 12.75% (28.70 lm W^{-1}), representing a 1.4 times enhancement in device efficiency as compared to

that of the undoped neat-film LECs. Such device efficiency approaches the upper limit (~15%) that one would expect from the PLQY of the emissive layer (~0.75) and an optical outcoupling efficiency of ~20% from a typical layered light-emitting device structure, consequently indicating superior balance of carrier mobilities in such doped emissive layer. These results confirm the strategy of introducing a proper carrier trapper into the CTMC neat films would improve the balance of carrier mobilities in the emissive layer, offering a general approach for optimizing device efficiencies of CTMC-based neat-film LECs.

5.2 Results and Discussion

5.2.1 Photoluminescent Studies

Molecular structures of the CTMC and the carrier trapper used in this study are shown in Fig. 5-1. The cyan-emitting CTMC $[\text{Ir}(\text{dfppz})_2(\text{dtb-bpy})]^+(\text{PF}_6^-)$ (where dfppz is 1-(2,4-difluorophenyl)pyrazole and dtb-bpy is [4,40-di(tert-butyl)-2,20-bipyridine]) reported previously by Tamayo *et al.*[22] was used as the emissive material. $[\text{Ir}(\text{dfppz})_2(\text{dtb-bpy})]^+(\text{PF}_6^-)$ was synthesized according to the procedures reported in the literature.[22] The cationic fluorescent NIR laser dye 3,30-diethyl-2,20-oxathiacarbocyanine iodide (DOTCI), which has been reported as an active material in efficient NIR dye lasers, was utilized as the carrier trapper. DOTCI was purchased from

Sigma-Aldrich Co. and was used as received. The PL spectrum of the $[\text{Ir}(\text{dfppz})_2(\text{dtb-bpy})]^+(\text{PF}_6^-)$ neat films and absorption/PL spectra of DOTCI in dilute ethanol solutions are shown in Fig. 5-2. Neat films of $[\text{Ir}(\text{dfppz})_2(\text{dtb-bpy})]^+(\text{PF}_6^-)$ exhibit cyan phosphorescent PL centered at 490 nm. Highly retained PLQY of $[\text{Ir}(\text{dfppz})_2(\text{dtb-bpy})]^+(\text{PF}_6^-)$ in neat films (0.75)[100] in comparison with that in dilute solutions (1.00)[100] reveals reduced self-quenching in neat films possibly resulting from the sterically bulky di-*tert*-butyl groups of the bipyridine ligand,[22] suggesting its suitability for use as the emissive material of neat-film LECs. DOTCI in EtOH solutions (10^{-5} M) exhibits concentrated NIR PL spectra centered at 720 nm. It is noted that since the absorption spectrum of DOTCI and the PL spectrum of $[\text{Ir}(\text{dfppz})_2(\text{dtb-bpy})]^+(\text{PF}_6^-)$ exhibit poor spectral overlap (Fig. 5-2), inefficient energy transfer between them would be expected. Thus, significant DOTCI emission in the NIR region, which would lead to a considerable color shift in the $[\text{Ir}(\text{dfppz})_2(\text{dtb-bpy})]^+(\text{PF}_6^-)$ emission, would be prevented at low DOTCI doping concentrations. However, even at low DOTCI doping concentrations, the large offset in the energy levels between $[\text{Ir}(\text{dfppz})_2(\text{dtb-bpy})]^+(\text{PF}_6^-)$ and DOTCI would still be effective to induce significant carrier trapping and consequently result in an altered balance of carrier mobilities.

Doping of the carrier trapper DOTCI in $[\text{Ir}(\text{dfppz})_2(\text{dtb-bpy})]^+(\text{PF}_6^-)$ neat films to modify the balance of carrier mobilities may simultaneously lead to additional DOTCI emission, which deteriorates color purity of the $[\text{Ir}(\text{dfppz})_2(\text{dtb-bpy})]^+(\text{PF}_6^-)$ emission. To clarify the energy transfer properties between $[\text{Ir}(\text{dfppz})_2(\text{dtb-bpy})]^+(\text{PF}_6^-)$ and DOTCI, Fig. 5-3 depicts the PL spectra of the $[\text{Ir}(\text{dfppz})_2(\text{dtb-bpy})]^+(\text{PF}_6^-)$ films containing various concentrations of DOTCI. The excitation wavelength is 365 nm, at which the absorption of $[\text{Ir}(\text{dfppz})_2(\text{dtb-bpy})]^+(\text{PF}_6^-)$ is much higher than that of DOTCI at low doping concentrations, minimizing direct absorption of DOTCI and thus ensuring DOTCI emission mainly coming from energy transfer. Since in LECs, an ionic liquid $[\text{BMIM}^+][\text{PF}_6^-]$ of 20 wt% was added to provide additional mobile ions and to shorten the device response time,[84] PL properties of the $[\text{BMIM}^+][\text{PF}_6^-]$ (20 wt%) blended films were characterized. With the increase of the DOTCI concentration, the relative intensity of the DOTCI emission with respect to the $[\text{Ir}(\text{dfppz})_2(\text{dtb-bpy})]^+(\text{PF}_6^-)$ emission is larger due to a relatively higher energy transfer rate at a higher DOTCI concentration. However, it is noted that the DOTCI emission is weak at low DOTCI concentrations (0.01 – 0.1 wt%) and the PL spectra are predominantly the $[\text{Ir}(\text{dfppz})_2(\text{dtb-bpy})]^+(\text{PF}_6^-)$ emission, confirming inefficient energy transfer in the $[\text{Ir}(\text{dfppz})_2(\text{dtb-bpy})]^+(\text{PF}_6^-)$

PF_6^-)/DOTCI system at such low DOTCI concentrations. Hence, color shift in the $[\text{Ir}(\text{dfppz})_2(\text{dtb-bpy})]^+(\text{PF}_6^-)$ emission induced by dilute doping of DOTCI for tailoring the balance of carrier mobilities would not be significant.

5.2.2 EL characteristics of the LEC devices

To study the EL properties of the LECs doped with a carrier trapper, the EL characteristics of the LECs based on $[\text{Ir}(\text{dfppz})_2(\text{dtb-bpy})]^+(\text{PF}_6^-)$ containing various concentrations of DOTCI were measured and are summarized in Table 5-1. The LECs have the structure of indium tin oxide (ITO)/ PEDOT:PSS (30 nm)/emissive layer (200 nm)/Ag (100 nm), where the emissive layer contains $[\text{Ir}(\text{dfppz})_2(\text{dtb-bpy})]^+(\text{PF}_6^-)$ [(80-x) wt%], DOTCI (x wt%) and $[\text{BMIM}^+][\text{PF}_6^-]$ (20 wt%) and $x = 0, 0.01, 0.1$ and 1 for **Devices I, II, III, and IV**, respectively. The ionic liquid $[\text{BMIM}^+][\text{PF}_6^-]$ was added to provide additional mobile ions and to shorten the device response time.[84] The EL spectra of the LECs based on $[\text{Ir}(\text{dfppz})_2(\text{dtb-bpy})]^+(\text{PF}_6^-)$ containing various concentrations of DOTCI and $[\text{BMIM}^+][\text{PF}_6^-]$ (20 wt%) at 3.3 V are shown in Fig. 5-4. For the emission coming from $[\text{Ir}(\text{dfppz})_2(\text{dtb-bpy})]^+(\text{PF}_6^-)$, EL spectra are basically similar to PL spectra, indicating similar emission mechanisms. However, the relative intensity of the DOTCI emission with respect to the $[\text{Ir}(\text{dfppz})_2(\text{dtb-bpy})]^+(\text{PF}_6^-)$ emission in EL (Fig. 5-4) is smaller than that in PL (Fig. 5-3) at the same

DOTCI concentration. This phenomenon would be explained as follows. The PL emission of DOTCI (Fig. 5-3) mainly comes from the Förster energy transfer[143] from triplet excitons of $[\text{Ir}(\text{dfppz})_2(\text{dtb-bpy})]^+(\text{PF}_6^-)$ to singlet excitons of DOTCI. Dexter energy transfer[64] from triplet excitons of $[\text{Ir}(\text{dfppz})_2(\text{dtb-bpy})]^+(\text{PF}_6^-)$ to triplet excitons of DOTCI, which decay nonradiatively, would be insignificant when the pumping level (and thus the concentration of triplet excitons) is low.[145] For host–guest LECs, electrochemically doped regions of the emissive layer result in ohmic contacts with metal electrodes and consequently facilitate carrier injection onto both the host and the guest. Hence, both exciton formation on the host followed by host–guest energy transfer (Förster and/or Dexter energy transfer) and direct exciton formation on the guest induced by carrier trapping contribute to the guest emission. Direct exciton formation on the guest would be significant in a host–guest system exhibiting large offsets in the energy levels between the host and the guest since carrier trapping would be facilitated by such energy level alignment. The energy level diagram of $[\text{Ir}(\text{dfppz})_2(\text{dtb-bpy})]^+(\text{PF}_6^-)$ and DOTCI estimated by cyclic voltammetry is shown in the inset of Fig. 5-5. A large energy offset (1.36 eV) in the HOMO levels between $[\text{Ir}(\text{dfppz})_2(\text{dtb-bpy})]^+(\text{PF}_6^-)$ and DOTCI would lead to significant hole trapping. The maximum current density

versus voltage characteristics of LECs based on $[\text{Ir}(\text{dfppz})_2(\text{dtb-bpy})]^+(\text{PF}_6^-)$ containing various concentrations of DOTCI and $[\text{BMIM}^+][\text{PF}_6^-]$ (20 wt%) are shown in Fig. 5-5. The maximum device current density under the same bias voltage decreases as the concentration of DOTCI increases and thus confirms significant carrier trapping, resulting in direct exciton formation on DOTCI. As a result, only singlet excitons (~25% of total excitons directly formed on DOTCI) contribute to the EL emission from DOTCI (Fig. 5-4). Triplet excitons (~75% of total excitons directly formed on DOTCI) cannot be harvested due to the spin selection rule. On the other hand, Dexter energy transfer may not be ignored in devices under electrical driving, in which the concentration of triplet excitons would be higher than that in thin films under illumination of low-power UV light. Dexter energy transfer takes place between host triplets and guest triplets, which decay nonradiatively, when the concentration of host triplets increases and thus would degrade the EL efficiency of phosphorescent sensitized (phosphorescent host doped with fluorescent guest) LECs.[99] Thus, it would be responsible for the lower relative intensity of the DOTCI emission with respect to the $[\text{Ir}(\text{dfppz})_2(\text{dtb-bpy})]^+(\text{PF}_6^-)$ emission in EL (Fig. 5-4) as compared to that in PL (Fig. 5-3). These results reveal that doping of DOTCI in $[\text{Ir}(\text{dfppz})_2(\text{dtb-bpy})]^+(\text{PF}_6^-)$ films at concentrations lower than 0.1 wt% renders

almost unaffected EL spectra of $[\text{Ir}(\text{dfppz})_2(\text{dtb-bpy})]^+(\text{PF}_6^-)$ (Fig. 5-4) while carrier trapping induced by DOTCI at such low concentrations (Fig. 5-5) would still significantly modify the balance of carrier mobilities in the LEC devices.

The LECs based on $[\text{Ir}(\text{dfppz})_2(\text{dtb-bpy})]^+(\text{PF}_6^-)$ doped with various DOTCI concentrations and $[\text{BMIM}^+][\text{PF}_6^-]$ (20 wt%) exhibited similar time-dependent EL characteristics under constant-bias operation. Fig. 5-6(a) shows the time-dependent brightness and current density under constant biases of 3.3–3.7 V for **Device II**. After the bias was applied, the current first increased and then stayed rather constant. On the other hand, the brightness first increased with the current and reached the maxima of 16.62, 24.28 and 42.50 cd m^{-2} under biases of 3.3, 3.5 and 3.7 V, respectively. The brightness then dropped with time with a rate depending on the bias voltage (or current). Corresponding time-dependent EQEs and power efficiencies of the same device are shown in Fig. 5-6(b). When a forward bias was just applied, the EQE was rather low due to poor carrier injection. During the formation of the *p*- and *n*-type regions near electrodes, the capability of carrier injection was improved and the EQE thus rose rapidly. The peak EQE and the peak power efficiencies at 3.3, 3.5 and 3.7 V are 12.75% and 28.70 lm W^{-1} , 12.30% and 26.53 lm W^{-1} and 11.27% and 22.12 lm W^{-1} , respectively. The drop of device efficiency after reaching the peak

value, as commonly seen in solid-state LECs, may be associated with a few factors. Before the device current reaches a steady value, the carrier recombination zone may keep moving closer to one electrode due to a discrepancy in electron and hole mobilities, which would induce exciton quenching such that the device efficiency would decrease with time while the current and the brightness are still increasing. Further, the decrease in brightness and efficiency under a relatively steady device current may be rationally attributed to the degradation of the emissive material during the LEC operation.[45]

Peak EQEs and peak power efficiencies (at current densities $< 0.1 \text{ mA cm}^{-2}$) of the LECs based on $[\text{Ir}(\text{dfppz})_2(\text{dtb-bpy})]^+(\text{PF}_6^-)$ doped with various DOTCI concentrations and $[\text{BMIM}^+][\text{PF}_6^-]$ (20 wt%) are shown in Fig. 5-7. The device efficiency first increases, then decreases as the DOTCI concentration increases from 0 to 1 wt%. The undoped LECs based on $[\text{Ir}(\text{dfppz})_2(\text{dtb-bpy})]^+(\text{PF}_6^-)$ show an EQE up to 9.06%. However, this result is much lower than the upper limit ($\sim 15\%$) that one would expect from the PLQY of the emissive layer (~ 0.75)[100] and an optical outcoupling efficiency of $\sim 20\%$ from a typical layered light-emitting device structure. Since the electrochemically doped regions near electrodes of LECs ensure balanced carrier injection,[1,59] such

lowered device efficiency would be attributed to the imperfect balance of carrier mobilities in the $[\text{Ir}(\text{dfppz})_2(\text{dtb-bpy})]^+(\text{PF}_6^-)$ films. As the carrier injection at both electrodes is becoming balanced, the carrier recombination zone may consequently locate near one of the electrodes due to discrepancy in electron and hole mobilities of the emissive layer. The recombination zone in the vicinity of an electrode may cause exciton quenching such that the EQE of the device would decrease. The ppz-based complex $\text{Ir}(\text{ppz})_3$ (where ppz is 1-phenylpyrazole) has been reported to be a hole transporting/electron blocking material.[146] Furthermore, the cationic complex $[\text{Ir}(\text{dfppy})_2(\text{bpy})]^+(\text{PF}_6^-)$ (where dfppy is 2-(2,4-difluorophenyl) pyridine and bpy is 2,20-bipyridine) was shown to exhibit higher hole mobility than electron mobility.[147] Thus, a similar complex $[\text{Ir}(\text{dfppz})_2(\text{dtb-bpy})]^+(\text{PF}_6^-)$ containing ppz and bpy moieties would also prefer hole transport. The suggested schematic diagram of the position of the exciton recombination zone for the LECs based on $[\text{Ir}(\text{dfppz})_2(\text{dtb-bpy})]^+(\text{PF}_6^-)$ and $[\text{BMIM}^+][\text{PF}_6^-]$ (20 wt%) is depicted in Fig. 8(a). The exciton recombination zone approaching the cathode leads to exciton quenching and thus deteriorates the device efficiency. To balance the carrier mobilities for moving the exciton recombination zone toward the center of the emissive layer, a low-gap carrier trapper DOTCI is doped in the

$[\text{Ir}(\text{dfppz})_2(\text{dtb-bpy})]^+(\text{PF}_6^-)$ films. A large energy offset (1.36 eV) in the HOMO levels between $[\text{Ir}(\text{dfppz})_2(\text{dtb-bpy})]^+(\text{PF}_6^-)$ and DOTCI (the inset of Fig. 5-5) impedes hole transport in the emissive layer. On the other hand, similar energies in the LUMO levels of $[\text{Ir}(\text{dfppz})_2(\text{dtb-bpy})]^+(\text{PF}_6^-)$ and DOTCI (the inset of Fig. 5-5) keep the electron mobilities of the emissive layer relatively unchanged. As a result, doping of DOTCI would improve the balance of carrier mobilities in $[\text{Ir}(\text{dfppz})_2(\text{dtb-bpy})]^+(\text{PF}_6^-)$ films and consequently move the exciton recombination zone toward the center of the emissive layer (Fig. 5-8(b)), improving the device efficiencies. With the DOTCI concentration of 0.01 wt%, the peak EQE and the peak power efficiency of the LECs reach 12.75% and 28.70 lm W^{-1} , respectively (Fig. 5-7). Such device efficiencies are enhanced by 1.4 times as compared to those of the undoped devices and approach the upper limit ($\sim 15\%$) that one would expect from the PLQY of the emissive layer (~ 0.75)[100] and an optical outcoupling efficiency of $\sim 20\%$ from a typical layered light-emitting device structure. These results confirm characteristics of preferred transport of hole for $[\text{Ir}(\text{dfppz})_2(\text{dtb-bpy})]^+(\text{PF}_6^-)$ and the improved balance of carrier mobilities in the doped emissive layer. To the best of our knowledge, these device efficiencies are among the highest reported values for neat-film cyan emitting LECs. Further increasing the concentration of DOTCI

would result in overmodified hole mobilities and thus deteriorate the balance of carrier mobilities as well (Fig. 5-8(c)). With the DOTCI concentration of 0.1 wt%, severe hole trapping leads to lower hole mobility compared with electron mobility and the exciton recombination zone would be pushed toward the anode in consequence. Exciton quenching near the anode also causes a deteriorated EQE of 6.94% (Fig. 5-7). These results reveal that doping of a proper carrier trapper in CTMC neat films would modify the balance of carrier mobilities of the emissive layer and thus enhance device efficiencies of neat-film LECs.

The turn-on time (the time required to reach the maximal brightness) as a function of bias voltage for LECs is shown in Fig. 5-9(a). An electrochemical junction between p- and n-type doped layers of LECs is formed during device operation. The higher electric field in the device induced by a higher bias voltage accelerates redistribution of mobile ions, which facilitates formation of ohmic contacts with the electrodes and thus fastens the device response. It is noted that the turn-on time of the LECs under the same bias voltage increases as the DOTCI concentration increases. More pronounced carrier trapping in LECs with higher DOTCI concentrations decreases the effective bias voltage across the emissive layer and consequently leads to a lower electric field, rendering a slower device response under the same bias voltage. Carrier trapping induced by

doping of DOTCI also decreases the device current density (Fig. 5-5) and thus is beneficial in device stability. As shown in Fig. 5-9(b), the device lifetime (the time for the brightness of the device to decay from the maximum to half of the maximum under a constant bias voltage) of LECs increases as the DOTCI concentration increases. It may be associated with the fact that the lower electric field or current density decelerates degradation (multiple oxidation and subsequent decomposition)[84] of the CTMC materials. Detailed degradation mechanisms of LECs based on CTMCs remain unclear and further studies are still needed to achieve practical device lifetimes. Recently published literature revealed that device current and brightness of sandwiched LECs first increase with extension of the p- and n-type electrochemically doped regions. As the width of the doping layers increases, the width of the neutral layer decreases and thus the number of excitons being quenched increases, leading to reduced brightness. Adding a hole trapper to decrease the hole mobility would reduce the speed of formation of the p-type doped layer and thus would slow down the evolution rate of the device current and brightness, leading to lengthened turn-on times and lifetimes. Our observed results are consistent with the reported model of LECs.[60]

5.3 Experimental

5.3.1 Photoluminescent Characterization

The mixed films for PL studies were spin-coated at 3000 rpm onto quartz substrates (0.5 cm^2) using mixed solutions (in acetonitrile) of various ratios. Since in LECs, an ionic liquid $[\text{BMIM}^+][\text{PF}_6^-]$ of 20 wt% was added to provide additional mobile ions and to shorten the device response time,[84] PL properties of the $[\text{BMIM}^+][\text{PF}_6^-]$ blended films were characterized. The mass ratio of solute component of $[\text{Ir}(\text{dfppz})_2(\text{dtb-bpy})]^+(\text{PF}_6^-)$, DOTCI and $[\text{BMIM}^+][\text{PF}_6^-]$ in acetonitrile solutions for spin coating of the mixed films is $(80 - x)$, x and 20, respectively ($x = 0, 0.01, 0.1, 1$). The concentrations of all solutions for spin coating are 80 mg mL^{-1} . The thickness of each spin-coated film was ca. 200 nm, as measured using profilometry. UV-Vis absorption spectra were recorded using a Hitachi U2800A spectrophotometer. PL spectra were recorded using a Hitachi F9500 fluorescence spectrophotometer. PLQYs for thin-film samples were determined with a calibrated integrating sphere system (HAMAMATSU C9920).

5.3.2 LEC Device Fabrication and Characterization

ITO-coated glass substrates ($2 \times 2 \text{ cm}^2$) were cleaned and treated with UV/ozone prior to use. A PEDOT:PSS layer was spin-coated at 4000 rpm onto

the ITO substrate in air and baked at 150 °C for 30 min. The emissive layer (~200 nm, as measured by profilometry) was then spin-coated at 3000 rpm from mixed acetonitrile solutions. The mass ratio of solute component and the concentrations of solutions for spin coating of the emissive layers were the same as those used for spin coating of the mixed films containing [BMIM⁺][PF₆⁻] for PL studies described above. The ionic liquid [BMIM⁺][PF₆⁻] was added to enhance the ionic conductivity of thin films and thus to reduce the turn-on time of the LEC device.[84] All solution preparing and spin-coating processes were carried out under ambient conditions. After spin coating, the thin films were then baked at 70 °C for 10 hours in a nitrogen glove box (oxygen and moisture levels below 1 ppm), followed by thermal evaporation of a 100 nm Ag top contact in a vacuum chamber (~10⁻⁶ Torr). The electrical and emission characteristics of LEC devices were measured using a sourcemeasurement unit and a Si photodiode calibrated with the Photo Research PR-650 spectroradiometer. All device measurements were performed under a constant bias voltage (3.3–3.7 V) in a nitrogen glove box. The EL spectra were taken with a calibrated CCD spectrograph.

5.4 Summary

In this work, we demonstrate improvements in the balance of carrier mobilities in neat-film LECs utilizing a cyan-emitting phosphorescent CTMC $[\text{Ir}(\text{dfppz})_2(\text{dtb-bpy})]^+(\text{PF}_6^-)$ as the emissive material and a cationic fluorescent NIR laser dye DOTCI as the carrier trapper. This low-gap carrier trapper is chosen such that a significant energy offset in the HOMO levels between $[\text{Ir}(\text{dfppz})_2(\text{dtb-bpy})]^+(\text{PF}_6^-)$ and DOTCI impedes hole transport in the emissive layers while similar LUMO levels of these two materials result in a relatively unaffected electron transport. Therefore, the balance of carrier mobilities in the CTMC neat films, which would intrinsically exhibit characteristics of preferred transport of holes, would be improved by doping such carrier trapper. PL measurements reveal inefficient energy transfer between $[\text{Ir}(\text{dfppz})_2(\text{dtb-bpy})]^+(\text{PF}_6^-)$ and DOTCI due to poor spectral overlap between the $[\text{Ir}(\text{dfppz})_2(\text{dtb-bpy})]^+(\text{PF}_6^-)$ emission and DOTCI absorption, ensuring unapparent DOTCI emission and thus reducing color shift in the $[\text{Ir}(\text{dfppz})_2(\text{dtb-bpy})]^+(\text{PF}_6^-)$ emission at low doping concentrations of DOTCI. However, even at low doping concentrations, carrier trapping would still be effective due to the large energy offset in the HOMO levels between $[\text{Ir}(\text{dfppz})_2(\text{dtb-bpy})]^+(\text{PF}_6^-)$ and DOTCI. EL measurements show that the peak

EQE (power efficiency) of the neat-film LECs doped with the carrier trapper reaches 12.75% (28.70 lm W^{-1}), representing a 1.4 times enhancement in device efficiency as compared to that of the undoped neat-film LECs. Such device efficiency approaches the upper limit ($\sim 15\%$) that one would expect from the PLQY of the emissive layer (~ 0.75) and an optical outcoupling efficiency of $\sim 20\%$ from a typical layered light-emitting device structure, consequently indicating superior balance of carrier mobilities in such doped emissive layer. These results confirm the strategy of introducing a proper carrier trapper into the CTMC neat films would improve the balance of carrier mobilities in the emissive layer, offering a general approach for optimizing device efficiencies of CTMC-based neat-film LECs.

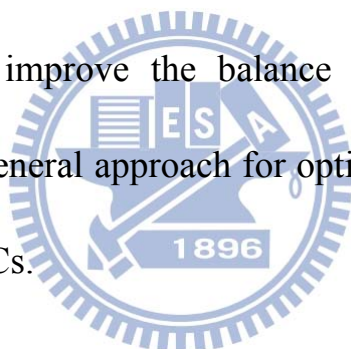


Table 5-1 Summary of the LEC device characteristics.

Device (DOTCI concentration)	Bias (V)	t_{\max} (min) ^a	L_{\max} (cd m^{-2}) ^b	$\eta_{\text{ext, max}}$ (%) ^c	$\eta_{\text{p, max}}$ (lm W^{-1}) ^d	$t_{1/2}$ (min) ^e
I (0.0 wt.%)	3.3 V	49	10.94	9.06	19.14	40
	3.5 V	32	19.41	8.54	16.78	24
	3.7 V	23	25.21	7.51	13.96	15
II (0.01 wt.%)	3.3 V	62	16.62	12.75	28.70	45
	3.5 V	34	24.48	12.30	26.53	27
	3.7 V	25	42.50	11.27	22.12	16
III (0.1 wt.%)	3.3 V	68	6.03	6.94	15.06	48
	3.5 V	54	11.03	6.62	13.53	31
	3.7 V	28	14.00	6.55	12.36	18
IV (1.0 wt.%)	3.3 V	295	0.95	0.72	1.56	233
	3.5 V	161	1.86	0.74	1.46	53
	3.7 V	119	2.78	0.73	1.27	23

[a] Time required to reach the maximal brightness. [b] Maximal brightness achieved at a constant bias voltage. [c] Maximal external quantum efficiency achieved at a constant bias voltage. [d] Maximal power efficiency achieved at a constant bias voltage. [e] The time for the brightness of the device to decay from the maximum to half of the maximum under a constant bias voltage.

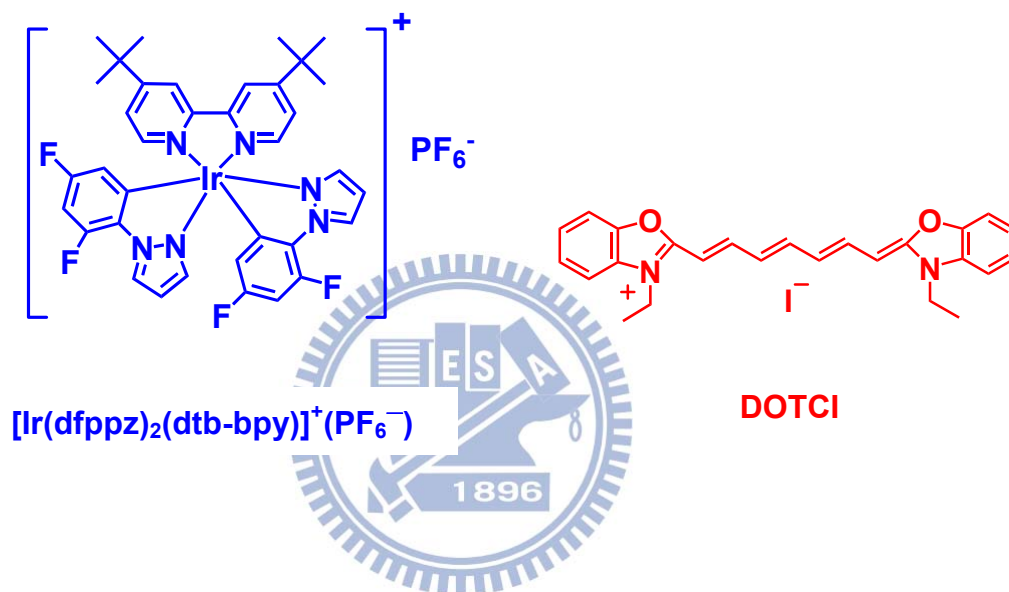


Figure 5-1 Molecular structures of the CTMC $[\text{Ir}(\text{dfppz})_2(\text{dtbbpy})]^+(\text{PF}_6^-)$ and the carrier trapper DOTCI.

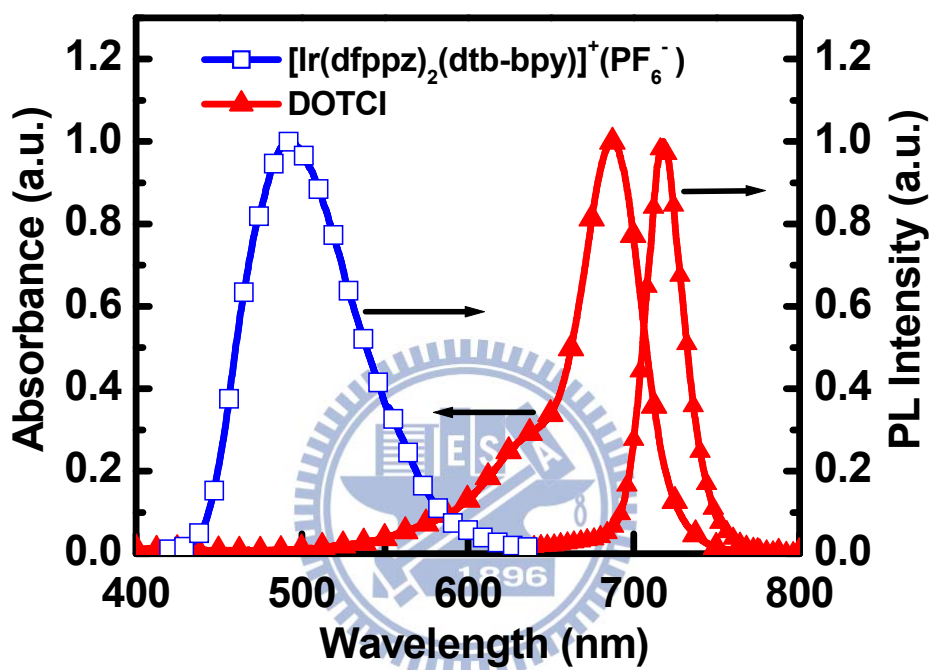


Figure 5-2 PL spectrum of the $[\text{Ir}(\text{dfppz})_2(\text{dtbbpy})]^+(\text{PF}_6^-)$ neat film and absorption/PL spectra of DOTCI in ethanol solution (10^{-5} M).

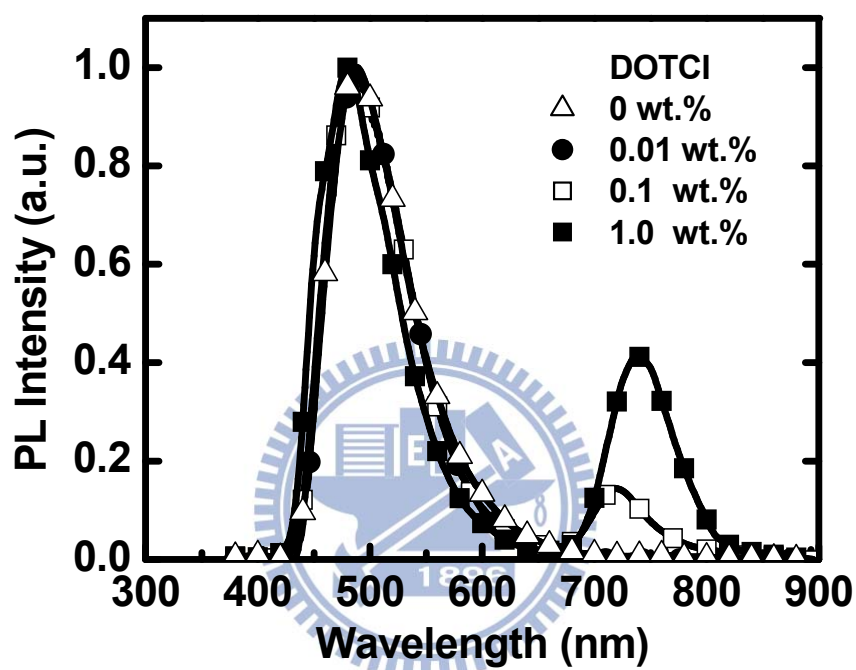


Figure 5-3 PL spectra of the $[\text{Ir}(\text{dfppz})_2(\text{dtb-bpy})]^+(\text{PF}_6^-)$ films containing various concentrations of DOTCI and $[\text{BMIM}^+][\text{PF}_6^-]$ (20 wt.%).

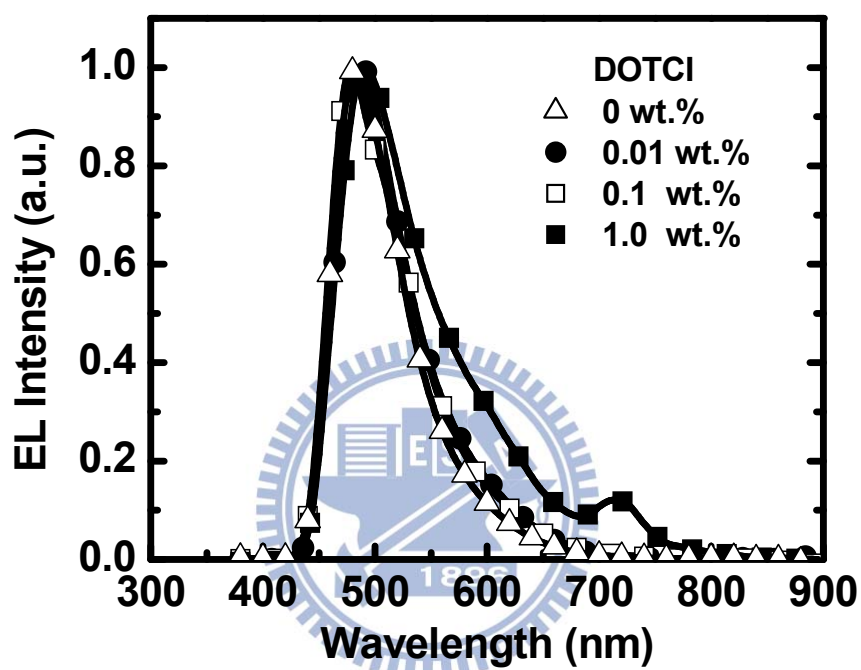


Figure 5-4 EL spectra for the LECs based on $[\text{Ir}(\text{dfppz})_2(\text{dtb-bpy})]^+(\text{PF}_6^-)$ containing various concentrations of DOTCI and $[\text{BMIM}^+][\text{PF}_6^-]$ (20 wt.%) at 3.3 V.

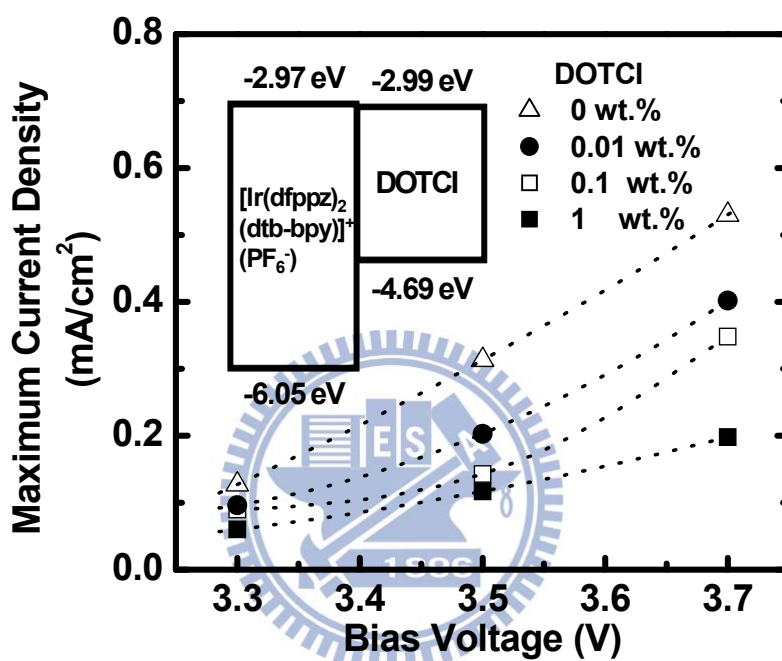


Figure 5-5 Maximum current density vs voltage characteristics for the LECs based on $[\text{Ir}(\text{dfppz})_2(\text{dtb-bpy})]^+(\text{PF}_6^-)$ containing various concentrations of DOTCI and $[\text{BMIM}^+][\text{PF}_6^-]$ (20 wt.%). Inset: the energy level diagram of $[\text{Ir}(\text{dfppz})_2(\text{dtb-bpy})]^+(\text{PF}_6^-)$ and DOTCI molecules.

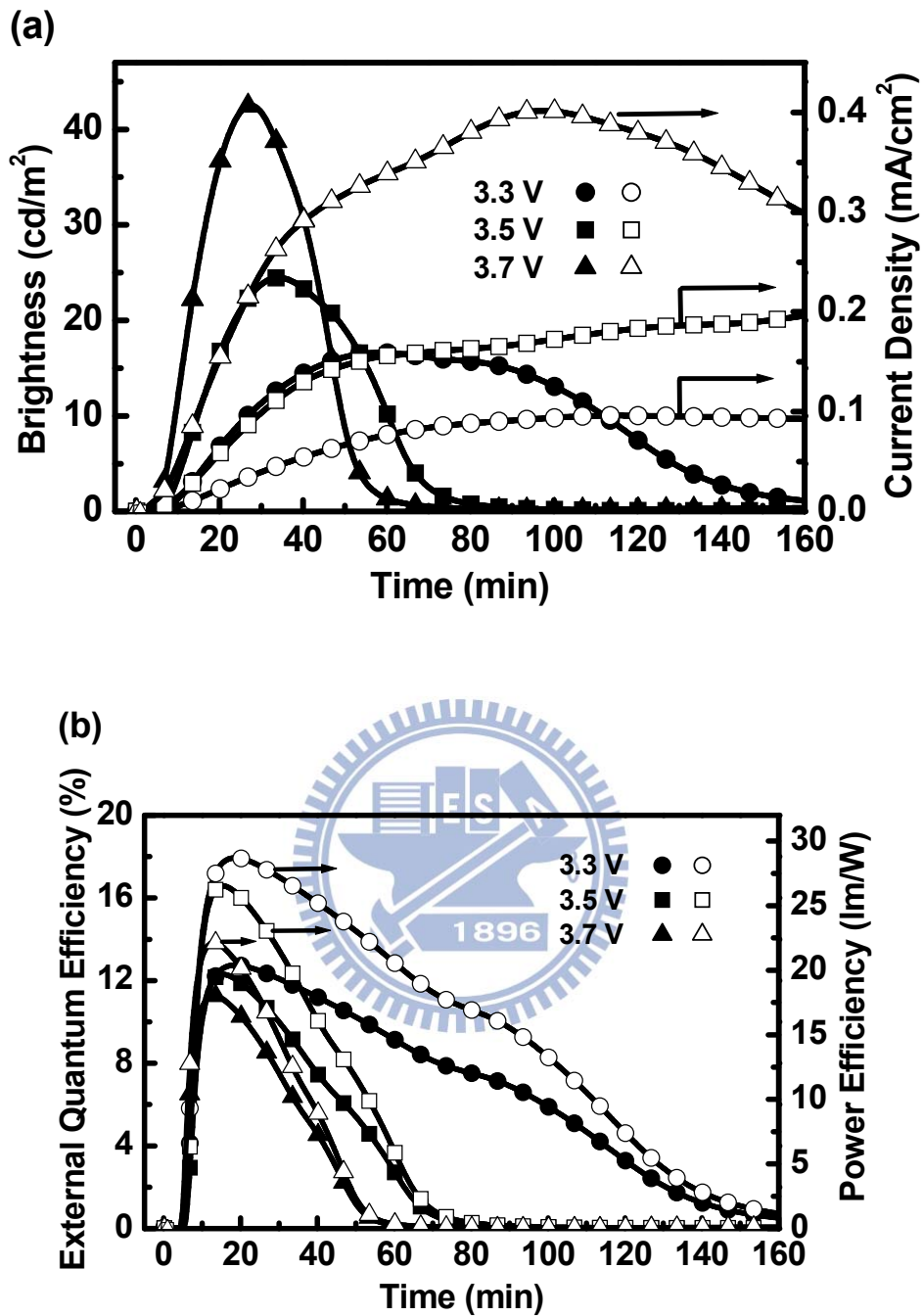


Figure 5-6 (a) Brightness (solid symbols) and current density (open symbols) and (b) external quantum efficiency (solid symbols) and power efficiency (open symbols) as a function of time under a constant bias voltage of 3.3–3.7 V for Device II.

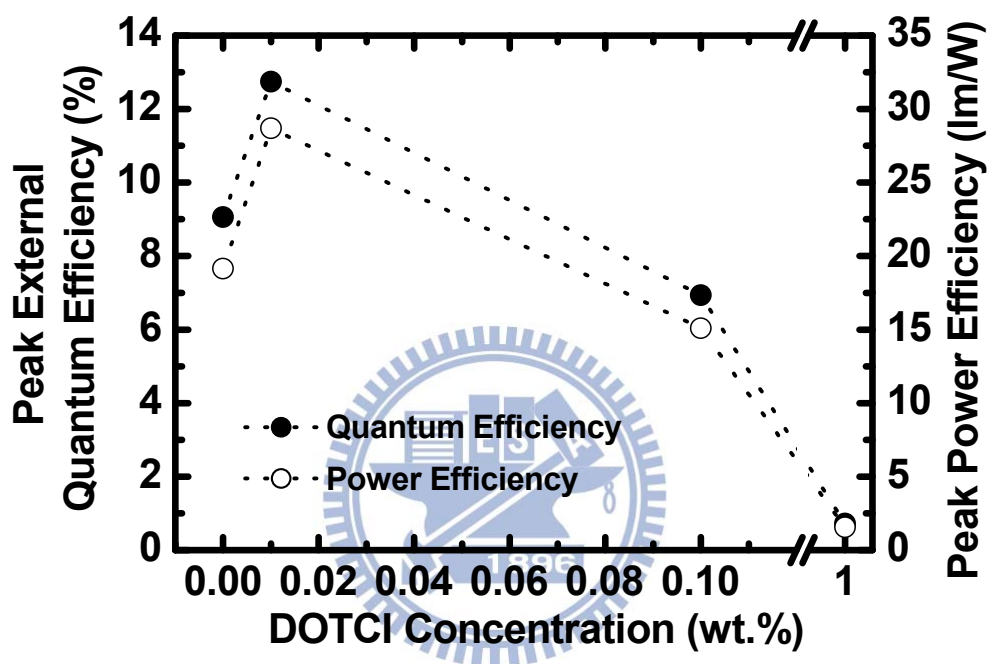


Figure 5-7 Peak external quantum efficiencies and peak power efficiencies (at current densities $<0.1 \text{ mA cm}^{-2}$) of the LECs as a function of the DOTCI concentration.

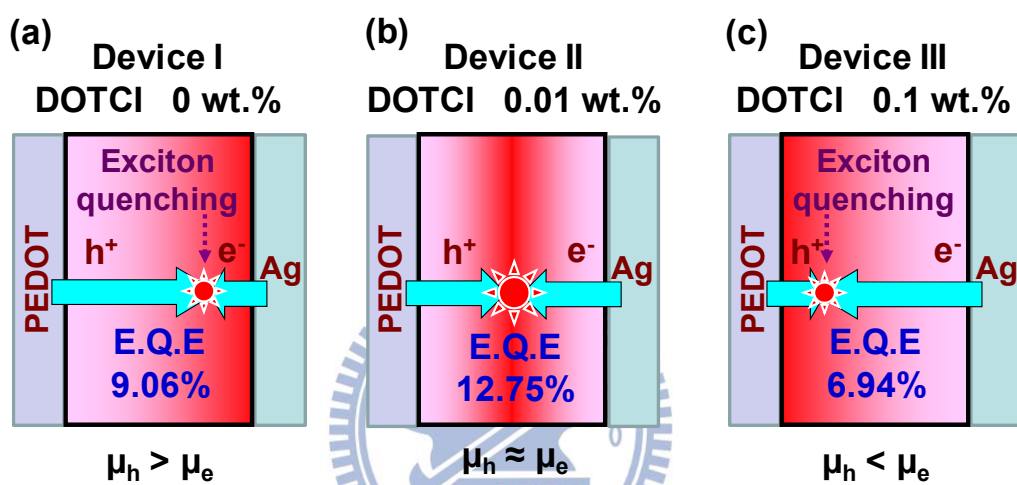


Figure 5-8 Schematic diagrams of the position of exciton recombination zone for (a) **Device I**, (b) **Device II** and (c) **Device III**. Electrochemically doped regions near electrodes are omitted for clarity.

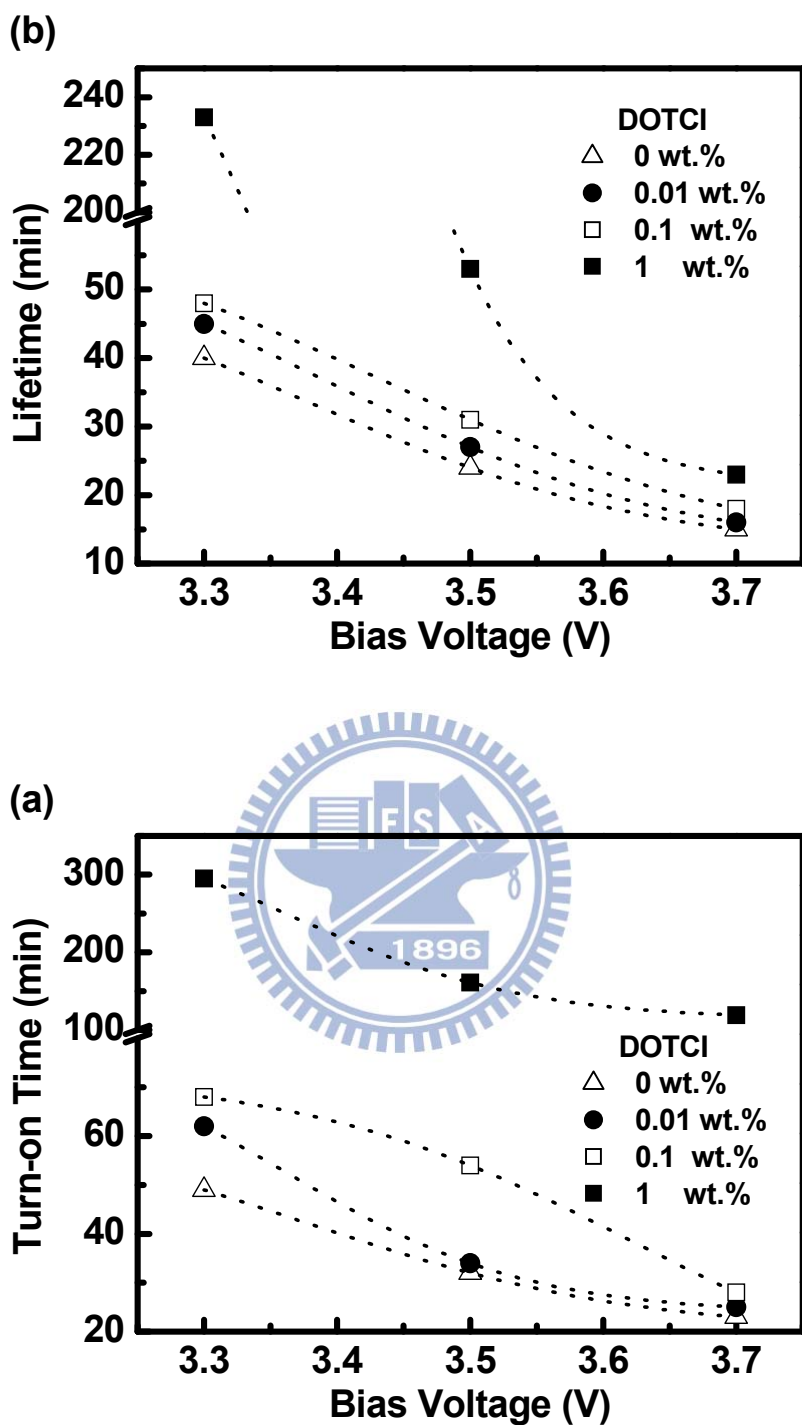


Figure 5-9 (a) Turn-on time and (b) lifetime as a function of bias voltage for the LECs based on $[\text{Ir}(\text{dfppz})_2(\text{dtb-bpy})]^+(\text{PF}_6^-)$ containing various concentrations of DOTCI and $[\text{BMIM}^+][\text{PF}_6^-]$ (20 wt.%).

Chapter 6 Tailoring Carrier Injection Efficiency to Improve Carrier Balance of Solid-State Light-Emitting Electrochemical Cells

6.1 Introduction

Solid-state LECs possess several advantages over conventional OLEDs. In LECs, electrochemically doped regions induced by spatially separated ions under a bias significantly reduce the barrier of carrier injection, giving balanced carrier injection, low operating voltages, and consequently high power efficiencies.[1,59] As such, LECs generally require only a single emissive layer, which can be easily processed from solutions and can conveniently use air-stable electrodes, while OLEDs typically require more sophisticated multilayer structures and low-work-function cathodes.[60-61] Compared with conventional polymer LECs that are usually composed of an emissive conjugated polymer, a salt and an ion-conducting polymer,[1,59] LECs based on CTMCs show several further advantages and have attracted much attention in recent years.[5,9,11-12,14,120-126] In such devices, no ion-conducting material is needed since these CTMCs are intrinsically ionic. Furthermore, higher EL efficiencies are expected due to the phosphorescent nature of CTMCs. Another benefit of employing CTMCs as the emissive materials is that they can be processed by spin coating rather than by thermal evaporation, which is

commonly used in fabricating conventional multilayered OLEDs. Thus, blue-green emitting complexes, which often contain fluorinated ligands, are not subject to high temperatures and subsequent de-fluorination at elevated temperatures.[155-156]

Device efficiencies of LECs based on CTMCs are determined by PLQYs of CTMCs, spin dependent exciton harvesting ratio, carrier balance of devices and optical outcoupling efficiency from a typical layered light-emitting device structure. Since CTMCs are phosphorescent materials, both singlet and triplet excitons can be harvested via efficient spin-orbital coupling mediated by the heavy-metal center. Carrier balance of devices depends on carrier injection efficiency and carrier transport mobilities of CTMCs. Optical outcoupling efficiency is ca. 20% for common layered bottom emitting device structure.[125]

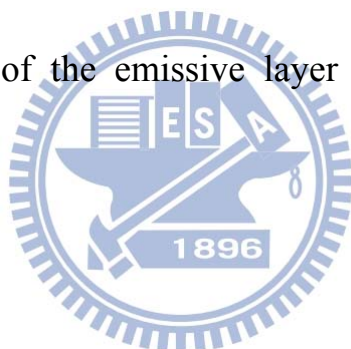
With perfect carrier balance in devices, carrier injection efficiency from electrodes and carrier transport mobilities of CTMCs compensate for each other, i.e., LECs based on CTMCs with higher and hole mobilities combined with device structures with higher hole and electron injection efficiencies, respectively. Hence, carrier recombination zone would be located near the center of emissive layer, eliminating exciton quenching near electrodes.[15,127] Under such condition, only PLQYs of CTMCs and optical outcoupling efficiency

would limit LEC device efficiencies. However, many reported device efficiencies of LECs based on CTMCs[17,23,33,38,39,50,53,86,102,152] were lower than the upper limits expected from the PLQYs of their emissive layers and optical outcoupling efficiencies of ~20%,[125] implying commonly observed imperfect carrier balance in CTMC-based LECs. Furthermore, altered device efficiencies of LECs based on CTMCs when cathodes with different work functions were used have been reported.[29,31,122,150] It reveals that electrochemical doping would lower carrier injection barrier, but would not always lead to an ohmic contact for carrier injection. Therefore, tailoring carrier injection efficiency would affect carrier balance and would be useful in optimizing device efficiencies of LECs. Effects of work functions of electrodes on device characteristics of planar type polymer LECs, which utilized interdigitated electrodes with spacings up to 1 mm have been systematically studied. These spacings are much larger than the interelectrode distance in sandwich type devices (typically < 200 nm). Carrier balance would be significantly different between planar and sandwich type LECs due to the large discrepancy in thickness of the active layer, which alters the intensity of electric field and consequently affects field-dependent mobilities of hole and electron. To clarify the effects of carrier injection on carrier balance and consequent

device efficiency of sandwich type LECs, which are more suitable for practical applications, systematic studies of the device characteristics influenced by carrier injection barriers are highly desired. To the best of our knowledge, related reports about this issue would still have been scarce up to now.

In this work, we systematically study the influence of carrier injection efficiency on the performance of LECs based on two CTMCs with oppositely preferred carrier transporting characteristics, i.e., one prefers hole transport and the other prefers electron transport. Carrier injection barrier is adjusted by employing proper hole injection layer (HIL) and/or electron injection layer (EIL). Experimental results show that an ohmic contact for hole injection of LECs based on CTMCs would be approximately formed by the p-type doped layer when hole injection barrier is not high, e.g., < 0.5 eV. However, for higher hole injection barrier, e.g., > 0.8 eV, some hole injection barrier would still exist even with the p-type doped layer and thus an additional HIL enhances hole injection efficiency. Similarly, for higher electron injection barrier, e.g., > 1.2 eV, electron injection efficiency would be enhanced by adding an EIL since some electron injection barrier would still be present even with the n-type doped layer. Therefore, carrier balance would be tailored by adding proper carrier injection layers for CTMC-based LECs with relatively higher carrier injection barriers. To

optimize device efficiency, carrier injection efficiency of CTMC-based LECs should be modified according to carrier transporting characteristics of CTMCs. Hole-preferred transporting CTMCs should be combined with an LEC structure with higher electron injection efficiency while higher hole injection efficiency would be required for LECs based on electron-preferred transporting CTMCs. As such, the carrier recombination zone would locate near the center of the emissive layer and exciton quenching near electrodes would be significantly mitigated, rendering an improved device efficiency approaching the upper limit expected from the PLQY of the emissive layer and the optical outcoupling efficiency.



6.2 Experimental

6.2.1 Materials

Molecular structures of the two CTMCs used in this study are shown in Fig. 6-1. The cyan-emitting CTMC $[\text{Ir}(\text{dfppz})_2(\text{dtb-bpy})]^+(\text{PF}_6^-)$ (**1**) (where dfppz is 1-(2,4-difluorophenyl) pyrazole and dtb-bpy is [4,4'-di(tert-butyl)-2,2'-bipyridine]) reported previously by Tamayo *et al.*, [22] was used as the emissive material with hole-preferred transporting characteristics. [102] The ppz-based complex $\text{Ir}(\text{ppz})_3$ (where ppz is 1-phenylpyrazole) has been reported to be a hole transporting/electron blocking

material.[146] In addition, a similar cationic complex $[\text{Ir}(\text{dfppy})_2(\text{bpy})]^+(\text{PF}_6^-)$ (where dfppy is 2-(2,4-difluorophenyl)pyridine and bpy is 2,2'-bipyridine) was shown to exhibit higher hole mobility than electron mobility.[147] The device efficiencies of the LECs based on complex **1** have been shown to be significantly enhanced by doping a low-gap hole trapping guest.[102] Since carrier balance is improved by lowering hole mobility of the emissive layer, complex **1** would be further proved to exhibit hole-preferred transporting characteristics.[102] On the other hand, the orange-emitting CTMC $[\text{Ir}(\text{ppy})_2(\text{dasb})]^+(\text{PF}_6^-)$ (**2**) (where ppy is 2-phenylpyridine and dasb is 4,5-diaza-9,9'-spirobifluorene)[34] was used as the emissive material with electron-preferred transporting characteristics. 4,5-diaza-9,9'-spirobifluorene (dasb) is a ligand with good electron affinity, which has been used to improve the electron injection and transport properties of OLEDs for blue emitters.[157] A europium complex incorporating dasb ligand has also been shown to exhibit good electron-transporting ability.[158] With a device structure preferring hole injection, the LECs based on complex **2** showed high EQEs up to ca. 9.2%, which are approaching the upper limit (c.a. 10%) expected from the PLQY of the emissive layer (0.49) and an optical outcoupling efficiency of ~20% from a typical layered light-emitting device structure. Such high device efficiency

suggests superior carrier balance and thus would imply electron-preferred transporting characteristics of complex **2** for compensating imbalanced carrier injection. Complexes **1** and **2** were synthesized according to the procedures reported in the literatures.[22,34] Thin films of the hole transporting material *N,N'*-diphenyl-*N,N'*-bis(3-methylphenyl)-1,1'-biphenyl-4,4'-diamine (TPD) was used as HILs to facilitate hole injection. For comparison, the hole transporting material *N,N'*-dicarbazolyl-3,5-benzene (mCP) with a high ionization potential was utilized to impede hole injection. Thin films of low-work-function metal Ca were used as EILs to facilitate electron injection. High-work-function metal Au was used to impede electron injection for comparison. To reduce turn-on times of the LEC devices, the ionic liquid [BMIM⁺][PF₆⁻] was added in the emissive layer to enhance the ionic conductivity of thin films.[84] TPD (Lum Tech) and [BMIM⁺][PF₆⁻] (Alfa Aesar) were used as received.

6.2.2 LEC Device Fabrication and Characterization

ITO-coated glass substrates were cleaned and treated with UV/ozone prior to use. A PEDOT:PSS (~40 nm) layer was spin-coated at 4000 rpm onto the ITO substrate in air and baked at 150 °C for 30 min. For devices without an HIL (**Device 1-S**, **1-E**, **2-S**, **2-E** and **2-IE**), the emissive layer was deposited directly on the PEDOT:PSS layer. For LEC devices with an HIL (**Device 1-H**, **1-HE**,

2-H, 2-HE, 2-IH and **2-IHE**), TPD or mCP (~20 nm) was spin-coated at 5000 rpm from the chlorobenzene solutions on the PEDOT:PSS layer under ambient conditions and baked at 60 °C for 6 hours. After spin coating of PEDOT:PSS, PEDOT:PSS/TPD or PEDOT:PSS/mCP layer, the emissive layer of complex **1** (~200 nm, for **Device 1-S, 1-H, 1-E** and **1-HE**) or complex **2** (~200 nm, for **2-S, 2-H, 2-E, 2-HE, 2-IH, 2-IE** and **2-IHE**) was then spin-coated at 3000 rpm from the acetonitrile solutions under ambient conditions. The ionic liquid [BMIM⁺][PF₆⁻] (20 wt%) was added in the emissive layer to enhance the ionic conductivity of thin films and thus to reduce the turn-on time of the LEC device.[84] After spin coating of all organic layers, the thin films were then baked at 70 °C for 10 hours in a nitrogen glove box (oxygen and moisture levels below 1 ppm), followed by thermal evaporation of a 100-nm Ag film (**Device 1-S, 1-H, 2-S, 2-H** and **2-IH**), a 40-nm Ca film (EIL) capped with an 80-nm Ag film (**Device 1-E, 1-HE, 2-E** and **2-HE**) and a 20-nm Au film capped with an 80-nm Ag film (**Device 2-IE** and **2-IHE**) as the top contact in a vacuum chamber (~10⁻⁶ torr). Thicknesses of thin films were measured by ellipsometry. The electrical and emission characteristics of LEC devices were measured using a source-measurement unit and a Si photodiode calibrated with the Photo Research PR-650 spectroradiometer. All device measurements were performed

under a constant bias voltage (3.5 V for **Device 1-S**, **1-H**, **1-E** and **1-HE** and 2.4 V for **2-S**, **2-H**, **2-E**, **2-HE**, **2-IH**, **2-IE** and **2-IHE**) in a nitrogen glove box. The EL spectra were taken with a calibrated CCD spectrograph.

6.3 Results and Discussion

6.3.1 General LEC Device Characteristics

To clarify the effects of carrier injection on carrier balance and thus device efficiency LECs, EL characteristics of LECs of various configurations for carrier injection were measured and are summarized in Table 6-1. Device configurations of LECs under study and related energy levels alignments[14,50,61,66,67,68] are shown in Fig. 6-2. Standard LECs have the structure of [ITO/PEDOT:PSS (40 nm)/complex **1** (200 nm, for **Device 1-S**) or complex **2** (200 nm, for **Device 2-S**)/Ag (100 nm)]. LECs with HILs have the structure of [ITO/PEDOT:PSS (40 nm)/TPD (20 nm)/complex **1** (200 nm, for **Device 1-H**) or complex **2** (200 nm, for **Device 2-H**)/Ag (100 nm)]. For comparison, LECs with HILs to impede hole injection have the structure of [ITO/PEDOT:PSS (40 nm)/mCP (20 nm)/complex **2** (200 nm, for **Device 2-IH**)/Ag (100 nm)]. LECs with EILs have the structure of [ITO/PEDOT:PSS (40 nm)/complex **1** (200 nm, for **Device 1-E**) or complex **2** (200 nm, for **Device 2-E**)/Ca (40 nm)/Ag (80 nm)]. For comparison, LECs with EILs to impede

electron injection have the structure of [ITO/PEDOT:PSS (40 nm)/complex **2** (200 nm, for **Device 2-IE**)/Au (20 nm)/Ag (80 nm)]. LECs with both HILs and EILs have the structure of [ITO/PEDOT:PSS (40 nm)/TPD (20 nm)/complex **1** (200 nm, for **Device 1-HE**) or complex **2** (200 nm, for **Device 2-HE**)/Ca (40 nm)/Ag (80 nm)]. For comparison, LECs with both HILs and EILs to impede both hole and electron have the structure of [ITO/PEDOT:PSS (40 nm)/mCP (20 nm)/complex **2** (200 nm, for **Device 2-IHE**)/Au (20 nm)/Ag (80 nm)]. EL spectra of **Device 1-S, 1-H, 1-E and 1-HE** at 3.5 V and **2-S, 2-H, 2-E, 2-HE, 2-IH, 2-IE and 2-IHE** at 2.4 V are shown in Fig. 6-3. The LECs based on complex **1** (**Device 1-S, 1-H, 1-E and 1-HE**) exhibited similar EL spectra dominated by emission of complex **1**. For the LECs based on complex **2** (**2-S, 2-H, 2-E, 2-HE, 2-IH, 2-IE and 2-IHE**), predominant EL emission resulted from complex **2**. These results reveal that the carrier recombination zone is still mainly located in the CTMC layer even when carrier injection layers are added. Therefore, discrepancies in device characteristics when different device configurations are employed can be reasonably attributed to altered carrier balance induced by different carrier injection efficiencies.

Time-dependent current density, brightness and EQE of **Device 1-S, 1-H, 1-E and 1-HE** at 3.5 V, **Device 2-S, 2-H, 2-E and 2-HE** at 2.4 V and Device

2-IH, **2-IE** and **2-IHE** at 2.4 V are shown in Fig. 6-4(a)~(c), Fig. 6-5(a)~(c) and Fig. 6-6(a)~(c), respectively. All LECs exhibited similar trends in time-dependent EL characteristics under constant-bias operation. After the bias was applied, the device current, brightness and EQE increased due to enhanced carrier injection induced by gradually formed p- and n-type doped layers near electrodes.[153] The brightness and EQE first increased with the device current and reached the maximum values. Then they dropped with time with a rate depending on the bias voltage (or current). The drop of brightness and device efficiency after reaching the peak value, as commonly seen in solid-state CTMC-based LECs, may be associated with a few factors. When the device current is still increasing, the p- and n-type doped layers keep extending and the carrier injection efficiency is continuously enhanced. Therefore, the carrier recombination zone may keep moving closer to one electrode due to discrepancy in electron and hole mobilities, which would induce exciton quenching, deteriorating brightness and device efficiency.[15,127] The decrease in brightness and efficiency under a relatively steady device current may be rationally attributed to the degradation of the emissive material during the LEC operation.[45] Though all LECs exhibited similar trends in time-dependent EL characteristics, distinct carrier balance and thus device efficiency were observed

in LECs with different carrier-injection structures. Discussions of effects of improved carrier injection on device characteristics of LECs based on complex **1** and **2** are shown in the following subsections.

6.3.2 Effects of Improved Hole Injection on Device Characteristics of LECs

Standard LECs based on complex **1** and **2** have the structure of ITO/PEDOT:PSS/emissive layer/Ag, which have been commonly used in previous reports.[101,102,152,154] It is noted that **Device 2-S** exhibited slower device response (brightness is still increasing after ~10-hr operation), lower brightness and higher device efficiency as compared to previously reported LECs based on the same complex.[34] These results are attributed to different device thicknesses and bias voltages used in the two works. In Ref. 26, the device thickness is 100 nm and the bias voltages are 2.6 and 2.5 V while the thickness is 200 nm and the bias voltage is 2.4 V in this work. Thicker thickness and lower bias lower the electric field inside the emissive layer and thus lengthen the time required for accumulating mobile ions near electrodes, rendering slower device response. Since the brightness of LECs in this work has not yet shown significant decrease after 10-hr operation (Fig. 6-5(b)), extrapolation, which has been used in Ref. 34 to derive device lifetimes, cannot

be performed to estimate lifetimes of LECs in this work. Lowered electric field also leads to lower current density, which results in a lowered brightness. However, thicker emissive layer is beneficial in preventing exciton quenching near electrodes. Thus, device efficiency of **Device 2-S** is higher than that of LECs based on the same complex.[34] Hole injection efficiency of standard LECs based on complex **1** and **2** was tailored by adding an HIL (TPD) between the PEDOT:PSS and the emissive layer (**Device 1-H** vs. **1-S** and **Device 2-H** vs. **2-S**, Fig. 6-2). For the LECs based on complex **1**, device current was significantly enhanced by inserting an HIL (Fig. 6-4(a)). Although a slight voltage drop across a thin neutral HIL (20 nm) would exist, reduced hole injection barrier would still play a major role in device characteristics and thus the device current was enhanced. However, device current of LECs based on complex **2** remained approximately unchanged after an HIL was added (Fig. 6-5(a)). Furthermore, since the LECs based on complex **1** without and with an HIL exhibited similar brightness (Fig. 6-4(b)), the EQE of the device with an HIL, which exhibited a much higher device current, was much lower than that of the device without an HIL (Fig. 6-4(c)). On the other hand, for the LECs based on complex **2**, only slight discrepancies in brightness and consequent device efficiency were measured for devices without and with an HIL (Fig. 6-5(b) and

6-5(c)). These results reveal that the device characteristics of the LECs based on complex **2** are insensitive to hole injection barrier while carrier balance is significantly altered by insertion of an HIL for the LECs based on complex **1**.

For CTMCs with lower energy gaps, e.g., complex **2**, the energy barrier for hole injection is moderate (0.48 eV) and thus an ohmic contact for hole injection would be formed by the p-type doped layer. Similar maximum device current and time required for brightness to reach the maximum value for standard LECs based on complex **2** without and with an HIL (**Device 2-S** and **2-H**, Table 6-1) reveal similar hole injection efficiency and formation rates of the p-type doped layer, confirming ohmic contacts for hole injection for both devices. Thus, additional HIL has little effect on the p-type electrochemical doping processes and consequent carrier balance, leading to almost unchanged device efficiency (**Device 2-S** and **2-H**, Fig. 6-5(c)). Both standard LECs based on complex **2** without and with an HIL showed similarly high EQEs up to c.a. 9%, which are approaching the upper limit (9.8%) expected from the PLQY of the emissive layer (0.49) and an optical outcoupling efficiency of ~20% from a typical layered light-emitting device structure. Such high device efficiencies imply superior carrier balance of standard LECs based on complex **2**. Since the energy barrier for electron injection (1.22 eV) is much larger than that for hole injection

(0.48 eV) in standard LECs based on complex **2** (**Device 2-S**, Fig. 6-2), complex **2** would possess electron-preferred transporting characteristics to compensate imbalanced hole-preferred carrier injection, resulting in good carrier balance.

On the other hand, for CTMCs with higher energy gaps, e.g., complex **1**, the p-type doped layer would not be capable of providing an ohmic contact with the anode when hole injection barrier is large (0.85 eV, **Device 1-S**, Fig. 6-2). Higher maximum device current and shorter time required for brightness to reach the maximum value for standard LECs based on complex **1** with an HIL as compared to those without an HIL (**Device 1-H** vs. **1-S**, Table 1) reveal higher hole injection efficiency and faster formation of the p-type doped layer. Additional HIL significantly accelerates the p-type electrochemical doping processes since fewer accumulated anions near the anode are required to enhance hole injection for devices with smaller hole injection barrier (**Device 1-H**). As the p-type layer is well established, hole injection efficiency of standard LECs with an HIL is much higher than that without an HIL, confirming that ohmic contact for hole injection can not be achieved in devices with higher hole injection barrier (**Device 1-S**). Therefore, addition of an HIL in LECs based on complex **1** leads to altered carrier balance and device efficiency (**Device 1-H** vs. **1-S**, Fig. 6-4(c)). Since complex **1** has been reported to exhibit hole-preferred

transporting characteristics,[102] the carrier recombination zone in standard LECs based on complex **1** would locate near the cathode due to smaller hole injection barrier (**Device 1-S**, Fig. 6-2). Exciton quenching occurs when the carrier recombination zone approaches electrodes and the device efficiency consequently deteriorates.[12,127] Standard LECs based on complex **1** showed EQEs of c.a. 8.5%, which are much lower than that (15%) expected from the PLQY of the thin film of complex **1** (0.75)[102] and an optical outcoupling efficiency of ~20% from a typical layered light-emitting device structure. Such lowered device efficiency confirms poor carrier balance of standard LECs based on complex **1**. With an HIL, the carrier recombination zone of the LECs based on complex **1** (**Device 1-H**, Fig. 6-2) would be further pushed towards the cathode due to enhanced hole injection efficiency, resulting in more severer exciton quenching and even deteriorated EQE (c.a. 6.8%, Table 6-1). These results suggest that an ohmic contact for hole injection of LECs based on CTMCs could be formed only when the energy barrier for hole injection is not large. For most blue-emitting CTMCs, in which the HOMO levels are stabilized by fluoro substitution to increase energy gaps,[18,22,23,36,39,102,151,152,154] the energy barrier for hole injection is commonly large in standard LECs, e.g., utilizing ITO as anode materials. Hence, carrier balance of standard LECs based

on CTMCs with higher energy gaps can be feasibly adjusted by tailoring hole injection efficiency with proper HILs. However, enhanced hole injection efficiency may not necessarily lead to improved device efficiency, e.g., for LECs based on CTMCs with hole-preferred transporting characteristics. For such LECs, large hole injection barrier to reduce the number of holes would be beneficial in compensating for excess holes in the emissive layer, resulting in better carrier balance.

6.3.3 Effects of Improved Electron Injection on Device Characteristics of LECs

Electron injection efficiency of standard LECs based on complex **1** and **2** was tailored by inserting a low-work-function EIL (Ca) at the cathode (**Device 1-E** and **Device 2-E**, Fig. 6-2). Both devices employing Ca cathodes showed much higher device current as compared to standard devices with Ag cathodes (Fig. 6-4(a) and Fig. 6-5(a)) due to enhanced electron injection. However, when an EIL was incorporated, the device efficiency of LECs base on complex **1** increased while that of LECs base on complex **2** decreased as compared to their standard Ag-cathode counterparts (**Device 1-E** vs. **1-S**, Fig. 6-4(c) and **Device 2-E** vs. **2-S**, Fig. 6-5(c)). Therefore, addition of EILs in standard LECs based on complex **1** and **2** alters carrier balance of both devices. Since standard LEC

devices based on both complexes, which exhibit similar LUMO levels, possess high electron injection barriers when Ag is used as cathode (1.29 and 1.22 eV for complex **1** and **2**, respectively, Fig. 6-2), these results indicate that the n-type doped layer would not be capable of providing an ohmic contact with the cathode when electron injection barrier is high. Significantly higher maximum device current and much shorter time required for brightness to reach the maximum value for the LECs based on complex **1** and **2** with Ca cathodes as compared to those with Ag cathodes (**Device 1-E vs. 1-S** and **Device 2-E vs. 2-S**, Table 6-1) indicate higher electron injection efficiency and faster formation of the n-type doped layer. Low-work-function Ca cathode significantly accelerates the n-type electrochemical doping processes since much fewer accumulated cations near the cathode are required to enhance electron injection for almost eliminated electron injection barrier (**Device 1-E** and **Device 2-E**, Fig. 6-2). As the n-type layer is well established, electron injection efficiency of the LECs with Ca cathodes is much higher than that with Ag cathodes, confirming that ohmic contact for electron injection can not be achieved in devices with higher electron injection barrier (**Device 1-S** and **2-S**). Thus, addition of an EIL leads to altered carrier balance and device efficiency (**Device 1-E vs. 1-S**, Fig. 6-4(c) and **Device 2-E vs. 2-S**, Fig. 6-5(c)).

For the LECs based on complex **1**, enhanced electron injection induced by the Ca cathode pushes the carrier recombination zone away from the cathode and consequently mitigates exciton quenching, leading to improved device efficiency as compared to the devices with Ag cathodes (**Device 1-E** vs. **1-S**, Fig. 6-2). On the contrary, for the LECs based on complex **2**, enhanced electron injection induced by the Ca cathode deteriorates carrier balance and the carrier recombination zone is shifted to the proximity of the anode, resulting in severe exciton quenching and thus declined device efficiency (**Device 2-E** vs. **2-S**, Fig. 6-2). Improved device efficiencies of LECs based on CTMCs have been reported when low-work-function cathode metals were utilized.[13,16,36] These results also suggest that electron injection of LECs with higher injection barrier, e.g., using inert high-work-function cathodes, would not be ohmic and thus carrier balance would be altered when electron injection efficiency is adjusted. Additionally, in this work, we demonstrate that enhanced electron injection efficiency may not necessarily lead to improved device efficiency. Enhancing electron injection efficiency is beneficial in improving carrier balance of LECs based on CTMCs with hole-preferred transporting characteristics, e.g., complex **1**. Increased amount of injected electrons would compensate for imbalanced hole-preferred transporting characteristics of CTMCs, leading to better carrier

balance. However, for LECs based on CTMCs with electron-preferred transporting characteristics, e.g., complex **2**, enhanced electron injection efficiency would result in excess electron and thus would deteriorate carrier balance. For such devices, inert high-work-function cathodes, which are ineffective in electron injection, would be used instead to reduce the number of electrons in the emissive layer and thus to improve carrier balance.

6.3.4 Effects of Improved Hole and Electron Injection on Device Characteristics of LECs

Hole and electron injection efficiencies of standard LECs based on complex **1** and **2** were simultaneously tailored by adopting both an HIL and an EIL (**Device 1-HE** and **Device 2-HE**, Fig. 6-2). For the LECs based on complex **1** with an HIL and an EIL, the device current was higher than that of the HIL-only (**Device 1-H**) and the EIL-only devices (**Device 1-E**), confirming that both hole and electron injection efficiencies are enhanced (Fig. 6-4(a)). For the LECs based on complex **2** with an HIL and an EIL, the device current was also higher than that of the HIL-only devices (**Device 2-H**), indicating improved electron injection (Fig. 6-5(a)). However, the device current of the LECs based on complex **2** with an HIL and an EIL was similar to that of the EIL-only devices (**Device 2-E**) (Fig. 6-5(a)). It reveals that enhanced device current of

LECs based on complex **2** employing both an HIL and an EIL is dominated by increased electron current and the HIL shows little effect on altering hole injection efficiency, which is consistent with the results of comparison of the standard LECs based on complex **2** without and with an HIL (**Device 2-S** vs. **2-H**, Fig. 6-5(a)). The LECs based on complex **1** with an HIL and an EIL exhibited faster device response as compared to the HIL-only (**Device 1-H**) and the EIL-only devices (**Device 1-E**) since much fewer accumulated cations near the cathode and anions near the anode are required to enhance injection efficiency of electron and hole, respectively (Table 6-1). Faster device response was also observed for the LECs based on complex **2** with an HIL and an EIL when compared with the HIL-only devices (**Device 2-H**) (Table 6-1) for the same reason. However, it is noted that though the HIL has little effect on hole injection efficiency, the LECs based on complex **2** with an HIL and an EIL still exhibited faster device response than the EIL-only devices (**Device 2-E**) (Table 6-1). Since the electron injection barrier is rather small when Ca is used as the cathode, the n-type doped layer capable of achieving ohmic contact for electron injection would be rapidly formed at the cathode and thus most voltage drop takes place across the thinner intrinsic emissive layer before the p-type doped layer for efficient hole injection is well established.[153] Thus, with an

HIL for reducing the hole injection barrier, higher electric field in the thinner intrinsic emissive layer would accelerate accumulation of enough anions to form the p-type doped layer for efficient hole injection, leading to faster device response. After reaching the steady state, hole injection of both devices at the anode would approach ohmic due to relatively smaller hole injection barriers and thus the maximum device current of both devices were similar (**Device 2-E** and **Device 2-HE**, Fig. 6-5(a)). On the contrary, standard LECs based on complex **2** without and with an HIL (**Device 2-S** and **2-H**) exhibited comparable device response (Table 6-1). Since both devices employing Ag cathodes possess high electron injection barrier, device response is mainly dominated by the slower formation of the n-type doped layer. Similar device response times of both devices were thus measured (**Device 2-S** and **2-H**, Table 6-1).

The LECs based on complex **1** employing both an HIL and an EIL showed better device efficiency than the EIL-only devices (**Device 1-E**). It reveals that significantly enhanced electron injection in the EIL-only devices would result in more electrons than holes in the emissive layer and the carrier recombination zone would consequently be closer to the p-type doped layer. With an additional HIL, the number of injected holes increases and the carrier recombination zone would be moved toward the center of the emissive layer, rendering reduced

exciton quenching and thus higher device efficiency. Compared with the EQE of the standard LECs based on complex 1 (ca. 8.5%), the EQE of the LECs based on complex 1 employing both an HIL and an EIL (10.5%) was enhanced by 24% (**Device 1-HE** vs. **Device 1-S**, Table 6-1). Such result confirms that properly modifying carrier injection efficiency according to the carrier transporting characteristics of the emissive materials would be useful in optimizing device efficiencies of the LECs based on CTMCs. On the other hand, the LECs based on complex 2 employing both an HIL and an EIL exhibited similar device efficiencies as compared to the EIL-only devices (**Device 2-E**). Since the hole injection barrier is relatively low for the standard LECs based on complex 2, an ohmic contact for hole injection would be achieved with the p-type doped layer whether the HIL is added or not. Therefore, carrier balance of the LECs based on complex 2 employing both an HIL and an EIL would be similar to that of the EIL-only devices (**Device 2-HE** vs. **Device 2-E**, Fig. 6-2). Significantly reduced device efficiencies of both LECs (5.37 and 5.66% for **Device 2-E** and **Device 2-HE**, respectively) in comparison with standard LECs based on complex 2 (ca. 9.2%, **Device 2-S**) indicate that over-enhancing of electron injection of the LECs based on CTMCs with electron-preferred transporting characteristics would deteriorate carrier balance. Similarly, over-enhancing of hole injection of the

LECs based on CTMCs with hole-preferred transporting characteristics would also lead to poor carrier balance (**Device 1-H**, Fig. 6-2). To optimize device efficiency, carrier injection efficiency should be tailored to compensate for the imbalance in carrier transporting characteristics of the CTMCs. Such technique would be useful in optimizing LECs with higher carrier injection barriers since electrochemically doped layers would not be capable of providing ohmic contacts for carrier injection and carrier injection efficiency and consequent carrier balance would be feasibly modified by employing proper carrier injection layers.

6.3.5 Effects of Impeded Hole, Electron and Both Hole and Electron Injection on Device Characteristics of LECs

Since LECs based on complex **2** exhibited deteriorated carrier balance with enhance hole and/or electron injection, it would be interesting to study the device characteristics when carrier injection is impeded. Impeded hole and electron injection of LECs based on complex **2** was achieved by inserting a hole transporting layer with a high ionization potential (mCP) at the anode and employing a high-work-function metal (Au) at the cathode, respectively (**Device 2-IH**, **Device 2-IE** and **Device 2-IHE**, Fig. 6-2). As shown in Fig. 6-6(a), LECs based on complex **2** with impeded hole (**Device 2-IH**) and electron injection

(**Device 2-IE**) showed lowered device current as compared to the standard LECs based on complex **2** (**Device 2-S**) under the same bias voltage. With impeded both hole and electron injection (**Device 2-IHE**), the device current further declined. It further revealed that electrochemically doped layers would not be capable of providing ohmic contacts for large carrier injection barrier (> 0.7 eV, Fig. 6-2). Compared with **Device 2-S**, LECs based on complex **2** with impeded carrier injection also exhibited slower device response (Fig. 6-6(b) and Table 6-1) since the time required for accumulation of mobile ions near electrodes to facilitate carrier injection is lengthened when carrier injection barrier is large. Furthermore, much lower brightness of LECs based on complex **2** with impeded carrier injection implied significantly deteriorated device efficiency as compared to **Device 2-S**. As shown in Fig. 6-6(c), LECs based on complex **2** with impeded hole or electron injection showed low EQEs $< 5\%$, which is only half of that obtained in **Device 2-S**. With a large hole injection barrier, carrier balance of **Device 2-S** would be deteriorated and thus the carrier recombination zone would be pushed toward the anode, resulting in exciton quenching and lowered EQEs (**Device 2-IH**, Fig. 6-2). On the other hand, significantly increased electron injection barrier would shift the carrier recombination zone toward the cathode and would consequently lead to exciton quenching and lowered EQEs as well

(**Device 2-IE**, Fig. 6-2). Since enhancement in carrier injection barrier is more significant for electron (**Device 2-IE**) than for hole (**Device 2-IH**) as compared to **Device 2-S**, which possesses superior carrier balance, deteriorating in device efficiency would be more severer in **Device 2-IE** (Table 6-1). It is interesting that simultaneous enhancement in hole and electron injection barrier of LECs based on complex 2 (**Device 2-IHE**) lead to slight increase in device efficiency when compared to the devices with independently impeded hole or electron injection (**Device 2-IH** or **2-IE**) (Table 6-1). However, device efficiency of **Device 2-IHE** is still far below that of **Device 2-S**. These results indicate that simultaneous enhancement in hole and electron injection barrier is beneficial in improving deteriorated carrier balance of **Device 2-IH** and **2-IE**. However, improvement in device efficiency is not significant since the carrier recombination zone would be only slightly shifted away from the cathode due to imbalanced carrier injection (**Device 2-IHE**, Fig. 6-2). The results mentioned in above sections reveal that alternation (either increase or decrease) of carrier injection efficiency of LECs with superior carrier balance, e.g., **Device 2-S**, which exhibited high EQEs approaching the upper limit estimated from the PLQY of the emissive layer, would deteriorate carrier balance and thus worse device efficiency would be obtained.

With judiciously tailored carrier balance, the peak EQEs of our sky-blue and orange LECs reached 10.5 and 9.16%, respectively. These results are approaching the state-of-the-art EQEs reported previously for sky-blue (12.75%)[54] and orange LECs (10.4%).[62] Thus, proposed strategy of tailoring carrier balance by adjusting carrier injection efficiency is efficient in improving device efficiencies of LECs. However, compared with high EQEs ~20% achieved in conventional sky-blue[162] and orange[163] OLEDs, in which host-guest emissive layers are generally used, device efficiencies of neat-film LECs still have much room for improvement due to self-quenching of excitons in condensed neat films. To further enhance device efficiencies of LECs, electrochemically stable high-gap ionic host materials would be highly required, especially for blue-green LECs, to reduce self-quenching effect. High energy barrier for carrier injection from electrodes would be a general problem for high-gap hosts, in which electrochemically doped layers would not be capable of providing ohmic contacts for carrier injection. Tailoring carrier balance by adjusting carrier injection efficiency would also be effective in improving device efficiencies of host-guest LECs. It would be a potential technique for host-guest LECs to achieve device efficiencies comparable with conventional OLEDs in the future.

6.4 Summary

In summary, we have demonstrated the influence of carrier injection efficiency on the performance of LECs employing two CTMCs (complex **1** and **2**) with oppositely preferred carrier transporting characteristics. Even with electrochemically doped layers, ohmic contact for carrier injection could be formed only when carrier injection barrier is relatively lower. Adding carrier injection layers in LECs with relatively higher carrier injection barriers would enhance carrier injection efficiency and would affect carrier balance, consequently resulting in altered device efficiency. Furthermore, comparison of device characteristics of LECs based on complex **1** and **2** in various device structures indicates that carrier injection efficiency of CTMC-based LECs should be modified according to carrier transporting characteristics of CTMCs to optimize device efficiency. Hole-preferred transporting CTMCs should be combined with an LEC structure with relatively higher electron injection efficiency while relatively higher hole injection efficiency would be required for LECs based on electron-preferred transporting CTMCs. With properly tailored carrier balance, the carrier recombination zone would locate near the center of the emissive layer and exciton quenching near electrodes would be significantly mitigated, rendering an improved device efficiency approaching the upper limit

expected from the PLQY of the emissive layer and the optical outcoupling efficiency.



Table 6-1 Summary of the LEC device characteristics.

Device	Bias (V)	$\lambda_{\max, \text{EL}}$ (nm)	t_{\max} (min) ^a	J_{\max} (mA cm ⁻²) ^b	L_{\max} (cd m ⁻²) ^c	$\eta_{\text{ext, max}}$ (%) ^d	$\eta_{\text{p, max}}$ (lm W ⁻¹) ^e	Lifetime (min) ^f
1-S	3.5	483	36	0.31	19.63	8.52	16.96	27
1-H	3.5	487	29	0.45	19.05	6.76	13.55	18
1-E	3.5	484	18	0.57	73.98	9.58	18.79	12
1-HE	3.5	482	14	0.65	108.94	10.50	20.64	6
2-S	2.4	586	510	0.08	16.45	9.16	26.91	– ^g
2-H	2.4	589	532	0.08	14.26	8.68	24.91	– ^g
2-E	2.4	596	102	0.26	16.25	5.37	13.70	204
2-HE	2.4	595	73	0.27	16.52	5.66	14.83	115
2-IH	2.4	588	530	0.066	7.33	4.94	14.50	– ^g
2-IE	2.4	585	544	0.064	6.67	4.68	13.74	– ^g
2-IHE	2.4	585	600	0.056	6.61	5.27	15.48	– ^g

[a] Time required to reach the maximal brightness. [b] Maximal current density achieved at a constant bias voltage. [c] Maximal brightness achieved at a constant bias voltage. [d] Maximal external quantum efficiency achieved at a constant bias voltage. [e] Maximal power efficiency achieved at a constant bias voltage. [f] The time for the brightness of the device to decay from the maximum to half of the maximum under a constant bias voltage. [g] Lifetime can not be determined since the brightness has not decreased to half of the maximum value during measuring.

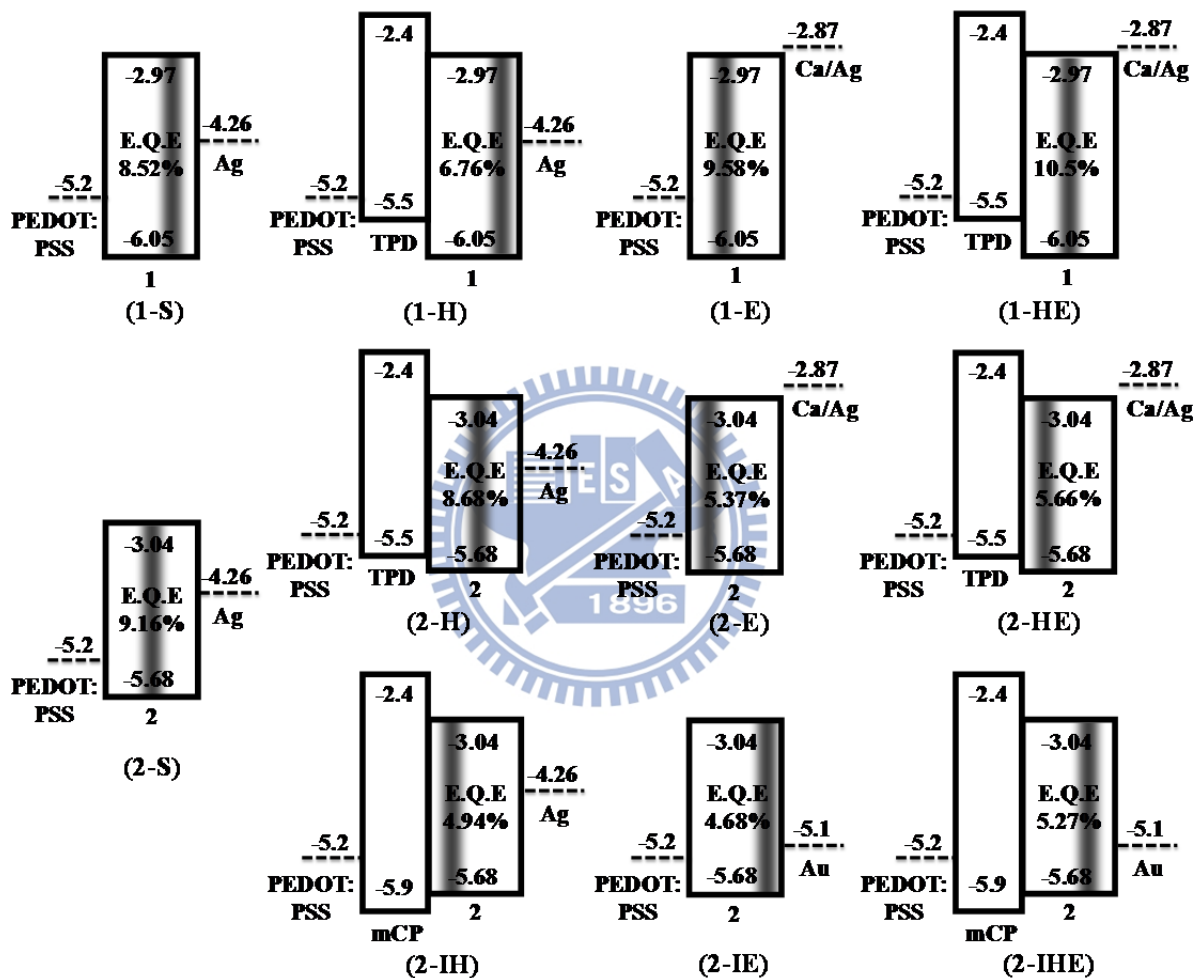


Figure 6-2 Device configurations, energy level alignments and schematic diagrams of the position of carrier recombination zone for the LECs under study. Electrochemically doped regions near electrodes are omitted for clarity.

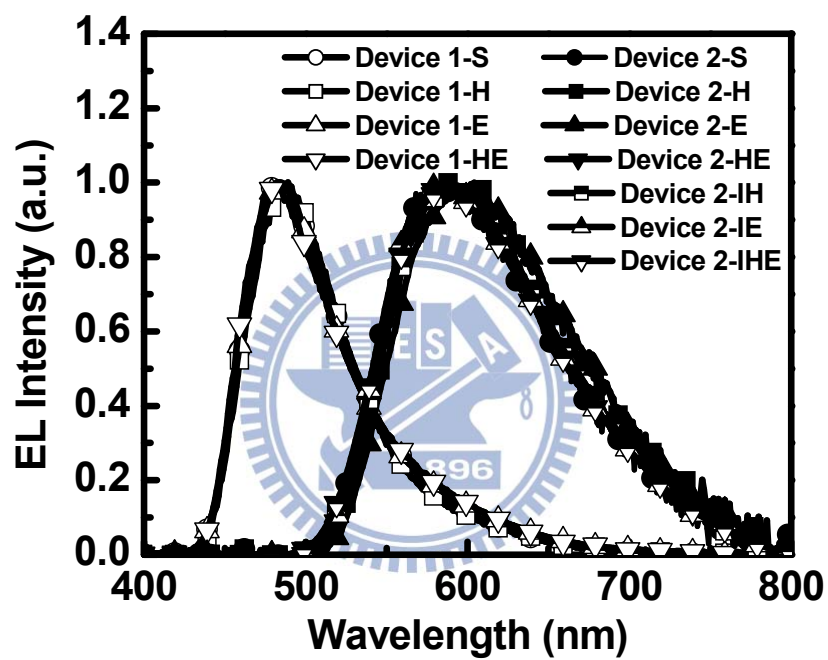


Figure 6-3 EL spectra of Device 1-S, 1-H, 1-E and 1-HE at 3.5 V and Device 2-S, 2-H, 2-E, 2-HE, 2-IH, 2-IE, 2-IHE at 2.4 V.

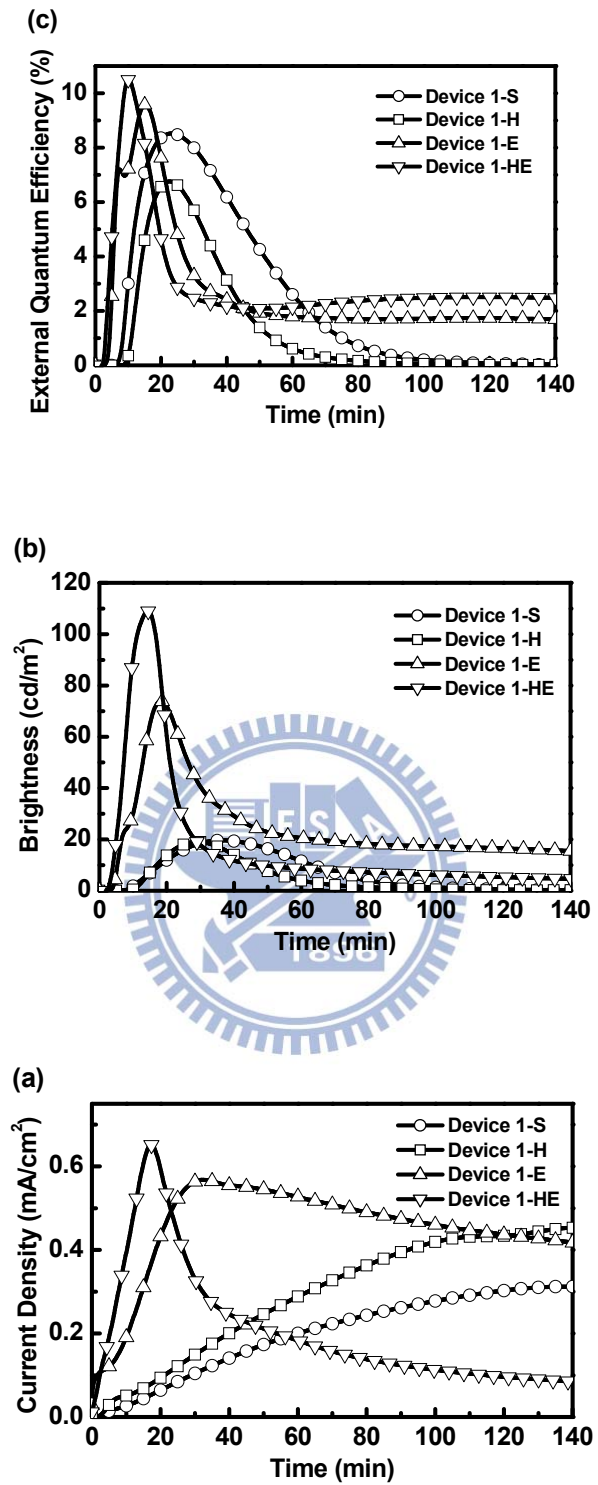


Figure 6-4 (a) Current density, (b) brightness and (c) external quantum efficiency as a function of time for **Device 1-S**, **1-H**, **1-E** and **1-HE** at 3.5 V.

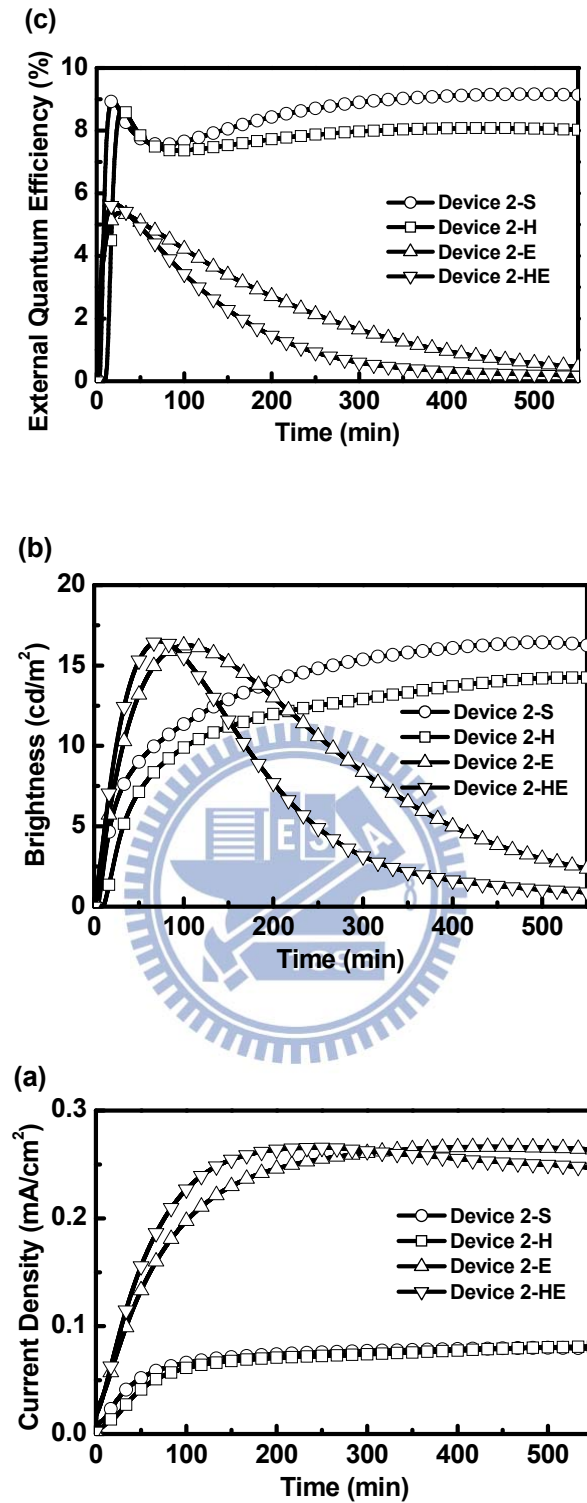


Figure 6-5 (a) Current density, (b) brightness and (c) external quantum efficiency as a function of time for **Device 2-S**, **2-H**, **2-E** and **2-HE** at 2.4 V.

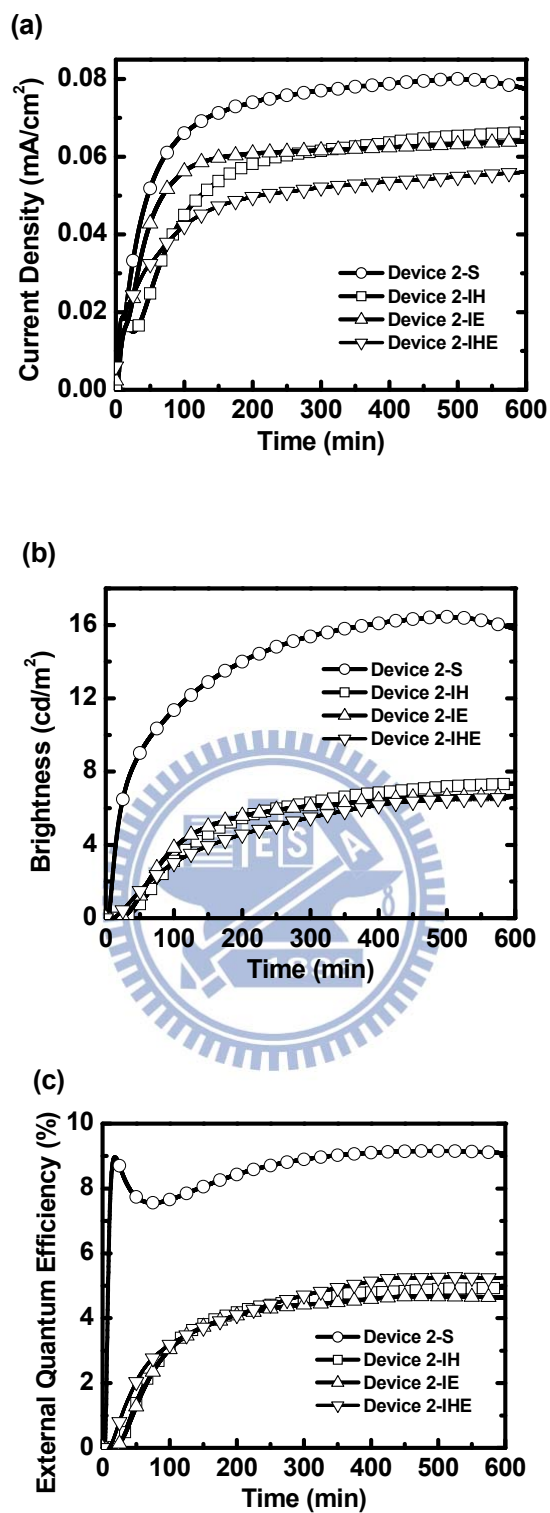


Figure 6-6 (a) Current density, (b) brightness and (c) external quantum efficiency as a function of time for **Device 2-S**, **2-IH**, **2-IE** and **2-IHE** at 2.4 V.

Chapter 7 Summary

In this thesis, we studied the high-gap ionic materials and carrier balance in LECs.

In chapter 2, we obtained saturated deep-blue EL from solid state LECs incorporating the ionic terfluorene derivative **1**. The peak external quantum efficiency and peak power efficiency of **1** in the presence of the ionic liquid reached 1.14% and 1.24 lm W^{-1} , respectively. These CIE coordinates are the most saturated blue emissions ever reported from LECs.

In chapter 3, UV LECs were, for the first time, achieved by the ionic 2,2'-bifluorene derivative. LEC devices incorporating bifluorene **1** exhibited UV EL emissions at 386 and 388 nm with maximum EQE and power efficiencies of 0.66 % and 0.23 lm W^{-1} . The EL emissions in the UV region are successfully achieved by LECs based on **1**, which are so far the shortest emission wavelength achieved in LECs.

In chapter 4, we report efficient host-guest solid-state LECs utilizing a cationic terfluorene derivative as the host and a red-emitting cationic transition metal complex as the guest. Experimental results confirm that in addition to reducing self-quenching of guest molecules, the strategy of utilizing a carrier transporting host doped with a proper carrier trapping guest would improve

balance of carrier mobilities in the host-guest emissive layer, offering an effective approach for optimizing device efficiencies of LECs.

In chapter 5, we demonstrate improving balance of carrier mobilities in neat-film LECs utilizing a CTMC as the emissive material and a cationic near-infrared laser dye as the carrier trapper. Experimental results confirm that balance of carrier mobilities in the CTMC neat films would be improved by doping a proper carrier trapper and such technique offers a general approach for optimizing device efficiencies of CTMC-based neat-film LECs.

In chapter 6, we study the influence of carrier injection efficiency on the performance of LECs based on a hole-preferred transporting CTMC $[\text{Ir}(\text{dfppz})_2(\text{dtb-bpy})]^+(\text{PF}_6^-)$ (complex 1) and an electron-preferred transporting CTMC $[\text{Ir}(\text{ppy})_2(\text{dasb})]^+(\text{PF}_6^-)$ (complex 2). Experimental results show that even with electrochemically doped layers, ohmic contacts for carrier injection could be formed only when carrier injection barriers are relatively lower. Thus, adding carrier injection layers in LECs with relatively higher carrier injection barriers would affect carrier balance and thus would result in altered device efficiency.

References

1. Q. Pei, G. Yu, C. Zhang, Y. Yang and A. J. Heeger, "Polymer light-emitting electrochemical cells", *Science*, **269**, 1086 (1995).
2. J. D. Slinker, J. A. DeFranco, M. J. Jaquith, W. R. Silveira, Y. W. Zhong, J. M. Moran-Mirabal, H. G. Craighead, H. D. Abruna, J. A. Marohn and G. G. Malliaras, "Direct measurement of the electric-field distribution in a light-emitting electrochemical cell", *Nat. Mater.*, **6**, 894 (2007).
3. P. Matyba, K. Maturova, M. Kemerink, N. D. Robinson and L. Edman, "The dynamic organic p-n junction", *Nat. Mater.*, **8**, 672 (2009).
4. J. D. Slinker, J. Rivnay, J. S. Moskowitz, J. B. Parker, S. Bernhard, H. D. Abruna and G. G. Malliaras, "Electroluminescent devices from ionic transition metal complexes", *J. Mater. Chem.*, **17**, 2976 (2007).
5. J. Slinker, D. Bernards, P. L. Houston, H. D. Abruna, S. Bernhard and G. G. Malliaras, "White-light emission from an assembly comprising luminescent Iridium and Europium complexes", *Chem. Commun.*, 2392 (2003).
6. C. Ulbricht, B. Beyer, C. Friebe, A. Winter and U. S. Schubert, "Recent developments in the application of phosphorescent Iridium(III) complex systems", *Adv. Mater.*, **21**, 4418 (2009).
7. E. Holder, B. M. W. Langeveld and U. S. Schubert, "New trends in the use of

- transition metal–ligand complexes for applications in electroluminescent devices”, *Adv. Mater.*, **17**, 1109 (2005).
8. M. S. Lowry and S. Bernhard, “synthetically tailored excited states: phosphorescent, cyclometalated Iridium(III) complexes and their applications”, *Chem.–Eur. J.*, **12**, 7970 (2006).
9. J. K. Lee, D. S. Yoo, E. S. Handy and M. F. Rubner, “Thin film light emitting devices from an electroluminescent ruthenium complex”, *Appl. Phys. Lett.*, **69**, 1686 (1996).
10. E. S. Handy, A. J. Pal and M. F. Rubner, “Solid-state light-emitting devices based on the tris-Chelated Ruthenium(II) complex. 2. tris(bipyridyl)ruthenium(II) as a high-brightness emitter”, *J. Am. Chem. Soc.*, **121**, 3525 (1999).
11. F. G. Gao and A. J. Bard, “Solid-state organic light-emitting diodes based on tris(2,2'-bipyridine)ruthenium(II) complexes”, *J. Am. Chem. Soc.*, **122**, 7426 (2000).
12. H. Rudmann and M. F. Rubner, “Single layer light-emitting devices with high efficiency and long lifetime based on tris(2,2' bipyridyl) ruthenium(II) hexafluorophosphate”, *J. Appl. Phys.*, **90**, 4338 (2001).
13. C. Y. Liu and A. J. Bard, “Individually addressable submicron scale

- light-emitting devices based on electroluminescence of solid $\text{Ru}(\text{bpy})_3(\text{ClO}_4)_2$ Films”, *J. Am. Chem. Soc.*, **124**, 4190 (2002).
- 14.H. Rudmann, S. Shimada and M. F. Rubner, “Solid-state light-emitting devices based on the tris-Chelated Ruthenium(II) complex. 4. High-efficiency light-emitting devices based on derivatives of the tris(2,2'-bipyridyl) Ruthenium(II) complex”, *J. Am. Chem. Soc.*, **124**, 4918 (2002).
- 15.C. Y. Liu and A. J. Bard, “Highly efficient and bright electroluminescent $\text{Ru}(\text{bpy})_3(\text{ClO}_4)/\text{Alq}^3$ device”, *Appl. Phys. Lett.*, **87**, 061110 (2005).
- 16.S. Bernhard, X. C. Gao, G. G. Malliaras and H. D. Abruna, “Efficient electroluminescent devices based on a chelated Osmium(II) complex”, *Adv. Mater.*, **14**, 433 (2002).
- 17.L. He, L. Duan, J. Qiao, R. J. Wang, P. Wei, L. D. Wang and Y. Qiu, “Blue-emitting cationic Iridium complexes with 2-(1H-Pyrazol-1-yl)pyridine as the ancillary ligand for efficient light-emitting electrochemical cells”, *Adv. Funct. Mater.*, **18**, 2123 (2008).
- 18.L. He, J. Qiao, L. Duan, G. F. Dong, D. Q. Zhang, L. D. Wang and Y. Qiu, “Toward highly efficient solid-state white light-emitting electrochemical cells: Blue-green to red emitting cationic Iridium complexes with Imidazole-type

- ancillary ligands”, *Adv. Funct. Mater.*, **19**, 2950 (2009).
- 19.M. A. Baldo, D. F. O’Brien, Y. You, A. Shoustikov, S. Sibley, M. E. Thompson and S. R. Forrest, “Highly efficient phosphorescent emission from organic electroluminescent devices”, *Nature*, **395**, 151 (1998).
- 20.J. K. Lee, D. S. Yoo, E. S. Handy and M. F. Rubner, “Thin film light emitting devices from an electroluminescent ruthenium complex”, *Appl. Phys. Lett.*, **69**, 1686 (1996).
- 21.V. Kalsani, M. Schmittel, A. Listorti, G. Accorsi and N. Armaroli, “Novel phenanthroline ligands and their kinetically locked Copper(I) complexes with unexpected photophysical properties”, *Inorg. Chem.*, **45**, 2061 (2006).
- 22.A. B. Tamayo, S. Garon, T. Sajoto, P. I. Djurovich, I. M. Tsyba, R. Bau and M. E. Thompson, “Cationic bis-cyclometalated Iridium(III) diimine complexes and their use in efficient blue, green, and red electroluminescent devices”, *Inorg. Chem.*, **44**, 8723 (2005).
- 23.H. C. Su, H. F. Chen, F. C. Fang, C. C. Liu, C. C. Wu, K. T. Wong, Y. H. Liu and S. M. Peng, “Solid-state white light-emitting electrochemical cells using Iridium-based cationic transition metal complexes”, *J. Am. Chem. Soc.*, **130**, 3413 (2008).
- 24.R. D. Costa, F. J. Cespedes-Guirao, E. Orti, H. J. Bolink, J. Gierschner, F.

- Fernandez-Lazaro and A. Sastre-Santos, "Efficient deep-red light-emitting electrochemical cells based on a perylenediimide-iridium-complex dyad", *Chem. Commun.*, 3886 (2009).
25. J. L. Rodriguez-Redondo, R. D. Costa, E. Orti, A. Sastre-Santos, H. J. Bolink and F. Fernandez-Lazaro, "Red-light-emitting electrochemical cell using a polypyridyl iridium(III) polymer", *Dalton Trans.*, 9787 (2009).
26. H. F. Chen, K. T. Wong, Y. H. Liu, Y. Wang, Y. M. Cheng, M. W. Chung, P. T. Chou and H. C. Su, "Bis(diphenylamino)-9,9'-spirobifluorene functionalized Ir(III) complex: a conceptual design en route to a three-in-one system possessing emitting core and electron and hole transport peripherals", *J. Mater. Chem.*, **21**, 768 (2011).
27. W. J. Xu, S. J. Liu, T. C. Ma, Q. Zhao, A. Pertegas, D. Tordera, H. J. Bolink, S. H. Ye, X. M. Liu, S. Sun and W. Huang, "*p-n* Metallophosphor based on cationic iridium(III) complex for solid-state light-emitting electrochemical cells", *J. Mater. Chem.*, **21**, 13999 (2011).
28. H. F. Chen, K. T. Wong, Y. H. Liu, Y. Wang, Y. M. Cheng, M. W. Chung, P. T. Chou and H. C. Su, "Bis(diphenylamino)-9,9'-spirobifluorene functionalized Ir(III) complex: a conceptual design en route to a three-in-one system possessing emitting core and electron and hole transport peripherals", *J.*

Mater. Chem., **21**, 768 (2011).

29. J. D. Slinker, A. A. Gorodetsky, M. S. Lowry, J. Wang, S. Parker, R. Rohl, S. Bernhard and G. G. Malliaras, "Efficient yellow electroluminescence from a Single Layer of a cyclometalated Iridium complex", *J. Am. Chem. Soc.*, **126**, 2763 (2004).

30. M. S. Lowry, W. R. Hudson, R. A. Pascal and Jr., S. Bernhard, "Accelerated luminophore discovery through combinatorial synthesis", *J. Am. Chem. Soc.*, **126**, 14129 (2004).

31. J. D. Slinker, C. Y. Koh, G. G. Malliaras, M. S. Lowry and S. Bernhard, "Green electroluminescence from an ionic Iridium complex", *Appl. Phys. Lett.*, **86**, 173506 (2005).

32. M. S. Lowry, J. I. Goldsmith, J. D. Slinker, R. Rohl, R. A. Pascal, Jr., G. G. Malliaras and S. Bernhard, "Single-layer electroluminescent devices and photoinduced hydrogen production from an ionic Iridium(III) complex", *Chem. Mater.*, **17**, 5712 (2005).

33. R. D. Costa, E. Orti, H. J. Bolink, S. Graber, S. Schaffner, M. Neuburger, C. E. Housecroft and E. C. Constable, "Archetype cationic Iridium complexes and their use in solid-state light-emitting electrochemical cells", *Adv. Funct. Mater.*, **19**, 3456 (2009).

- 34.H. C. Su, F. C. Fang, T. Y. Hwu, H. H. Hsieh, H. F. Chen, G. H. Lee, S. M. Peng, K. T. Wong and C. C. Wu, “Highly efficient orange and green solid-state light-emitting electrochemical cells based on cationic IrIII complexes with enhanced steric hindrance”, *Adv. Funct. Mater.*, **17**, 1019 (2007).
- 35.R. Terki, L. P. Simoneau and A. Rochefort, “Tailoring the photoluminescence properties of ionic iridium complexes”, *J. Phys. Chem. A*, **113**, 534 (2009).
- 36.M. Mydlak, C. Bizzarri, D. Hartmann, W. Sarfert, G. Schmid and L. De Cola, “Positively charged Iridium(III) triazole derivatives as blue emitters for light-emitting electrochemical cells”, *Adv. Funct. Mater.*, **20**, 1812 (2010).
- 37.C. H. Yang, J. Beltran, V. Lemaire, J. Cornil, D. Hartmann, W. Sarfert, R. Frohlich, C. Bizzarri and L. De Cola, “Iridium metal complexes containing N-Heterocyclic carbene ligands for blue-light-emitting electrochemical cells”, *Inorg. Chem.*, **49**, 9891 (2010).
- 38.C. Rothe, C.-J. Chiang, V. Jankus, K. Abdullah, X. Zeng, R. Jitchati, A. S. Batsanov, M. R. Bryce and A. P. Monkman, “Ionic Iridium(III) complexes with bulky side groups for use in light emitting cells: Reduction of concentration quenching”, *Adv. Funct. Mater.*, **19**, 2038 (2009).
- 39.L. He, L. Duan, J. Qiao, G. Dong, L. Wang and Y. Qiu, “Highly efficient

- blue-green and white light-emitting electrochemical cells based on a cationic Iridium complex with a bulky side group”, *Chem. Mater.*, **22**, 3535 (2010).
- 40.H.-C. Su, F.-C. Fang, T.-Y. Hwu, H.-H. Hsieh, H.-F. Chen, G.-H. Lee, S.-M. Peng, K.-T. Wong and C.-C. Wu, “Highly efficient orange and green solid-state light-emitting electrochemical cells based on cationic IrIII complexes with enhanced steric hindrance”, *Adv. Funct. Mater.*, **17**, 1019 (2007).
- 41.L. He, L. Duan, J. Qiao, D. Q. Zhang, L. D. Wang and Y. Qiu, “Enhanced stability of blue-green light-emitting electrochemical cells based on a cationic iridium complex with 2-(1-phenyl-1H-pyrazol-3-yl)pyridine as the ancillary ligand”, *Chem. Commun.*, **47**, 6467 (2011).
- 42.L. He, L. Duan, J. Qiao, G. F. Dong, L. D. Wang and Y. Qiu, “Highly efficient blue-green and white light-emitting electrochemical cells based on a cationic Iridium complex with a bulky side group”, *Chem. Mater.*, **22**, 3535 (2010).
- 43.L. He, L. Duan, J. Qiao, D. Q. Zhang, L. D. Wang and Y. Qiu, “Highly efficient solution-processed blue-green to red and white light-emitting diodes using cationic iridium complexes as dopants”, *Org. Electron.*, **11**, 1185 (2010).

44. B. Chen, Y. Li, W. Yang, W. Luo and H. Wu, "Efficient sky-blue and blue-green light-emitting electrochemical cells based on cationic iridium complexes using 1,2,4-triazole-pyridine as the ancillary ligand with cyanogen group in alkyl chain", *Org. Electron.*, **12**, 766 (2011).
45. G. Kalyuzhny, M. Buda, J. McNeill, P. Barbara and A. J. Bard, "Stability of thin-film solid-state electroluminescent devices based on tris(2,2'-bipyridine)ruthenium(II) complexes", *J. Am. Chem. Soc.*, **125**, 6272 (2003).
46. N. Rockstroh, K. Peuntinger, H. Gorgs, D. M. Guldi, F. W. Heinemann, B. Schafer and S. Rau, "Structural properties of Ruthenium biimidazole complexes determining the stability of their supramolecular aggregates", *Z. Naturforsch., B: Chem. Sci.*, **65**, 281 (2010).
47. L. J. Soltzberg, J. D. Slinker, S. Flores-Torres, D. A. Bernards, G. G. Malliaras, H. D. Abruna, J. S. Kim, R. H. Friend, M. D. Kaplan and V. Goldberg, "Identification of a quenching species in Ruthenium tris-bipyridine electroluminescent devices", *J. Am. Chem. Soc.*, **128**, 7761 (2006).
48. H. J. Bolink, L. Cappelli, E. Coronado, M. Gratzel, E. Orti, R. D. Costa, P. M. Viruela and M. K. Nazeeruddin, "Stable single-layer light-emitting

electrochemical cell using

4,7-Diphenyl-1,10-phenanthroline-bis(2-phenylpyridine)iridium(III)

Hexafluorophosphate”, *J. Am. Chem. Soc.*, **128**, 14786 (2006).

49.R. D. Costa, E. Orti, D. Tordera, A. Pertegas, H. J. Bolink, S. Graber, C. E. Housecroft, L. Sachno, M. Neuburger and E. C. Constable, “Stable and efficient solid-state light-emitting electrochemical cells based on a series of hydrophobic Iridium complexes”, *Adv. Energy Mater.*, **1**, 282 (2011).

50.H. J. Bolink, E. Coronado, R. D. Costa, E. Orti, M. Sessolo, S. Graber, K. Doyle, M. Neuburger, C. E. Housecroft and E. C. Constable, “Long-living light-emitting electrochemical cells – control through supramolecular interactions”, *Adv. Mater.*, **20**, 3910 (2008).

51.S. Graber, K. Doyle, M. Neuburger, C. E. Housecroft, E. C. Constable, R. D. Costa, E. Orti, D. Repetto and H. J. Bolink, “A supramolecularly-caged ionic Iridium(III) complex yielding bright and very stable solid-state light-Emitting electrochemical cells”, *J. Am. Chem. Soc.*, **130**, 14944 (2008).

52.R. D. Costa, E. Orti, H. J. Bolink, S. Graber, C. E. Housecroft, M. Neuburger, S. Schaffner and E. C. Constable, “Two are not always better than one: ligand optimisation for long-living light-emitting electrochemical cells”, *Chem. Commun.*, 2029 (2009).

- 53.R. D. Costa, E. Orti, H. J. Bolink, S. Graber, C. E. Housecroft and E. C. Constable, “Efficient and long-living light-emitting electrochemical cells”, *Adv. Funct. Mater.*, **20**, 1511 (2010).
- 54.R. D. Costa, E. Orti, H. J. Bolink, S. Graber, C. E. Housecroft and E. C. Constable, “Intramolecular π -stacking in a phenylpyrazole-based Iridium complex and Its use in light-emitting electrochemical cells”, *J. Am. Chem. Soc.*, **132**, 5978 (2010).
- 55.R. D. Costa, E. Orti, H. J. Bolink, S. Graber, C. E. Housecroft and E. C. Constable, “Light-emitting electrochemical cells based on a supramolecularly-caged phenanthroline-based iridium complex”, *Chem. Commun.*, **47**, 3207 (2011).
- 56.J. D. Slinker, A. A. Gorodetsky, M. S. Lowry, J. J. Wang, S. Parker, . Rohl, S. Bernhard and G. G. Malliaras, “Efficient yellow electroluminescence from a single layer of a cyclometalated Iridium complex”, *J. Am. Chem. Soc.*, **126**, 2763 (2004).
- 57.T. H. Kwon, Y. H. Oh, I. S. Shin and J. I. Hong, “New approach toward fast response light-emitting electrochemical cells based on neutral Iridium complexes via cation transport”, *Adv. Funct. Mater.*, **19**, 711 (2009).
- 58.R. D. Costa, A. Pertegás, E. Ortí, H. J. Bolink, “Improving the turn-on time

- of light-emitting electrochemical cells without sacrificing their stability”, *Chem. Mater.* **22**, 1288 (2010).
- 59.Q. Pei, Y. Yang, G. Yu, C. Zhang and A. J. Heeger, “Polymer light-emitting electrochemical cells: In situ formation of a light-emitting p–n junction”, *J. Am. Chem. Soc.*, **118**, 3922 (1996).
- 60.C. W. Tang and S. A. Van Slyke, “Organic electroluminescent diodes”, *Appl. Phys. Lett.*, 51, 913 (1987).
- 61.C.W. Tang, S. A. Van Slyke and C. H. Chen, “Novel current–voltage characteristics in an InP-based resonant-tunneling high electron mobility transistor”, *Appl. Phys. Lett.*, 65, 3610 (1989).
- 62.H.-C. Su, C.-C. Wu, F.-C. Fang and K.-T. Wong, “Efficient solid-state host-guest light-emitting electrochemical cells based on cationic transition metal complexes”, *Appl. Phys. Lett.*, **89**, 261118 (2006).
- 63.H. J. Bolink, L. Cappelli, S. Cheylan, E. Coronado, R. D. Costa, N. Lardiés, M. K. Nazeeruddin and E. Ortí, “Origin of the large spectral shift in electroluminescence in a blue light emitting cationic iridium(III) complex”, *J. Mater. Chem.*, **17**, 5032 (2007).
- 64.K. A. King and R. J. Watts, “Dual emission from an ortho-metalated iridium(III) complex”, *J. Am. Chem. Soc.*, **109**, 1589 (1987).

- 65.S. Lamansky, P. Djurovich, D. Murphy, F. A. Razzaq, R. Kwong, I. Tsyba, M. Bortz, B. Mui, R. Bau and M. E. Thompson, “Highly phosphorescent bis-cyclometalated Iridium complexes: synthesis, photophysical characterization, and use in organic light emitting diodes”, *Inorg. Chem.*, **40**, 1704 (2001).
- 66.T. Sajoto, P. I. Djurovich, A. Tamayo, M. Yousufuddin, R. Bau and M. E. Thompson, “Blue and near-UV phosphorescence from Iridium complexes with cyclometalated pyrazolyl or N-Heterocyclic carbene ligands”, *Inorg. Chem.*, **44**, 7992 (2005).
- 67.Q. Pei and Y. Yang, “Polymer Light-Emitting Electrochemical Cells: In Situ Formation of a Light-Emitting p–n Junction”, *J. Am. Chem. Soc.*, **118**, 7416 (1996).
- 68.A. W. Grice, D. D. C. Bradley, M. T. Bernius, M. Inbasekaran, W. W. Wu and E. P. Woo, “High brightness and efficiency blue light-emitting polymer diodes”, *Appl. Phys. Lett.*, **73**, 629 (1998).
- 69.U. Scherf and E. J. W. List, “Semiconducting polyfluorenes—towards reliable structure–property relationships”, *Adv. Mater.*, **14**, 477 (2002).
- 70.Y. Yang and Q. B. Pei, “Efficient blue-green and white light-emitting electrochemical cells based on poly [9, 9-bis (3, 6-dioxaheptyl)-fluorene-2,

7-diyl]”, *J. Appl. Phys.*, **81**, 3294 (1997).

71.T. Ouisse, M. Armand, Y. Kervella and O. Stéphan, “Fully transparent, organic light-emitting electrochemical cells”, *Appl. Phys. Lett.*, **81**, 3131 (2002).

72.M. Sun, C. Zhong, F. Li, Y. Cao and Q. Pei, “A fluorene–oxadiazole copolymer for white light-emitting electrochemical cells”, *Macromolecules*, **43**, 1714 (2010).

73.J.-I. Lee, D.-H. Hwang, H. Park, L.-M. Do, H. Y. Chu, T. Zyung and R. D. Miller, “Light-emitting electrochemical cells based on poly(9,9-bis(3,6-dioxaheptyl)-fluorene-2,7-diyl) ”, *Synth. Met.*, **111**, 195 (2000).

74.O. Stéphan, V. Collomb, J. Vial and M. Armand, “Blue-green light-emitting diodes and electrochemical cells based on a copolymer derived from fluorene”, *Synth. Met.*, **113**, 257 (2000).

75.D. Vak, S.-H. Oh and D.-Y. Kim, “Efficient single-component light-emitting electrochemical cells with an ion-conducting water-soluble polyfluorene”, *Appl. Phys. Lett.*, **94**, 243305 (2009).

76.K.-T. Wong, Y.-Y. Chien, R.-T. Chen, C.-F. Wang, Y.-T. Lin, H.-H. Chiang, P.-Y. Hsieh, C.-C. Wu, C. H. Chou, Y. O. Su, G.-H. Lee and S.-M. Peng,

“Ter(9,9-diarylfluorene)s: Highly efficient blue emitter with promising electrochemical and thermal stability”, *J. Am. Chem. Soc.*, **124**, 11576 (2002).

77.K.-T. Wong, R.-T. Chen, F.-C. Fang, C.-C. Wu and Y.-T. Lin, “4,5-Diazafluorene-Incorporated ter(9,9-diarylfluorene): A novel molecular doping strategy for improving the electron injection property of a highly efficient OLED blue emitter”, *Org. Lett.*, **7**, 1979 (2005).

78.C.-C. Wu, T.-L. Liu, W.-Y. Hung, Y.-T. Lin, K.-T. Wong, R.-T. Chen, Y.-M. Chen and Y.-Y. Chien, “Unusual nondispersive ambipolar carrier transport and high electron mobility in amorphous ter(9,9-diarylfluorene)s”, *J. Am. Chem. Soc.*, **125**, 3710 (2003).

79.C.-C. Wu, W.-G. Liu, W.-T. Hung, T.-L. Liu, Y.-T. Lin, H.-W. Lin, K.-T. Wong, Y.-Y. Chien, R.-T. Chen, T.-H. Hung, T.-C. Chao and Y.-M. Chen, “Spiroconjugation-enhanced intermolecular charge transport”, *Appl. Phys. Lett.*, **87**, 052103 (2005).

80.*Colorimetry*; Commission Internationale de l’Eclairage (CIE): Paris, 1986.

81.K. L. Billingsley, T. E. Barder and S. L. Buchwald, “An improved system for the palladium-catalyzed borylation of aryl halides with pinacol borane”, *Angew. Chem. Int. Ed.*, **46**, 5359 (2007).

- 82.G. Saikia and P. K. Iyer, "Facile C–H alkylation in water: enabling defect-free materials for optoelectronic devices", *J. Org. Chem.*, **75**, 2714 (2010).
- 83.K.-Y. Pu, Z. Fang and B. Liu, "Effect of charge density on energy-transfer properties of cationic conjugated polymers", *Adv. Funct. Mater.*, **18**, 1321 (2008).
- 84.S. T. Parker, J. D. Slinker, M. S. Lowry, M. P. Cox, S. Bernhard and G. G. Malliaras, "Improved turn-on times of Iridium electroluminescent devices by use of ionic liquids", *Chem. Mater.*, **17**, 3187 (2005).
- 85.V. Bulovic, A. Shoustikov, M. A. Baldo, E. Bose, V. G. Kozlov, M. E. Thompson and S. R. Forrest, "Bright, saturated, red-to-yellow organic light-emitting devices based on polarization-induced spectral shifts", *Chem. Phys. Lett.*, **287**, 455 (1998).
- 86.H.-C. Su, H.-F. Chen, C.-C. Wu and K.-T. Wong, "Decreased turn-on times of single-component light-emitting electrochemical cells by tethering an ionic iridium complex with imidazolium moieties", *Chem. Asian J.*, **3**, 1922 (2008).
- 87.C. Yang, Q. Sun, J. Qiao and Y. Li, "Ionic liquid doped polymer light-emitting electrochemical cells", *J. Phys. Chem. B*, **107**, 12981 (2003).

- 88.L. Edman, M. Pauchard, D. Moses and A. J. Heeger, “Planar polymer light-emitting device with fast kinetics at a low voltage”, *J. Appl. Phys.*, **95**, 4357 (2004).
- 89.F. P. Wenzl, P. Pachler, C. Suess, A. Haase, E. J. W. List, P. Poelt, D. Somitsch, P. Knoll, U. Scherf and G. Leising, The influence of the phase morphology on the optoelectronic “Properties of light-emitting electrochemical cells”, *Adv. Funct. Mater.*, **14**, 441 (2004).
- 90.J.-P. Choi, K.-T. Wong, Y.-M. Chen, J.-K. Yu, P.-T. Chou and A. J. Bard, “Electrogenerated chemiluminescence. 76. Excited singlet state emission vs excimer emission in ter(9,9-diarylfuorene)s”, *J. Phys. Chem. B*, **107**, 14407 (2003).
- 91.Q. Sun, H. Wang, C. Yang and Y. Li, “Synthesis and electroluminescence of novel copolymers containing crown ether spacers”, *J. Mater. Chem.*, **13**, 800 (2003).
- 92.M. K. Nazeeruddin, R. T. Wegh, Z. Zhou, C. Klein, Q. Wang, F. De Angelis, S. Fantacci and M. Grätzel, “Efficient green-blue-light-emitting cationic Iridium complex for light-emitting electrochemical cells”, *Inorg. Chem.*, **45**, 9245 (2006).
- 93.Y. Ohsawa, S. Sprouse, K. A. King, M. K. DeArmond, K. W. Hanck and R. J.

- Watts, "Electrochemistry and spectroscopy of ortho-metalated complexes of iridium(III) and rhodium(III)", *J. Phys. Chem.*, **91**, 1047 (1987).
- 94.S. Alem and J. Gao, "The effect of annealing/quenching on the performance of polymer light-emitting electrochemical cells", *Org. Electron*, **9**, 347 (2008).
- 95.Y. Hu and J. Gao, "Direct imaging and probing of the p-n junction in a planar polymer light-emitting electrochemical cell", *J. Am. Chem. Soc.*, **133**, 2227 (2011).
- 96.S. van Reenen, P. Matyba, A. Dzwilewski, R. A. J. Janssen, L. Edman and M. Kemerink, "A unifying model for the operation of light-emitting electrochemical cells", *J. Am. Chem. Soc.*, **132**, 13776 (2010).
- 97.J. Fang, P. Matyba, N. D. Robinson and L. Edman, "Identifying and alleviating electrochemical side-reactions in light-emitting electrochemical cells", *J. Am. Chem. Soc.*, **130**, 4562 (2008).
- 98.C. H. Lyons, E. D. Abbas, J. K. Lee and M. F. Rubner, "Solid-state light-emitting devices based on the trischelated Ruthenium(II) complex. 1. Thin film blends with poly(ethylene oxide)", *J. Am. Chem. Soc.*, **120**, 12100 (1998).
- 99.H.-C. Su, Y.-H. Lin, C.-H. Chang, H.-W. Lin, C.-C.Wu, F.-C. Fang, H.-F.

- Chen and K.-T. Wong, “Solid-state light-emitting electrochemical cells employing phosphor-sensitized fluorescence”, *J. Mater. Chem.*, **20**, 5521 (2010).
100. H.-C. Su, H.-F. Chen, Y.-C. Shen, C.-T. Liao and K.-T. Wong, “Highly efficient double-doped solid-state white light-emitting electrochemical cells”, *J. Mater. Chem.*, **21**, 9653 (2011).
101. C.-C. Ho, H.-F. Chen, Y.-C. Ho, C.-T. Liao, H.-C. Su and K.-T. Wong, “Phosphorescent sensitized fluorescent solid-state near-infrared light-emitting electrochemical cells”, *Phys. Chem. Chem. Phys.*, **13**, 17729 (2011).
102. C.-T. Liao, H.-F. Chen, H.-C. Su and K.-T. Wong, “Tailoring balance of carrier mobilities in solid-state light-emitting electrochemical cells by doping a carrier trapper to enhance device efficiencies”, *J. Mater. Chem.*, **21**, 17855 (2011).
103. C.-T. Liao, H.-F. Chen, H.-C. Su and K.-T. Wong, “Improving the balance of carrier mobilities of host–guest solid-state light-emitting electrochemical cells”, *Phys. Chem. Chem. Phys.*, **14**, 1262 (2012).
104. H.-F. Chen, C.-T. Liao, T.-C. Chen, H.-C. Su, K.-T. Wong and T.-F. Guo, “An ionic terfluorene derivative for saturated deep-blue solid state

- light-emitting electrochemical cells”, *J. Mater. Chem.*, **21**, 4175 (2011).
105. M. A. Baldo, S. Lamansky, P. E. Burrows, M. E. Thompson and S. R. Forrest, “Very high-efficiency green organic light-emitting devices based on electrophosphorescence”, *Appl. Phys. Lett.*, **75**, 4 (1999).
106. R. J. Holmes, S. R. Forrest, Y.-J. Tung, R. C. Kwong, J. J. Brown, S. Garon and M. E. Thompson, “Blue organic electrophosphorescence using exothermic host–guest energy transfer”, *Appl. Phys. Lett.*, **82**, 2422 (2003).
107. S. Tokito, T. Iijima, T. Tsuzuki and F. Sato, “High-efficiency white phosphorescent organic light-emitting devices with greenish-blue and red-emitting layers”, *Appl. Phys. Lett.*, **83**, 2459 (2003).
108. S.-J. Yeh, M.-F. Wu, C.-T. Chen, Y.-H. Song, Y. Chi, M.-H. Ho, S.-F. Hsu and C. H. Chen, “New Dopant and Host Materials for Blue-Light-Emitting Phosphorescent Organic Electroluminescent Devices”, *Adv. Mater.*, **17**, 285 (2005).
109. R. J. Holmes, B. W. D’Andrade, S. R. Forrest, X. Ren, J. Li and M. E. Thompson, “Efficient, deep-blue organic electrophosphorescence by guest charge trapping”, *Appl. Phys. Lett.*, **83**, 3818 (2003)
110. X. Ren, J. Li, R. J. Holmes, P. I. Djurovich, S. R. Forrest and M. E. Thompson, “Ultrahigh energy gap hosts in deep blue organic

- electrophosphorescent devices”, *Chem. Mater.*, **16**, 4743 (2004).
111. T.-C. Chao, Y.-T. Lin, C.-Y. Yang, T.-S. Hung, H.-C. Chou, C.-C. Wu and K.-T. Wong, “Highly efficient UV organic light-emitting devices based on Bi(9,9-diarylfluorene)s”, *Adv. Mater.*, **17**, 992 (2005).
112. K.-T. Wong, Y.-L. Liao, Y.-T. Lin, H.-C. Su and C.-C. Wu, “Spiro-configured bifluorenes: Highly efficient emitter for UV organic light-emitting device and host material for red electrophosphorescence”, *Org. Lett.*, **7**, 5131 (2005).
113. B. Liu, B. S. Gaylord, S. Wang, and G. C. Bazan, “Shape-adaptable water-soluble conjugated polymers”, *J. Am. Chem. Soc.*, **125**, 6705 (2003).
114. L. Wang, H. Liu and J. Hao, “Stable porphyrin vesicles formed in non-aqueous media and dried to produce hollow shells”, *Chem. Commun.*, 1353 (2009).
115. C. J. Medforth, Z. Wang, K. E. Martin, Y. Song, J. L. Jacobsenc and J. A. Shelnutt, “Self-assembled porphyrin nanostructures”, *Chem. Commun.*, 7261 (2009).
116. K. Kalyanasundaram and J. K. Thomas, “Environmental effects on vibronic band intensities in pyrene monomer fluorescence and their application in studies of micellar systems”, *J. Am. Chem. Soc.*, **99**, 2039

(1977).

117. G. Wyszecki, and W.S. Stiles, Color Science - Concepts and Methods, Quantitative Data and Formulae (2nd ed.). Wiley-Interscience (2000).
118. H. Rudmann, S. Shimada and M. F. Rubner, "Operational mechanism of light-emitting devices based on Ru (II) complexes: Evidence for electrochemical junction formation", *J. Appl. Phys.*, **94**, 115 (2003).
119. A. R. Hosseini, C. Y. Koh, J. D. Slinker, S. Flores-Torres, H. D. Abruña and G. G. Malliaras, "Addition of a phosphorescent dopant in electroluminescent devices from ionic transition metal complexes", *Chem. Mater.*, **17**, 6114 (2005).
120. N. Armaroli, G. Accorsi, M. Holler, O. Moudam, J. Nierengarten, Z. Zhou, R. T. Wegh and R. Welter, "Highly luminescent Cu^I complexes for light-emitting electrochemical cells", *Adv. Mater.*, **18**, 1313 (2006).
121. H. J. Bolink, L. Cappelli, E. Coronado, M. Grätzel and M. Nazeeruddin, "Stable single-layer light-Emitting electrochemical cell using 4,7-Diphenyl-1,10-phenanthroline-bis(2-phenylpyridine)iridium(III) hexafluorophosphate", *J. Am. Chem. Soc.*, **128**, 14786 (2006).
122. Q. Zhang, Q. Zhou, Y. Cheng, L. Wang, D. Ma, X. Jing and F. Wang, "Highly efficient electroluminescence from green-light-emitting

- electrochemical cells based on Cu^I Complexes”, *Adv. Funct. Mater.*, **16**, 1203 (2006).
123. H. J. Bolink, L. Cappelli, E. Coronado, A. Parham and P. Stössel, “Green light-emitting solid-state electrochemical cell obtained from a homoleptic Iridium(III) complex containing ionically charged ligands”, *Chem. Mater.*, **18**, 2778 (2006).
124. E. Z. Colman, J. D. Slinker, J. B. Parker, G. G. Malliaras and S. Bernhard, “Improved turn-on times of light-emitting electrochemical cells”, *Chem. Mater.*, **20**, 388 (2008).
125. H. J. Bolink, E. Coronado, R. D. Costa, N. Lardiés and E. Ortí, “Near-quantitative internal quantum efficiency in a light-emitting electrochemical cell”, *Inorg. Chem.*, **47**, 9149 (2008).
126. F.-C. Chen, Y. Yang and Q. Pei, “Phosphorescent light-emitting electrochemical cell”, *Appl. Phys. Lett.*, **81**, 4278 (2002).
127. K. W. Lee, J. D. Slinker, A. A. Gorodetsky, S. Flores-Torres, H. D. Abruña, P. L. Houston and G. G. Malliaras, “Photophysical properties of tris(bipyridyl)ruthenium(II) thin films and devices”, *Phys. Chem. Chem. Phys.*, **5**, 2706 (2003).
128. C. Adachi, M. A. Baldo, S. R. Forrest, S. Lamansky, M. E. Thompson

- and R. C. Kwong, “Endothermic energy transfer: A mechanism for generating very efficient high-energy phosphorescent emission in organic materials”, *Appl. Phys. Lett.*, **78**, 1622 (2001).
129. S. Tokito, T. Iijima, Y. Suzuri, H. Kita, T. Tsuzuki and F. Sato, “High-efficiency white phosphorescent organic light-emitting devices with greenish-blue and red-emitting layers”, *Appl. Phys. Lett.*, **83**, 569 (2003).
130. W.-Y. Hung, T.-H. Ke, Y.-T. Lin, C.-C. Wu, T.-H. Hung, T.-C. Chao, K.-T. Wong and C.-I. Wu, “Employing ambipolar oligofluorene as the charge-generation layer in time-of-flight mobility measurements of organic thin films”, *Appl. Phys. Lett.*, **88**, 064102 (2006).
131. A. P. Kulkarni, C. J. Tonzola, A. Babel and S. A. Jenekhe, “Electron transport materials for organic light-emitting diodes”, *Chem. Mater.*, **16**, 4556 (2004).
132. E. Tekin, E. Holder, V. Marin, B.-J. de Gans and U. S. Schubert, “Ink-jet printing of luminescent Ruthenium- and Iridium-containing polymers for applications in light-emitting devices”, *Macromol. Rapid Commun.*, **26**, 293 (2005).
133. V. Marin, E. Holder, M. M. Wienk, E. Tekin, D. Kozodaev and U. S. Schubert, “Ink-jet printing of electron donor/acceptor blends: towards bulk

- heterojunction solar cells”, *Macromol. Rapid Commun.*, **26**, 319 (2005).
134. E. Tekin, H. Wijlaars, E. Holder, D. A. M. Egbe and U. S. Schubert, “Film thickness dependency of the emission colors of PPE–PPVs in inkjet printed libraries”, *J. Mater. Chem.*, **16**, 4294 (2006).
135. C. Ulbricht, N. Rehmann, E. Holder, D. Hertel, K. Meerholz and U. S. Schubert, “Synthesis and characterization of oxetane-functionalized phosphorescent Ir(III)-complexes”, *Macromol. Chem. Phys.*, **210**, 531 (2009).
136. N. Tian, A. Thiessen, R. Schiewek, O. J. Schmitz, D. Hertel, K. Meerholz and E. Holder, “Efficient synthesis of carbazolyl- and thienyl-substituted β -diketonates and properties of their red- and green-light-emitting Ir(III) complexes”, *J. Org. Chem.*, **74**, 2718 (2009).
137. N. Rehmann, C. Ulbricht, A. Köhnen, P. Zacharias, M. C. Gather, D. Hertel, E. Holder, K. Meerholz and U. S. Schubert, “Advanced device architecture for highly efficient organic light-emitting diodes with an orange-emitting crosslinkable Iridium(III) complex”, *Adv. Mater.*, **20**, 129 (2008).
138. E. Holder, G. Schoetz, V. Schurig and E. Lindner, “Synthesis and enantiomer separation of a modified tris(2,2'-bipyridine)ruthenium(II)

- complex”, *Tetrahedron: Asymmetry*, **12**, 2289 (2001).
139. E. Holder, M. A. R. Meier, V. Marin and U. S. Schubert, *J. Polym. Sci., Part A: Polym. Chem.*, **41**, 3954 (2003).
140. V. Marin, E. Holder and U. S. Schubert, “Polymeric ruthenium bipyridine complexes: New potential materials for polymer solar cells”, *J. Polym. Sci., Part A: Polym. Chem.*, **42**, 374 (2004).
141. V. Marin, E. Holder, R. Hoogenboom and U. S. Schubert, “Mixed iridium(III) and ruthenium(II) polypyridyl complexes containing poly(ϵ -caprolactone)-bipyridine macroligands”, *J. Polym. Sci., Part A: Polym. Chem.*, **42**, 4153 (2004).
142. E. Holder, V. Marin, A. Alexeev and U. S. Schubert, “Greenish-yellow-, yellow-, and orange-light-emitting iridium(III) polypyridyl complexes with poly(ϵ -caprolactone)-bipyridine macroligands”, *J. Polym. Sci., Part A: Polym. Chem.*, **43**, 2765 (2005).
143. T. Förster, “10th Spiers Memorial Lecture. Transfer mechanisms of electronic excitation”, *Discuss. Faraday Soc.*, **27**, 7 (1959).
144. D. L. Dexter, “Theory of concentration quenching in inorganic phosphors”, *J. Chem. Phys.*, **21**, 836 (1954).
145. M. A. Baldo, M. E. Thompson and S. R. Forrest,

- “High-efficiency fluorescent organic light-emitting devices using a phosphorescent sensitizer”, *Nature*, **403**, 750 (2000).
146. R. J. Holmes, S. R. Forrest, T. Sajoto, A. Tamayo, P. I. Djurovich, M. E. Thompson, J. Brooks, Y.-J. Tung, B. W. D’Andrade, M. S. Weaver, R. C. Kwong and J. J. Brown, “Saturated deep blue organic electrophosphorescence using a fluorine-free emitter”, *Appl. Phys. Lett.*, **87**, 243507 (2005).
147. B. Park, Y. H. Huh, H. G. Jeon, C. H. Park, T. K. Kang, B. H. Kim and J. Park, “Solution processable single layer organic light-emitting devices with a single small molecular ionic iridium compound”, *J. Appl. Phys.*, **108**, 094506 (2010).
148. H. Rudmann, S. Shimada and M. F. Rubner, “Operational mechanism of light-emitting devices based on Ru (II) complexes: Evidence for electrochemical junction formation”, *J. Appl. Phys.*, **94**, 115 (2003).
149. A. A. Gorodetsky, S. Parker, J. D. Slinker, D. A. Bernards, M. H. Wong, G. G. Malliarasa S. Flores-Torres, H. D. Abruña, “Contact issues in electroluminescent devices from ruthenium complexes”, *Appl. Phys. Lett.*, **84**, 807 (2004).
150. X. Zeng, M. Tavasli, I. F. Perepichka, A. S. Batsanov, M. R. Bryce, C.-J.

- Chiang, C. Rothe, and A. P. Monkman, “Cationic bis-cyclometallated Iridium(III) phenanthroline complexes with pendant fluorenyl substituents: synthesis, redox, photophysical properties and light-emitting cells”, *Chem. Eur. J.*, **14**, 933 (2008).
151. C.-H. Yang, J. Beltran, V. Lemaire, J. Cornil, D. Hartmann, W. Sarfert, R. Fröhlich, C. Bizzarri and L. De Cola, “Iridium metal complexes containing N-heterocyclic carbene ligands for blue-light-emitting electrochemical cells”, *Inorg. Chem.*, **49**, 9891 (2010).
152. H.-C. Su, H.-F. Chen, Y.-C. Shen, C.-T. Liao and K.-T. Wong, “Highly efficient double-doped solid-state white light-emitting electrochemical cells”, *J. Mater. Chem.*, **21**, 9653 (2011).
153. M. Lenes, G. Garcia-Belmonte, D. Tordera, A. Pertegás, J. Bisquert and H. J. Bolink, “Operating Modes of Sandwiched Light-Emitting Electrochemical Cells”, *Adv. Funct. Mater.*, **21**, 1581 (2011).
154. H.-B. Wu, H.-F. Chen, C.-T. Liao, H.-C. Su and K.-T. Wong, “Efficient and color-stable solid-state white light-emitting electrochemical cells employing red color conversion layers”, *Org. Electron.*, **13**, 483 (2012).
155. Y. Zheng, A. S. Batsanov, R. M. Edkins, A. Beeby and M. R. Bryce, “Thermally induced defluorination during a mer to fac transformation of a

- blue-green phosphorescent cyclometalated Iridium(III) complex”, *Inorg. Chem.*, **51**, 290 (2012).
156. V. Sivasubramaniam, F. Brodkorb, S. Hanning, H. P. Loebel, V. V. Elsbergen, H. Boerner, U. Scherf and M. Kreyenschmidt, “Investigation of FIrpic in PhOLEDs via LC/MS technique”, *Cent. Eur. J. Chem.*, **7**, 836 (2009).
157. C. C. Chi, C. L. Chiang, S. W. Liu, H. Yueh, C. T. Chen and C. T. Chen, “Achieving high-efficiency non-doped blue organic light-emitting diodes: charge-balance control of bipolar blue fluorescent materials with reduced hole-mobility”, *J. Mater. Chem.*, **19**, 5561 (2009).
158. S. Wang, J. Zhang, Y. Hou, C. Du and Y. Wu, “4,5-Diaza-9,9'-spirobifluorene functionalized europium complex with efficient photo- and electro-luminescent properties”, *J. Mater. Chem.*, **21**, 7559 (2011).
159. Y. Shao, G. C. Bazan and A. J. Heeger, “Long-lifetime polymer light-emitting electrochemical cells”, *Adv. Mater.*, **19**, 365 (2007).
160. M. Cocchi, V. Fattori, D. Virgili, C. Sabatini, P. D. Marco, M. Maestri and J. Kalinowski, “Highly efficient organic electrophosphorescent light-emitting diodes with a reduced quantum efficiency roll off at large

current densities”, *Appl. Phys. Lett.*, **84**, 1052 (2004).

161. Y. Sun and S. R. Forrest, “High-efficiency white organic light emitting devices with three separate phosphorescent emission layers”, *Appl. Phys. Lett.*, **91**, 263503 (2007).

162. N. Chopra, J. Lee, Y. Zheng, S.-H. Eom, J. Xue and F. So, “High efficiency and low roll-off blue phosphorescent organic light-emitting devices using mixed host architecture”, *Appl. Phys. Lett.*, **93**, 143307 (2008).

163. R. Wang, D. Liu, H. Ren, T. Zhang, H. Yin, G. Liu and J. Li, “Highly efficient orange and white organic light-emitting diodes based on new orange Iridium complexes”, *Adv. Mater.*, **23**, 2823 (2011).

